Scientific merits and analytical challenges of tree-ring densitometry

J. Björklund[1, 2, 3], G. von Arx[1], D. Nievergelt[1], R. Wilson[4, 10], J. Van den Bulcke[5, 6], B. Günther[7], N.J. Loader[8], M. Rydval[2], P. Fonti[1], T. Scharnweber[9], L. Andreu-Hayles[10], U. Büntgen[11, 1], R. D'Arrigo[10], N. Davi[12], T. De Mil[5, 6], J. Esper[13], H. Gärtner[1], J. Geary[12], B.E. Gunnarson[14], C. Hartl[13], A. Hevia[15, 16], H. Song[17, 18], K. Janecka[9, 19], R.J. Kaczka[19], A.V. Kirdyanov[20, 21], M. Kochbeck[13], Y. Liu[17, 18], M. Meko[22], I. Mundo[23, 24], K. Nicolussi[25], R. Oelkers[10], T. Pichler[25], R. Sánchez-Salguero[26], L. Schneider[1], F. Schweingruber[1], M. Timonen[27], V. Trouet[22], J. Van Acker[5, 6], A. Verstege[1], R. Villalba[23], M. Wilmking[9] and D. Frank[1, 22]

[1] DendroSciences, Swiss Federal Research Institute for Forest Snow and Landscape, **Switzerland**
[2] Faculty of Forestry and Wood Sciences, Czech University of Life Sciences, Prague, **Czech Republic**
[3] Gothenburg University Laboratory for Dendrochronology, Earth Science Center, Gothenburg University, **Sweden**
[4] School of Earth and Environmental Sciences, University of St. Andrews, **UK**
[5] UGent-Woodlab, Laboratory of Wood Technology, Department of Environment, Faculty of Bioscience Engineering, Ghent University, Ghent, **Belgium**
[6] Ghent University Centre for X-ray Tomography (UGCT), Proeftuinstraat 86, B-9000 Gent, **Belgium**
[7] Technische Universität Dresden, **Germany**
[8] Department of Geography, Swansea University, **UK**
[9] Dendrogreif, University of Greifswald, **Germany**
[10] Tree-Ring Laboratory, Lamont-Doherty Earth Observatory of Columbia University, **USA**
[11] Department of Geography, University of Cambridge, **UK**
[12] Department of Environmental Science, William Paterson University, **USA**
[13] Department of Geography, Johannes Gutenberg-University, Mainz, **Germany**
[14] Bolin Centre for Climate Research, Stockholm University, **Sweden**
[15] Forest and Wood Technology Research Centre (CETEMAS), Asturias, **Spain**
[16] Dpto. Ciencias Agroforestales, Universidad de Huelva, **Spain**
[17] State Key Laboratory of Loess and Quaternary Geology, Institute of Earth Environment, Chinese Academy of Sciences, Xi'an 710061, **China**
[18] Center for Excellence in Quaternary Science and Global Change, Chinese Academy of Sciences, Xi'an 710061, **China**
[19] University of Silesia in Katowice, Faculty of Earth Sciences, **Poland**
[20] Sukachev Institute of Forest SB RAS, Krasnoyarsk, **Russia**
[21] Institute of Ecology and Geography, Siberian Federal University, Krasnoyarsk, **Russia**
[22] Laboratory of Tree-Ring Research, University of Arizona, **USA**
[23] Instituto Argentino de Nivología, Glaciología y Ciencias Ambientales (IANIGLA), CONICET, Mendoza, **Argentina**
[24] Facultad de Ciencias Exactas y Naturales, UNCuyo, Mendoza, **Argentina**
[25] Institute of Geography, University of Innsbruck, **Austria**
[26] Dept. Sistemas Físicos, Químicos y Naturales, Universidad Pablo de Olavide, **Spain**
[27] Natural Resources Institute, **Finland**

Corresponding author: Jesper Björklund (jesper.bjoerklund@wsl.ch)

Key Points:

- We review the merits and state-of-the-art of tree-ring wood microdensitometry and its associated analytical challenges
- We show that systematic level offsets in mean wood density from different techniques and laboratories require correction
- Measurement resolution – notoriously difficult to control – is identified as the major challenge for future research applications

Abstract

X-ray microdensitometry on annually-resolved tree-ring samples has gained an exceptional position in last-millennium paleoclimatology through the maximum latewood density parameter (MXD), but also increasingly through other density parameters. For fifty years, X-ray based measurement techniques have been the *de facto* standard. However, studies report offsets in the mean levels for MXD measurements derived from different laboratories, indicating challenges of accuracy and precision. Moreover, reflected visible light-based techniques are becoming increasingly popular and wood anatomical techniques are emerging as a potentially powerful pathway to extract density information at the highest resolution. Here we review the current understanding and merits of wood density for tree-ring research, associated microdensitometric techniques, and analytical measurement challenges. The review is further complemented with a careful comparison of new measurements derived at 17 laboratories, using several different techniques. The new experiment allowed us to corroborate and refresh "long-standing wisdom", but also provide new insights. Key outcomes include; i) a demonstration of the need for mass/volume based re-calibration to accurately estimate average ring density; ii) a substantiation of systematic differences in MXD measurements that cautions for great care when combining density datasets for climate reconstructions; and iii) insights into the relevance of analytical measurement resolution in signals derived from tree-ring density data. Finally, we provide recommendations expected to facilitate future inter-comparability and interpretations for global change research.

Plain Language Summary

Paleoclimatology, the study of how the climate has changed throughout earth history, is an important component of climate change research. The wood density of tree-rings is a widely used parameter to study past temperature changes. Despite wood density being widely used and considered excellent for this type of research, deriving comparable measurements at different laboratories and using a variety of techniques is proving challenging. This review compiles the current understanding and merits of wood density as a proxy in paleoclimate research. We further describe and review prevalent measurement techniques and associated analytical measurement challenges. The review is also complemented with a careful comparison of a set of new measurements derived at 17 laboratories, using several different techniques. We find that there are substantial differences in measurements performed among laboratories. The main challenge is associated with the analytical resolution when measuring small features such as the density of the latewood. We provide recommendations for future work to overcome systematic differences and towards the prospect of combining measurements from different techniques in integrative studies.

Key words

Microdensitometry, Maximum latewood density (MXD), X-ray densitometry, Blue intensity, Anatomical density, Paleoclimatology

1 Introduction

Polge [1978] declared that the true wood factory, i.e. the cell-producing *cambium* inside the bark of forest trees, is imperfect because the characteristics of wood substantially change from year to year, and within each growing season. This heterogeneity of wood may well be disadvantageous from a material science perspective [*Zobel & Van Buijtenen*, 1989], but is the very basis of discerning annual tree rings, as well as of all inter-disciplinary applications of tree-ring research [*Cook & Kairiukstis*, 2013; *Fritts*, 1976]. The coherence among sequences of ring characteristics, such as annual ring width, from nearby trees (meters to even hundreds of kilometers apart) is indicative of underlying common environmental drivers of growth [*Fonti et al.*, 2010; *Fritts*, 1976; *Jones et al*., 2009; *Vaganov et al*., 2011]. This coherence permits verifiable dating of tree rings to their exact year of formation by comparing growth sequences of many neighboring trees via a process called cross-dating [*Black et al., 2016*; *Stokes & Smiley*, 1968]. Thus, these environmentally sensitive archives enable the understanding of ecosystem dynamical processes, both natural and anthropogenically driven [e.g., *Seidl et al.*, 2017], and also serve as longer-term surrogates or proxies for comparably short meteorological observations [*Fritts*, 1976]. The significance of tree-ring proxies for last millennium climate change studies is clearly illustrated by the fact that tree-ring datasets outnumber all other proxy records, including ice cores, sediments, corals, speleothems and documentary evidence, in global paleoclimate databases [*Emile-Geay et al*., 2017]. Although the majority of tree-ring datasets are based upon ring width, the measurements of wood density at annual or higher (i.e., microdensitometry) resolution play a significant role in late Holocene paleoclimatology [*Briffa et al.,* 2004]. For conifers, and particularly those growing in cooler high-latitude and high-altitude environments, the density of wood tissue formed towards the end of the growing season, maximum latewood density or simply maximum density (MXD; Figure 1), is particularly tightly coupled (with strong positive correlations) to growing season air temperature [*Schweingruber et al.,* 1978].

FIGURE 1 *The concept of deriving microdensitometric data on a digitized X-ray radiograph of a Pinus sylvestris sample from Northern Finland. In a) a photo sensor is moved from left to right in the X-ray radiograph (from pith to bark along the radial axis) producing two measurement profiles in b). The difference between the measurement profiles is the sensor aperture. The red profile displays the result of using a narrow aperture, and the blue line a wide aperture, i.e. high and low measurement resolutions respectively. From the measurement profiles and annual ring demarcations, maximum density (MXD), the highest value for every ring (year) can be derived. Similarly, minimum density (MND) is the lowest value per ring. Ring density is the average density integrated over the entire ring. Extracted MXD values at high and low measurement resolutions illustrate the potential distortion effect on the inter-annual variability. The horizontal solid white lines in a) denote the tangential sensor-width and the photo-sensor aperture is illustrated with the various thicknesses of the vertical dotted white lines. The sensor is ideally moved across ring boundaries at an obliquity of 0° compared to the ring boundary. The obliquity is the angle offset of the photo sensor with regard to each passed ring boundary, illustrated with the three differently angled dotted white lines in a).*

However, it is also clear that density measurements are far more complex [*Schweingruber*, 1988] than the less time- and labor-intensive ring-width measurements [e.g., *Briffa et al.,* 2002; *Esper et al.,* 2012]. Although high coherence in the inter-annual to long-term variation of MXD is reproduced among various laboratories and using various techniques, many studies report mean level offsets in MXD data [*Clauson & Wilson,* 1991; *De Ridder et al.,* 2010; *Gunnarson et al.,* 2011; *Ivkovich & Koshy,* 1997; *Mannes et al.,* 2007; *Melvin et al.,* 2013; *Kaczka et al.,* 2018; *Klesse et al.,* 2015; *Park & Telewski,* 1993]. Such offsets indicate challenges of accurately and precisely measuring and/or consistently defining and quantifying wood density. The accuracy and precision of density parameters is not only vital when used directly (e.g., g/cm^3) for purposes such as biomass estimations [e.g., *Babst et al.,* 2014b; *Bouriaud et al.,* 2015; *Vannoppen et al.,* 2018]. But it is also necessary to address and correct for systematic bias when using density parameters as climate proxies. In this sense, it is well recognized that mixing MXD data with different mean levels due to measurement idiosyncrasies can negatively impact the reliability of climate reconstructions [*Esper et al.,* 2014; *Gunnarson et al.,* 2011; *Klesse et al.,* 2015; *Melvin et al.,* 2013; *Zhang et al.,* 2015].

With an increasing demand for high-quality wood density data to study environmental change [e.g., *Wilson et al.,* 2016; *Anchukaitis et al.,* 2017], compounded by a growing body of research documenting measurement inconsistencies, it is now a timely and necessary endeavor to review the accumulated state-of-the-art knowledge, and to empirically examine and review how wood density measurements are reproduced using various techniques in various laboratories. The review is focused on the application of density measurements on conifer tree-rings in paleoclimatology because wood density measurements of deciduous trees have to date not been widely used nor shown great promise. In Section 2, we consolidate and discuss the current theoretical understanding, and the basic application of microdensitometry on wood, including the associated scientific merits and analytical challenges. Section 3 is dedicated to a description of the primary, and currently applied, microdensitometric techniques. Section 4 comprises a full-scale inter-comparison experiment of microdensitometric measurements, conducted across a representative range of techniques and laboratories. The fifth and final section is dedicated to a synthesis of the empirical findings of Section 4 in the context of existing knowledge and technique idiosyncrasies, along with some recommendations for future work.

2 Current understanding of wood density in tree rings

"The concept of density is deceptively simple. Measurements of the physical characteristics of weight and volume of a body would seem to be among the easiest physical parameters to describe. In reality, for a porous, hygroscopic, polymeric material such as wood the measurement of one of these parameters – the volume component – is extremely controversial."

Kellogg and Wangaard [1969]

As researchers have long struggled with direct densitometry based on measurements of mass/volume of wood, it should come as no surprise that indirect determinations of density at minute scales (on tree ring or sub-ring level) using microdensitometric approaches also are associated with significant challenges.

2.1 Defining density in tree rings

When studying environmental change with tree rings, it is essential that the measured characteristics – such as density – are absolutely bound to each specific annual ring. Mobile compounds in the wood such as water or resins, that also have an effect on wood density, do not belong to one particular ring and are preferably removed or kept constant [*Lenz et al.,* 1976; *Schweingruber*, 1988; *Schweingruber et al.,* 1978]. Wood density in a tree-ring context is ideally a function of the woody tissue or xylem (Figure 2), where the tracheid cell (also referred to as fiber or grain) should be considered the base unit.

FIGURE 2 *Rendering of a small piece of the xylem of a Pinus sylvestris wood sample (image, property of UGCT – Ugent-Woodlab, captured with the Nanowood, X-ray CT scanner at 0.65 µm resolution [Dierick et al., 2014; Van den Bulcke et al., 2009]). The figure indicates important directions in the wood and illustrates the typical morphology of tracheid cells constituting the xylem. Note that the tracheid cells are axially elongated, and that the radial dimension of the tracheid determines whether the xylem is classified as earlywood or latewood. The abrupt change from smaller radial dimension tracheids to larger indicates the tree-ring boundary between two growing seasons. The empty space within each tracheid is called lumen or plur. lumina. A single row of cells along the radial direction in the xylem is often referred to as a radial file.*

The tracheid is the major component of the conifer xylem, and is developed in a few defined stages: cell division, cell expansion (axial elongation and radial enlargement), cell wall thickening (involving cellulose, hemicelluloses, cell wall proteins, and lignin biosynthesis and deposition) and programmed cell death [*Plomion et al.,* 2001]. The mature tracheids provide both a hydraulic system for water conductance and primary mechanical support for the tree [*Tyree & Zimmermann,* 2002]. With this single cell type, the tracheid anatomy varies continuously to accommodate both of these functions [*Lachenbruch & Mcculloh*, 2014]. Within a growing season, trees first produce large and thin-walled tracheids. As the season progresses, cells gradually become smaller and thicker-walled. This change in cell characteristic is often regarded to reflect the functional switch from optimizing the hydraulic performance (earlywood) to the mechanical support (latewood) of the xylem [*Lachenbruch & Mcculloh,* 2014; *Rossi et al.,* 2006; *Wodzicki,* 1971]. There is considerable debate about how this intra-seasonal (i.e., within a single ring) change in xylem morphology is organized. Some advocate that it is actively/genetically driven by a need for reinforcement of the tree structure by latewood tissue [*Bowyer & Shmulski,* 2003; *Brown et al.,* 1949; *Gartner,* 1995; *Hannrup,* 2007; *Sperry et al.,* 2006; *Yasue et al.,* 2000; *Zobel and van Buijtenen,* 1989], while others advocate that it is passively/environmentally driven by a reduced need and/or availability of water later in the season (reduced radial cell expansion from lowered turgor pressure) that manifests itself as latewood [*Antonova & Stasova,* 1997; *Hansen et al.,* 1997; *Moehring et al.,* 1975; *Olano et al.,* 2014; *Petit & Crivellaro,* 2014; *Plomion et al.,* 2001; *Simard et al.,* 2013; *Uggla et al.,* 2001]. Regardless, it appears that the more modest year-to-year (i.e., inter-annual) variability in tracheid dimensions of both earlywood and latewood components is mainly driven by external environmental influences [*Bryukhanova & Fonti,* 2013; *Fonti & Jansen,* 2012; *Pritzkow et al.,* 2014].

The density of the xylem is first determined by the tracheid dimensions including the size of the cell, the thickness of the wall, where the anatomical density is defined as the proportion of cell wall per tracheid for the tracheids of interest [*Polge,* 1978; *Rathgeber et al.,* 2006; *Vaganov et al.*, 2006; *Wimmer,* 1995]. The density is further modulated by the density variations of the solid cell wall stemming from the molecular composition of the tracheids, i.e. the relative abundance of the three macromolecular classes: cellulose, hemicelluloses and lignin [*Lachenbruch & Mcculloh,* 2014; *Savidge,* 2003]. To the first order the cell wall density is found to be more or less constant among tree species at ca. 1.5 g/cm^3 [*Kellogg et al.,* 1975; *Kellogg & Wangaard*, 1969; *Siau,* 1984; *Stamm & Sanders,* 1966]. The cell wall density also appears to play a minor role in determining density variation from earlywood to latewood [*Decoux et al.,* 2004]. Hence, the variability of wood density must primarily be determined by changes in anatomical dimensions [*Elliott & Brook,* 1967; *Jagels & Telewski,* 1990; *Polge,* 1978; *Tsoumis,* 1964]. Within a tree ring, density increases from earlywood to latewood, mainly as a function of diminishing sizes of tracheids as the wall area per cell varies modestly within an annual ring [e.g., *Cuny et al.,* 2014; *Rathgeber et al.,* 2006]. From one year to the next, variations of earlywood density are also mainly controlled by variation in tracheid sizes [*Björklund et al.,* 2017; *Yasue et al.,* 2000], while latewood density fluctuations have mainly been attributed to variations in the amount of deposited cell-wall material [*Vaganov et al.,* 2006; *Wang et al.,* 2002; *Yasue et al.,* 2000]. A complex interplay between tracheid size and cell-wall material, however, has also been identified and proposed [*Björklund et al.,* 2017].

2.2 Environmental relationship and associated scientific merits of tree-ring density

In temperature-limited environments, the density of the latewood and thus the MXD parameter is tightly correlated with growing season air temperature. While high temperatures result in both larger cells and more deposited cell wall material, the MXD exhibits a net increase [*Björklund et al.,* 2017]. The cell dimensions that drive earlywood density variation are also controlled by growing season temperature, but because variations in deposited cell wall material is secondary to earlywood cell enlargement variations, high temperatures mainly mean larger cells and thus lower density [*Björklund et al.,* 2017]. Likewise, in drought prone environments, dry years appear to have a negative effect on earlywood cell enlargement and to yield high density [*Camarero et al.,* 2017; *Camarero et al.,* 2014]. Latewood density appears to modestly increase in wet years [*Cleaveland,* 1986], most likely due to increased deposition in the cell wall, but this has not been explicitly studied. Interestingly, this robust earlywood and latewood dichotomy of Northern Hemisphere conifers does not generally apply to Australasian conifers where earlywood and latewood density are both negatively influenced by increased temperatures [*Drew et al.,* 2012; *O'Donnell et al.,* 2016]. Drew et al. [2012] suggests that for Australasian conifers, increased temperatures reduce the duration of the wall thickening leading to a net decrease in latewood density.

The most important direct application of the prominent link between wood density and climate is realized through high-quality growing season air temperature reconstructions using the MXD parameter of Northern Hemisphere conifers [e.g., *Esper et al.,* 2018]. The benefits of using MXD compared to ring width are numerous and substantial enough to outweigh the greater costs including time associated with these measurements. The strong positive association between year-to-year MXD and temperature variation often include the warmer half of the year, a substantially longer period than for ring width [e.g., *Anchukaitis et al., 2017*; *Björklund et al.*, 2017; *Briffa et al.*, 2002, 2004; *Frank & Esper*, 2005; *Wilson et al.,* 2016]. The latitudinal and altitudinal temperature response space is greater for MXD than for ring width, where MXD displays a significant positive response in many areas where ring widths do not [*Björklund et al.,* 2017]. In addition to this, MXD measurements are less susceptible than ring width to some types of non-climatic noise, such as large-scale disturbances [*Rydval et al.,* 2018]. Ring width has been shown to exhibit muted short-term responses to extreme events and exaggerated decadal to centennial scale fluctuations compared to instrumental records [*Franke et al.*, 2013] and climate model simulations [*Franke et al.*, 2013; *Schneider et al.,* 2015; *Wilson et al.,* 2016]. MXD has been shown to be superior when assessing short-term climate perturbations from volcanic eruptions [*Anchukaitis et al.,* 2012; *D'Arrigo et al.,* 2013; *Esper et al.*, 2015; *Frank et al.,* 2007; *Jones et al.,* 1995; *Stoffel et al.,* 2015]. However, Battipaglia et al. [2010] note that MXD may be less faithful to warm extremes than cold extremes. MXD appears to be less affected by amplified reactions to environmental variability, that is, short-term climatic perturbations invoke muted responses in ring width, but also a lagged recovery to normal growth when the perturbation has ended (so-called biological memory effects) [*Esper et al.*, 2015; *Fritts,* 1976]. Moreover, in contrast to ring width, MXD has been advocated to better represent millennial-scale variability [*Esper et al.,* 2012], but more long-term studies are needed to firmly establish this. Considering these merits, MXD is increasingly the preferred or sole parameter for large-scale temperature reconstructions [e.g., *Briffa et al.,* 2002; *Schneider et al.*, 2015]. In large-scale temperature reconstructions based on both MXD and ring width, MXD is often the stronger explanatory variable and carries more weight [e.g., *Anchukaitis et al.*, 2017; *Esper et al*., 2018; *Guillet et al*., 2017; *Stoffel et al.*, 2015; *Wilson et al.,* 2016].

Whereas MXD provides superior information about growing season temperature than ring width, further densitometric-based tree-ring parameters are also measured, and may improve the skill of a reconstruction [*Cleaveland,* 1986; *Schweingruber et al.,* 1978]. The density of the wood formed at the start of the growing season, in particular the minimum density of the earlywood (Figure 1), has been shown to be sensitive to water availability in drought-prone environments [*Camarero et al.,* 2017; *Camarero et al.,* 2014; *Cleaveland*, 1986]. The minimum density parameter, when subtracted from the MXD parameter, creates a new parameter (i.e., “delta density”), which has been shown to express stronger correlations with temperature with improved fidelity of multi-centennial scale variability [*Björklund*, 2014]. The density integrated over the entire ring, ring density, is useful for carbon cycle research [*Babst et al.,* 2014a], with specific equations relating wood dimensional measurements to carbon quantities [*Babst et al.,* 2014b; *Bouriaud et al.,* 2015]. Interestingly, failing to consider ring density can lead to overestimation of long-term trends of aboveground biomass increment for species such as beech (*Fagus sylvatica*), but underestimations for oak (*Quercus petraea*) [*Vannoppen et al.,* 2018]. Density measurements can thus improve estimates of terrestrial carbon fluxes – one of the most important challenges in environmental science [*Baker et al.,* 2004] – as well as help explain ecological strategies of trees by evaluating life history trends in density [*Nock et al.,* 2009; *Woodcock & Shier,* 2002]. Moreover, the earlywood to latewood dynamics of ring density profiles (Figure 1) can also be used as proxies of adaptive traits linked to resistance to drought [*Britez et al.,* 2014].

2.3 The basics of X-ray based microdensitometry of tree-rings

Early on, various radiation, light, electrical, and mechanical techniques were developed to study the density of tree-rings [*Cameron et al.,* 1959; *Green*, 1965; *Green & Worrall,* 1964; *Harris*, 1969; *Marian & Stumbo*, 1960] but the most prevalent approach is based on X-ray radiation, pioneered by *Polge* [1963, 1965b, 1966, 1970], *Fletcher and Hughes* [1970] and *Parker and Henoch* [1971]. Both *Polge* [1966] and *Parker and Henoch* [1971] correlated MXD chronologies with climate variables with promising results. A few years later, Ernst Schär and Fritz Schweingruber (Swiss Federal Institute of Forest, Snow and Landscape WSL) started the development of a measurement technology from modified commercial components that by the mid 1970s was operational [*Lenz et al.,* 1976]. Using this device and later commercial updates, Fritz Schweingruber and co-workers created a database of wood density time series covering wide areas of North America, most of Europe, and transects across the Eurasian Northern boreal zone [*Briffa et al.,* 1998; *Briffa et al.,* 2002; *Schweingruber & Briffa*, 1996; *Schweingruber et al.*, 1988; *Schweingruber et al.,* 1993]. This network constitutes the beginning for MXD, as the state-of-the-art parameter of current tree-ring based temperature reconstructions. Subsequently, a great number of devices for measuring wood density have been developed, where some are more successful than others in their longevity and acceptance within the research community.

The first stage in X-ray densitometry is to produce an X-radiograph of a transversal cross section of wood. The transversal section provides an axial view of tracheids forming tree rings (Figure 2). This is achieved by transmitting X-ray radiation through the wood section onto a sheet of X-ray sensitive film [e.g., *Parker & Jozsa,* 1973; *Polge,* 1963, 1966] or using an electronic detector [e.g., *Cown & Clement,* 1983; *Woods & Lawhon,* 1974]. Alongside the wood sample, a material standard with a known density and attenuation properties of X-ray radiation similar to the cell walls of wood is exposed. This reference standard material is designed as a stepped wedge of different thicknesses, i.e., variable optical depths [*Parker et al.,* 1985] enabling a range of transmissions to be related to the reference material (Figure 3a).

***FIGURE 3** a) A stepped calibration wedge constructed from a reference material of known density used to refer all the brightness values of the X-radiograph of the wood sample to a density scale. b) The concept of internal image distortion (parallax) in X-ray images, note that the conical beam 2-D representation of the objects become more distorted when the X-rays are increasingly less parallel. c) The assumption of direct comparability between homogenous and heterogeneous materials in X-ray densitometry. While the two objects have the same density, their spatial configuration causes a difference in the detected transmission.*

Note that a radial cross section of wood is, in contrast to the standard material, not a homogeneous material, at the spatial scales of relevance, but rather a mesh of cell walls and

cell voids called lumina (Figure 2). X-rays are distributed in a cone-shaped fashion from the source, and when the X-rays penetrate the mesh, image distortion of the internal structure will occur where the rays are non-perpendicular to the surface of the sample (Figure 3b). Thus the microstructure will only appear sharp in the radiographs if the X-rays are parallel with the fiber direction [e.g., *Bergsten et al.,* 2001; *Lenz et al.,* 1976]. However, transmitting parallel X-rays through meshed structures may induce incorrect estimates of its density. This is because the relationships between wood density and the transmission of X-rays are different for homogenous and heterogeneous materials [*Moschler & Winistorfer,* 1990]. In fact, it can numerically be shown that the sum of detected radiation will be larger if transmitted through a material where the solid material is parallel structured with the beams, compared to if the material is organized orthogonally (see Figure 3c for a conceptual example). Even though this bias may be relevant, there is a tendency within the microdensitometry community to prioritize sharpness of the microstructure [*Vaganov et al.,* 2006].
In order for the X-rays to be as close to parallel to the fiber angle upon exposure as possible, the X-ray source is placed at a far distance from the samples (a few meters), or by passing the X-rays through a collimator that focuses the emitted rays into a narrower beam. The images of the sample and the standard are then projected in a densitometer (a device that measures brightness of the radiograph) or displayed on a computer screen. By comparing the wood samples' brightness (grey-scale) values with the brightness values for the co-assessed standard of known density, spatially variable wood densities within the sample image can be obtained. The output is often presented as a radial measurement profile with the y-axis representing fluctuations in density and the x-axis representing the radial extension of the sample (Figure 1).

In order to ensure consistent measurements, there are a few aspects that need further elaboration. By definition, the transmittance of a sample material is related to its optical depth and to its opacity or attenuation of X-ray radiation. The optical depth of the sample is controlled by preparing thin wood strips, or laths, of near-even thickness using a twin-blade saw [*Kusec,* 1972] or microtome [*Thetford,* 1991]. Due to variations in wood moisture content, saw blade temperature changes etc., that can affect the volume of the sample and/or the saw blades, the resulting sample thicknesses are measured with a caliper and documented on a sample-by-sample basis [*Parker et al.,* 1985]. It is critical that the saw cut is performed perpendicular to the fiber direction because any deviation to this will affect the clarity of the image and thus the final density profile [*Lenz et al.,* 1976]. The fiber direction can vary substantially throughout the same sample. Thus, several cuts are often made to ensure adequately consistent fiber orientation for all parts of the sample [*Vaganov et al.,* 2006].

The X-ray opacity of wood is dependent on the attenuation coefficient, associated with the molecular composition of the xylem cell walls, but also to some degree on mobile compounds (so-called extractives) [*Bergsten et al.,* 2001; *Helama et al.,* 2012; *Helama et al.,* 2010; *Kanowski & Wright,* 1985; *Lloyd,* 1978; *Schweingruber et al.,* 1978], and moisture content [*Schweingruber et al.,* 1978]. The material standard (of similar mixing ratios of lignin, cellulose and hemicellulose as wood) is invalid for resins, crystals, metallic inclusions etc. This is because these compounds have potentially different X-ray interactions [*Schweingruber et al.,* 1978]. Because these extractives can change appreciably along a tree-ring sequence (e.g., heartwood to sapwood), removal of these extractives is highly recommended. The extractives may be removed from the wood by use of solvents, without changing the cellular structural characteristics [*Pereira et al.,* 2003]. Samples can be boiled in water to remove hydrophilic compounds such as phenols and tannins etc., and refluxed in alcohol, benzene, acetone or toluene to remove lipophilic substances such as resins or oils [*Parker et al.,* 1985]. The complete (i.e., 100%) removal of these compounds is difficult to achieve.

Water is strongly opaque to low energy X-rays, and furthermore changes the volume and density of wood [*Bergsten et al.,* 2001; *Williamson & Wiemann,* 2010]. Ideally, wood samples should thus be X-rayed in an oven-dry state. However, related technical difficulties have resulted in a standard procedure where moisture content is kept relatively constant by placing the X-ray device in an acclimatized room. This means that established measurement technical definitions for gravimetric/volumetric density, such as "basic density" [*Elliott,* 1970], or “dry wood density” [Zobel & Van *Buijtenen,* 1989], are not directly comparable to commonly produced microdensitometric measurements. For microdensitometry, the specification behind the density unit (e.g., g/cm^3) is a wood sample conditioned to a defined relative humidity (usually 40-60% depending on the laboratory) at a specified temperature (usually 20-23°C, also depending on the laboratory), corresponding to a moisture content of roughly 10% by weight during radiography [*Lenz et al.,* 1976]. For “basic density” and “dry wood density”, the wood is either oven dried or air-dried prior to gravimetric determination, whereas the volume is determined on fresh samples when water is not removed (so-called “green volume”).

2.4 The challenges of analytical scale for microdensitometric measurements

The purpose of microdensitometry for e.g., dendroclimatology is to produce consecutive measurements of density at ring or sub-ring level, such as density of the earlywood or latewood, or the minimum or maximum density per ring (Figure 1). Because X-ray microdensitometry is indirectly measured through detected light transmission, it is fundamental to cross-validate the performance by comparing with basic, yet accurate, mass/volume based density measurements. Experiments involving the production of intra-ring gravimetric/volumetric density measurements with serial tangential wood shavings (using a microtome) have been conducted [*Ifju et al.,* 1965; *Kennedy,* 1966], but this is a rather imprecise approach because determination of volume is unreliable for small samples [*Kellogg & Wangaard,* 1966; *Mothe et al.,* 1998] and moreover it is tremendously tedious. Microdensitometry is therefore cross-validated by comparing integrated measurements of X-ray density from full samples that can be easily volumetrically determined [e.g., *Bergsten et al.,* 2001; *De Ridder et al.,* 2010; *Evans,* 1994; *Lenz et al.,* 1976]. Full samples often comprise multiple decades of rings and >1 cm^3 of wood volume. Upon comparison it is important that mass/volume based density is determined under similar acclimatization conditions as prevalent during the X-ray exposure. It can be demonstrated that, using the appropriate precautions, X-ray microdensitometric measurements precisely [*Vaganov et al.,* 2006], but not necessarily accurately [Lenz et al., 1976], reproduce those obtained gravimetrically/volumetrically. That is, the measurement noise level is low, but there could be a systematic mean level bias. In fact, *Lenz et al.* [1976] formulated the hypothesis that observed differences could be a product of the chemical differences between the tracheid wall and the material standard, and proposed a set of correction factors for different types of wood species. However, the discrepancy could also be attributed to the heterogeneity of wood as a material compared to the homogenous material standard. In that case, the differently configured mesh structure of earlywood and latewood, as well as the different earlywood and latewood percentages and morphologies of different conifer genera [*Schweingruber et al.,* 2011] should prompt the use of different correction factors rather than the chemical difference of the materials.

Even if a perfect cross-validation of full sample density was possible, the fact that maximum, minimum, earlywood and latewood density parameters are not directly validated is indicative of further challenges with regard to the analytical scale of measurements. It is often stated in the literature that minimum and maximum density are completely dependent of measurement resolution [*Evans,* 1994; *Lenz et al.,* 1976; *Parker et al.,* 1985; *Polge,* 1978; *Vaganov et al.,* 2006]. *Jacquin et al.* [2017] contemplates that even if *"separate devices provide about the same densities on average, one might suspect that density extrema and variance are more sensitive to the measuring method"*. Thus, the selected literature conveys the impression that we should not expect to obtain comparable MXD measurements using different techniques if they differ in measurement resolution. To the best of our knowledge, this has not been rigorously assessed prior to the current review and comparative investigation.

The MXD parameter, which is often of particular interest to dendroclimatologists, may, on the anatomical scale, be a function of only one or two latewood tracheids in the radial direction within a tree ring [*Vaganov et al.,* 2006]. Thus, to faithfully represent the MXD of every ring, a spatial resolution of ≤10 µm would be needed because this is the typical size of a latewood tracheid in the radial direction [*Vaganov et al.,* 2006]. For most current techniques, the MXD parameter is extracted from a measurement profile produced by a photo sensor traversing across a tree-ring sample (see Figure 1). If the spatial resolution were coarser than 10 µm, the amplitude of the profile, moving from minimum to maximum density within a tree-ring, would be proportionally suppressed. The measurement resolution is in theory dependent on the aperture of the slit width of the photo sensor [*Evans,* 1994; *Lenz et al.,* 1976; *Polge,* 1978; *Schweingruber et al.,* 1978] but is in practice also dependent on the photo sensor being held parallel to the ring boundaries during measurement [*Evans,* 1994; *Lenz et al.,* 1976; *Park and Telewski,* 1993; *Schweingruber,* 1988; *Schweingruber et al.,* 1978; *Vaganov et al.,* 2006; *Van den Bulcke et al.,* 2014]. A blurred radiograph may further limit the potential to obtain a measurement resolution determined by the slit width.
As discussed previously, the sharpness of the radiograph depends on the extent of parallax, the distortion of the internal structure of the object, that arises when the X-rays from a point source diverge and penetrate the wood at non-orthogonal beam angles to the sample surface [*Jacquin et al.,* 2017; *Parker et al.,* 1985]. Since the parallax problem is mitigated at the design phase of each measurement system, the more important factor likely is high-precision sample preparation to ensure that tracheid angles match the incidence of the X-rays [*Lenz et al.,* 1976]. The impact of all these features on a specific measurement profile, henceforth collectively referred to as apparent measurement resolution, can conceptually be illustrated by using an increasingly wider sensor aperture on a sharp radiograph, where wider aperture corresponds to reduced measurement resolution (Figure 1). Conceptually demonstrated in *Jacquin et al.,* [2017] and empirically demonstrated in *Lenz et al.,* [1976] and *Helama et al.,* [2012], and illustrated in

Figure 1, it is clear that density maxima in particular, but also minima, are affected by apparent measurement resolution. Notably, a reduced apparent measurement resolution results in a deflated profile with systematically lower mean levels of MXD. Even more noteworthy is that the narrow ring profiles become relatively more deflated than wide ring profiles, and this can in special cases alter the inter-annual direction of change or ranking of MXD values (Figure 1), and likely also affect the overall variance. Moreover, because narrower rings are often non-randomly distributed in time with respect to wider rings, due primarily to so-called biological growth trends [*Fritts,* 1976] or low-frequency environmental changes, MXD measurements from techniques with differing apparent measurement resolution could also potentially attain measurement-derived differences in long-term trends [*Helama et al.,* 2012].

3 Primary and currently applied microdensitometric techniques

Following the early work on microdensitometry, continuing research has led to numerous alterative measurement systems and techniques: Walesch electronics [*Eschbach et al.,* 1995], Itrax Multiscanner [*Bergsten et al.,* 2001], SilviScan [*Evans,* 1994], High-Frequency densitometry [*Schinker et al.,* 2003], Resistograph [*Rinn et al.,* 1996], radiography on microtome sections [*Telewski et al.,* 1987], 3D X-ray Computed Tomography [*Dierick et al.,* 2014], neutron imaging [*Mannes et al.,* 2007], anatomical relative density [*Decoux et al.,* 2004], visible light reflectance [e.g., *Clauson & Wilson* 1991; *Jagels & Telewski,* 1990; *Sheppard et al.,* 1996; *Thetford et al.,* 1991], blue light reflectance [*McCarroll et al.,* 2002], Tetrahertz pulse imaging [*Jackson et al.,* 2009] and laser-sandblasting of wood surfaces [*Lesnino,* 1989]. In this chapter we provide a background for the development rationale, current use, brief technical specifications and required sample preparations for the primary and most promising microdensitometric techniques in the present era.

3.1 X-ray techniques

3.1.1 The Dendro2003 – WALESCH *Electronic GmbH*

The DENDRO2003 X-ray microdensitometer is the third generation of densitometers developed by WALESCH Electronic GmbH (Switzerland), where the first generation was introduced in the beginning of the 1990's in cooperation with WSL [*Eschbach et al.,* 1995]. There are currently 14 devices in the world. The device is largely based on the early versions of densitometry technology developed by Fritz Schweingruber and co-workers at WSL. Since the development of the vast data network created at WSL, the Walesch technique has continued to be used predominantly for temperature reconstructions and interpretations thereof, including millennial length [e.g., *Briffa et al.,* 1990, 1992; *Büntgen et al.,* 2006; *Esper et al.,* 2012; *Klippel et al.,* 2018; *Luckman & Wilson*, 2005] and multi-centennial length reconstructions [e.g., *Anchukaitis et al.,* 2013; *Büntgen et al.,* 2008, 2011, 2017; *Chen et al.,* 2012; *Davi et al.,* 2003; *Klesse et al.,* 2015; *Luckman et al.,* 1997; *Sun et al.,* 2012; *Yuan et al.,* 2013], studies of climate growth relationships [e.g., *Briffa et al.,* 2002; *Büntgen et al.,* 2010, 2007; *Düthorn et al.,* 2016; *Levanič et al.,* 2009; *Trouet, et al.,* 2012] or comparing alternative techniques in a climate reconstruction context [e.g., *Kaczka et al.,* 2018; *Mannes et al.,* 2007; *McCarroll et al.,* 2002; *Wang et al.,* 2002; *Wilson et al.,* 2014].

Each sample (e.g., chemically extracted ≥5 mm increment cores) is usually cut into short segments (e.g., typically 5 cm or shorter) depending on local deviations of fiber direction, and affixed to wooden mounting blocks at a fiber-angle orthogonal to the saw blades. The fiber-angle is determined with the aid of a crosshair under a microscope. The samples are usually cut with a twin-blade saw to an axial thickness of 1.2 mm. The thickness of each sample is measured and recorded using a dial gauge and the value is included in the density transformation of film brightness values into density. A stationary soft X-ray source, located in a room with controlled temperature and relative humidity (usually 50% RH at 20°C), is used to expose the samples placed on a cassette with an X-ray sensitive film. Very fine-grained and high-contrast technical X-ray films are used, such as the Kodak Industrex MX125 with a dimension of approximately 20 x 30 cm. Because the focal spot of the X-ray beam is uncontrolled, and all samples are exposed continuously, the X-ray source is placed 1.5-3 meters away to mitigate parallax. A material standard, a calibration step-wedge of either cellulose acetate ($\rho = 1.27$ g/cm^3) or cellulose propionate ($\rho = 1.24$ g/cm^3) is placed among the samples on the cassette. After exposure, the film is chemically developed preferably with an automatic processor under standardized conditions (e.g., with an X-O-Mat for 90 seconds). Before starting the measurement procedure on a developed film, the DENDRO2003 densitometer is calibrated using brightness values from five fields of different thickness on the calibration step-wedge (Figure 3a). Because of the hypothesized mismatch in chemistry of the tracheid wall and the step-wedge, empirically obtained correction factors are used (different factors for different species) [*Lenz et al.,* 1976].

On the display projector of the densitometer, a photo sensor divided into 7 segments is used to analyze the brightness of the film. The measurement dimension of the photo sensor depends on the magnification used, but is usually operated at the highest magnification, where the radial extension of the sensor is 10 µm, and each sensor is 0.14 mm in the tangential direction. Each segment can independently be switched on or off. For narrow rings, fewer photocells and larger projector magnification tend to be used, leading to a variable measurement resolution within most samples. Projected on the display, the developed negative is moved across the photo sensor and a density value is recorded every 10 µm building up a measurement profile segmented with annual boundaries. A pedagogic cartoon of the entire process is provided in *Schweingruber* [1988].

3.1.2 The Itrax Multiscanner

The Itrax multiscanner by Cox Analytical Systems (Sweden) was mainly, but not exclusively, developed for wood samples – the functionality permits the analysis of speleothems and other small flat samples, and additionally offers information about chemical composition of the samples when equipped with an X-ray fluorescence detector [*Hevia et al.,* 2018; *Scharnweber et al.,* 2016]. Available since 2004, an increasing number of laboratories (at present 15) have used the Itrax Multiscanner to produce density data for a number of dendroecological and/or dendroclimatological studies [e.g., *Björklund et al.,* *2015*; *Björklund et al.,* 2013; *Cameron et al.,* 2015; *Duan et al.,* 2014; *Gunnarson et al.,* 2011; *Gunnarson et al.,* 2012; *Helama et al.,* 2014; *Liang et al.,* 2016; *Linderholm et al.,* 2015; *Melvin et al.,* 2013; *McCarroll et al.,* 2013; *Xing et al.,* 2014; *Zhang et al.,* 2015, 2016]. Many of these studies combine new or updated measurements with previously published MXD data acquired by other analytical techniques such as the Walesch technique. Further dendrochronological applications of the Itrax multiscanner include studies on tropical wood [Haines et al., 2018], reconstructions of salmon abundance [*Starheim* *et al.,* 2013], glacier mass balances [*Wood et al.,* 2011; *Wood & Smith,* 2013], or studies comparing X-ray based wood density of the Itrax with data obtained with the Walesch technique [*Helama et al.,* 2012], wood density surrogates derived with blue intensity techniques [*Björklund et al.,* 2014; *Campbell et al.,* 2007; *Rydval et al.,* 2014] and wood anatomical parameters [*Pritzkow et al.,* 2014]. A reference list of studies using the Itrax multiscanner can be downloaded from the manufacturer's website (http://www.coxsys.se/).

Sample preparation for microdensitometric measurements on wood with the multiscanner largely follows the same protocol as with the Walesch technique, but 10-12 mm diameter core samples are more often used, due to the sample holder design. The multiscanner is equipped with an X-ray source that produces soft high intensity X-rays, emitted as a flattened cone beam located at a short distance from the samples [*Bergsten et al.,* 2001]. The transmitted radiation is passed through a slit (10-20 µm aperture) and digitally detected by an array sensor. The wood samples are positioned in a vertical sample holder that is moved in stepwise short (10 µm) distances relative to the fixed X-ray source. The small focal spot and the short distance between sample and beam ensures that the beams are close to parallel with the fiber angle throughout the wood sample. However, as mentioned above, when transmitting perfectly parallel X-rays to produce sharp radiographic images, this approach tends to yield compromised density values [*Moschler & Winistorfer,* 1990]. The developer has addressed this by using the flattened X-ray cone beam. Consider that the density fluctuations of interest in dendrochronology are radially directed, i.e. across ring boundaries, whereas density is not expected to vary much in the tangential direction, along ring boundaries [*Bergsten et al.,* 2001]. When exposing the wood sample with a radially flattened cone beam, the ray direction will be very close to parallel with the tracheids in the radial direction, while being non-parallel with the tracheids in the tangential direction. This allows for most of the rays to pass through cell wall and avoids direct transmission through the empty space of the lumina, making the wood material more homogenous. Theoretically the resolution and sharpness of the radiograph will be highest in the radial direction where it matters most, and lower in the tangential direction where it is of little consequence. The sensitivity of preparing the samples' fiber angles is reduced in the tangential direction but still critical in the radial direction. By stepwise moving the sample relative to the X-ray source and detector, entire radiographic images are built up by successively adding line by line. By using a thin slit between the object and the array sensor, the geometric aberration and the contribution of scattered radiation can be reduced to practically zero in the radial direction. The 16 bit radiographs are then calibrated to densities using a simultaneously scanned material standard with steps of varying thickness, usually cellulose acetate or acrylic (Poly(methyl methacrylate)) (ρ = 1.18 g/cm^3). Density profiles are then commonly produced and analyzed in WinDendro™ [*Campbell et al.,* 2011; *Guay et al.,* 1992], using a pre-determined analysis track-width for each sample (commonly 1 mm). The digital sensor line within the WinDendro software can be adjusted to match the ring boundary, but if the ring boundaries are curved or slightly oblique to the plane of the flattened cone beam in the X-ray phase, the divergent radiation will cause optical aberrations also in the radial direction [*Moschler & Winistorfer,* 1990] and reduce the apparent radial sample resolution of the radiograph.

3.1.3 The Nanowood 3D X-ray Computed Tomography

The Nanowood X-ray CT scanner is developed and built by the Radiation Physics group (Prof.

Luc Van Hoorebeke and Prof. Matthieu Boone) of the UGCT (University Ghent Centre for X-ray Tomography, Belgium) and was installed at UGent-Woodlab in 2010. The system was mainly developed for non-invasive research on wood and wood-based materials. In recent years, several papers have been published which make use of tree-ring data, ring-width series and / or density profiles, measured on 3D scanned increment cores [e.g., *De Groote et al.,* 2018; *Maes et al.,* 2017; *Vannoppen et al.,* 2017; *Vannoppen et al.,* 2018; *Vanhellemont et al.,* 2019]. The use of the Nanowood system for the purpose of tree-ring analysis was first reported in *De Ridder et al.* [2010], where the original principles of 3D densitometry are highlighted and the proof of concept is validated in terms of accuracy compared to conventional density measurements, i.e. gravimetric/volumetric measurements. This was further elaborated on in *Van den Bulcke et al.* [2014], introducing a software toolbox for processing of dendrochronological helical XCT images (DHXCT), and scaled up to high-throughput analyses as presented in *De Mil et al.* [2016]. To date, there are no publications that have used this system to derive MXD for dendroclimatological studies, but the functionality is available, evidenced by the successful production of data for the comparison experiment in Section 4 of this review, and several other studies are underway.

The Nanowood was specifically designed to enable scanning at a wide range of image resolutions needed to cover the hierarchical nature of wood and wood-based products. Therefore two complementary X-ray sources are implemented, more specifically a closed tube allowing a focal spot size down to 5 µm and a maximal power of 39 W suitable for scanning larger samples. The second X-ray tube consists of a transmission target and has a maximum power of 3 W, with a very small focal spot of 400 nm making it suitable for sub-micron CT on smaller samples. Two different X-ray detectors were implemented as well, with sensitivities tuned to the energies of the two X-ray sources. For more information on the technical details of the Nanowood X-ray CT scanner, the reader is referred to *Dierick et al.* [2010, 2014].

The samples are exposed throughout a helical motion in front of the stationary cone-beam X-ray source. The transmitted energy is digitally captured and a tomographic wood volume is reconstructed with algorithms developed in *Katsevich* [2002]. Because the volume of the sample is quantified during the scan, meticulous sample preparation prior to exposure is not needed. However, X-ray CT derived densities are also most accurate when samples are oven-dried and non-wood components are removed with solvents. As for X-ray microdensitometry, the grey-scale values of the voxels in the reconstructed volume are converted to density bounded by the density of a solid material standard and air. The sample holder is constructed with the calibration material of similar molecular composition as the tracheid cell wall (ρ = 1.40 g/cm^3). The resulting density values are acknowledged to be very precise and accurate and allow for density estimations for biomass purposes [*Vanoppen et al.,* 2018]. Also with this technique density values are derived from profiles, such as in Figure 1. The profiles are produced, instead of applying a sensor line to a sample on a 2D radiograph, by adapting a software-created plane within the reconstructed volume, to both the tree-ring boundaries and the axial fiber angles within the DHXCT software [*De Mil et al.,* 2016]. The plane area can be changed for every sample but is fixed within a sample. The aperture, or the plane thickness, is typically the same as the obtained approximate voxel pitch. Furthermore, the operator can choose how much of the plane area to use according to a specified hierarchy (i.e. one could opt for 20% of the brightest voxels (high density voxels) in the plane for the MXD parameter to mitigate artefacts from ring boundary irregularities and resin ducts). If the wood samples' characteristics are analyzed for dendrochronological purposes, it is necessary to use lower resolution X-ray functionality. Currently the device has been used to scan at voxel pitches of 110, 50 and 35 μm. Moreover, 17.5 μm resolution is also feasible, and was applied for the comparison experiment in section 4 of this review. The finer the resolution, the longer scan time and volume reconstruction time is needed, but the team at UGent anticipates that both the finest measurement resolutions and process times will be improved upon in the near future.

3.1.4 The SilviScan™ technology

The SilviScan technology is developed by The Commonwealth Scientific and Industrial Research Organisation (CSIRO) in Melbourne, Australia, under the leadership of Dr. Robert Evans. The SilviScan system was originally developed for the analysis of wood properties with regard to pulp and wood quality [*Evans,* 1994]. Traditionally, wood density was the major criterion for these commercial end-uses, but with this instrument, other important anatomical properties and tracheid dimensions became available and could be routinely measured. Although it is being used in Australia, Sweden and Canada for a wide range of basic and applied research, the device in Australia is the only one currently used for dendroclimatological studies. These studies have predominantly been conducted in Australia uncovering significant climate information imprinted in various density and tracheid dimensions, for trees where ring width has been unusable [*Allen et al.,* 2013; *Drew et al.,* 2012]. *O'Donnell et al.* [2016] and *Allen et al.* [2018] reconstructed temperature and *Allen et al.* [2015] explored stream flow in Tasmania using density data. Outside of Australia, SilviScan wood density has been used in reconstructing summer temperature [*Wood & Smith,* 2015] and partially involved in reconstructing Glacier mass balance [*Wood & Smith,* 2013] in Canada. In Norway, *Rosner et al.* [2013] found wood density to be an indicator of drought sensitivity.

The SilviScan is a system that combines X-ray densitometry, optical microscopy and X-ray diffraction to measure wood density and various anatomical properties. The X-ray source emits a flattened cone beam through the side of the axially placed sample, i.e. the sample is exposed in the tangential direction (Figure 2) [*Evans,* 1994] and thus X-rays cannot pass through lumina, in contrast to most other devices. Similar to the Itrax multiscanner, this feature makes the wood material more homogenous and appropriate for X-ray analysis. The sample is positioned on a goniometer that can rotate around its horizontal axis. During the scan, a video microscope placed above the sample detects ring boundary orientation and, in tandem with image analysis software, an automatic adjustment of the sample is made so as to always X-ray the sample in parallel to the ring boundary [*Downes et al.,* 2002]. The system usually provides density profiles with a radial interval of 25 μm [e.g., *Auty et al.,* 2014]. Because the sample is irradiated with X-rays from the side and video microscope from the top, both the tangential and axial dimensions of the samples are critical. Samples are meticulously prepared with a twinblade saw, preferably from 10-12 mm cores, into slices of 6 or 7 mm in the axial direction and 2 mm in the tangential direction. The top transverse surface is hand polished with a series of fine abrasive sheets [*sensu Schnell & Sell,* 1989]. Resins are removed from the samples with acetone and dried and acclimatized to 23°C and 50% RH prior to exposure. In contrast to other systems, the calibration is not achieved with a material standard, but the dimensions and weights of the cut samples are used to calculate average conditioned densities for the calibration of the densitometer.

SilviScan was designed to rapidly analyze samples for many different characteristics. This has resulted in some compromise with spatial resolution [*Downes et al.,* 2002]. Although SilviScan analysis provides information on growth ring angle to maximize the resolution for latewood density, the latewood density may be slightly underestimated by the theoretical maximum measurement resolution of 25 µm [*Evans et al.,* 1996]. However, SilviScan also has the functionality of analyzing anatomical features. In theory these features could be used to create density measurements at a higher resolution and also allow the environmental signals evident in density to be resolved into cell size or wall thickness changes [*Downes et al.,* 1994].

3.2 Reflected light techniques – Blue intensity

For decades, the merits of using video image analysis to capture reflected visible light from the surface of tree ring samples in order to examine their anatomical characteristics and visual properties have been recognized and the technique has been applied in a range of studies [e.g., *Clauson & Wilson,* 1991; *Thetford et al.,* 1991; *Jagels & Telewski,* 1990; *Sheppard & Graumlich,* 1996; *Yanosky & Robinove,* 1986; *Yanosky et al.,* 1987]. As cell wall density appears to be rather constant [*Kellogg & Wangaard,* 1969; *Stamm & Sanders,* 1966], it has been possible to apply imaging analysis techniques with the hypothesis that wood density can be derived solely from properties such as the proportion of cell-wall area to the full cell area [*Park & Telewski,* 1993]. Early pioneering work by *Yanosky and Robinove* [1986], and *Yanosky et al.* [1987] recognized that reflected visible light had the potential to act as a surrogate for wood density and was followed by further detailed investigations into the relationship between wood density and the optical properties of wood [*Clauson & Wilson,* 1991]. *Sheppard et al.* [1996] investigated earlywood maximum and latewood minimum brightness (analogous to minimum density and MXD, respectively), and demonstrated that temperature could successfully be reconstructed.
Although the relationship between density and reflected brightness is strongly coupled, it may be distorted for several reasons. A decoupling between brightness and density is primarily a manifestation of differential discoloration of cell walls linked to heartwood and sapwood staining, and uneven distribution of extractives in the xylem [*Raven*, 2004]. In the absence of other discoloring agents, the light absorbance properties of wood have been found to be strongly coupled with lignin content. Although the absorption properties of lignin span a broad range of wavelengths [*Austin & Ballaré,* 2010], the strong relationship of its concentration in the cell wall and ultra violet absorption has long been recognized [e.g., *Fukazawa,* 1992]. The link between latewood lignin content and temperature was also proposed, as (late) summer temperatures were found to be influential on lignification of the secondary cell wall [*Gindl et al.,* 2000]. *McCarroll et al.* [2002], also reported a strong link between reflected light from the latewood and MXD, and detailed their findings insofar that the brightness from the blue spectrum was slightly better correlated with MXD than the green, ultraviolet and red light reflections. In line with that shorter radiation wavelengths being more readily absorbed by lignin, this has resulted in the analysis of reflected light within the blue spectrum becoming a standard tree-ring measurement technique; termed blue reflectance or more commonly blue intensity (BI) [*Campbell et al.,* 2007].
In contrast with X-ray densitometric measurements, sample preparation and measurement of BI can be performed rather quickly and at considerably lower cost. Samples are usually treated to remove extractives and then surfaced by either sanding with gradually finer sand paper or using a microtome. Samples are then either scanned using a commercial flatbed scanner, involving a

color-card calibration step, or photographed with a microscope-mounted camera [*Campbell et al.,* 2011; *Levanič,* 2007; *Österreicher et al.,* 2015]. For scanning, the use of a color calibration card is recommended to ensure consistent reproduction of colors and brightness over time and irrespective of the equipment used. This is because some un-calibrated scanners are known to have severely skewed color rendering, where areas of low, but non-zero reflection, are rendered as zero reflection, while other un-calibrated scanners may render a color scale that is non-linearly related to calibrated colors (for more information, contact the corresponding author). Although sample preparation is quite straightforward, it is important that the surfaces of the samples are prepared in such a way that the captured images have comparable reflection across the sample. If that quality is met *Babst et al.* [2009] and *Rydval et al.* [2014] argue that images of at least 1200 dpi (dot size of c. 20 µm) should be captured in order to produce BI measurements of reasonable quality. Important to note is that manufacturers of flatbed scanners are notoriously ambiguous in their reporting of scanner resolution (https://www.imageaccess.de/_WhitePapers/PDF/WhitePaper_The_Resolution_Myth.pdf, accessed September 2019). To be able to report an accurate measurement resolution from a flatbed scanner, a resolution target needs to be utilized (https://www.filmscanner.info/en/FilmscannerTestberichte.html, accessed September 2019). A high-end reflective scanner can typically resolve 10 µm in theory, and in practice likely substantially less due to a narrow focus depth. Thus, the flatbed scanning systems lack the ability to render cell structure, which particularly affects BI measurements of narrow rings. While microscope photography has the benefit of producing clearer, higher resolution images, this approach can suffer from uneven illumination of the sample and image distortion, which must be corrected or calibrated [*Österreicher et al.,* 2015; *Sheppard & Singavarapu,* 2006]. *Sheppard et al.* [1996] proposed a procedure to correct anomalous latewood brightness using the brightness of earlywood. Another potential bias is that regardless of image acquisition hardware, lumina of the tracheids are typically filled with near-white wood dust during sanding or with highly reflective white chalk following microtoming to increase contrast [*Evans,* 1994; *Gärtner & Nievergelt,* 2010; *Österreicher et al.,* 2015]. Note that the reflective properties of wood dust and chalk are different and the mean levels of the BI measurement accordingly are expected to be different even if the colors of the cell walls are similar.

From the images, BI profiles can be produced with multiple types of specialized software including WinDendro [*Campbell et al.,* 2011; *Guay et al.,* 1992], CDendro/CooRecorder [*Larsson,* 2014; *Rydval et al.,* 2014], Lignovision (http://www.rinntech.com/), or generic image analysis software such as Image Pro Plus (Media Cybernetics, USA) or ImageJ (developed by W. Rasband, National Institutes of Health, Bethesda, MD, USA). When analyzing resulting measurements, discoloration or staining of samples (including pronounced heartwood-sapwood color differences in some conifers, discoloration caused by the action of fungal and bacterial agents and decay, staining caused by resins and other extractives) have been found to induce biases in the trends of latewood BI series [e.g., *Björklund et al.,* 2014, 2015; *Buckley et al.,* 2018; *Rydval et al.,* 2014]. Although refluxing tree cores in acetone, ethanol, toluene:ethanol or even peroxide, usually with a Soxhlet apparatus (https://en.wikipedia.org/wiki/Soxhlet_extractor, accessed Jan 2019) has been applied as a way to remove extractives, the treatment is imperfect as it only reduces discoloration related to mobile substances and so does not eliminate discoloration biases entirely [*Björklund et al.,* 2014; *Rydval et al.,* 2014; *Sheppard &*

Wiedenhoeft, 2007]. While heartwood-sapwood discoloration can be minimal in some species such as spruce (*Picea Sp.*) [*Rydval et al.,* 2018; *Wilson et al.,* 2014], discoloration in general is an issue that usually requires attention. Analogously to the brightness adjustment outlined by *Sheppard et al.* [1996], *Björklund et al.* [2014] demonstrated that the discoloration in latewood BI can be mitigated by subtracting earlywood BI for each tree ring, producing a third parameter, the "delta BI" parameter. However, as this correction was found to be imperfect in fully correcting discoloration biases, *Björklund et al.* [2015] proposed a BI contrast adjustment prior to the calculation of delta BI, producing encouraging results. Features of discoloration bias can also be mathematically filtered out [*Rydval et al.,* 2017a, 2017b], though this approach typically only retains up to decadal scale variability.

As BI (reflectance) measurements are inversely correlated with density (i.e. higher density wood appears darker and reflects less light [*Sheppard,* 1999]), the measurements are usually inverted prior to dendroclimatic analyses [*Rydval et al.,* 2014] or expressed in terms of light absorbance [*Björklund et al.,* 2014]. The current range of terminology of "maximum blue absorption intensity" [*Björklund et al.,* 2014], "minimum blue intensity" [*Campbell et al.,* 2007] or "latewood blue intensity" are all corresponding measurements to the MXD parameter. Below we employ the use of the absorbed BI definition.

Despite limitations, maximum BI has featured in a number of climate response and reconstruction studies (primarily summer temperature) that have been partly (or entirely) derived from this parameter, covering many regions, including northern [*Björklund et al.,* 2015; *Fuentes et al.,* 2018; *Linderholm et al.,* 2015; *McCarroll et al.,* 2013], northwest [*Rydval et al.,* 2017a, 2017b; *Tene et al.,* 2011; *Wilson et al.,* 2012], western [*Trachsel et al.,* 2012] and eastern Europe [*Kaczka et al.,* 2017, 2018; *Rydval et al.,* 2018], North America [*Wilson et al.,* 2014; 2017a] and the Caucasus [*Dolgova et al.,* 2016]. The parameter has also been included in large-scale (hemispheric) reconstructions of temperature [*Anchukaitis et al.,* 2017; *Wilson et al.,* 2016] and the development of a temperature reconstruction in the tropics [*Buckley et al.,* 2018]. As a result of its relative ease of development, maximum BI has also found applications in dendroarchaeology by assisting in the dating of historical wooden material from conifers with potential applications also in the provenancing of historical wood [*Mills et al.,* 2017; *Spyt et al.,* 2016; *Wilson et al.,* 2017b]. In addition to using the sensitivity of maximum BI to temperature, the potential of using the sensitivity of earlywood blue intensity to precipitation has also been examined [*Dannenberg & Wise*, 2016].

3.3 Wood anatomical density

Although anatomical density has been explored in early works as the proportion of tracheid wall of the full tracheid, for assemblages of tracheids at an intra-annual [*Elliott & Brook,* 1967; *Green,* 1965] and inter-annual basis [*Park & Telewski,* 1993], recent work on anatomical density is based on averages of individual tracheid cell dimensions [*Björklund et al.,* 2017; *Decoux et al.,* 2004; *Rathgeber et al.,* 2006]. Because anatomical density is based on measurements of individual tracheid cell dimensions, other cell types in the wood such as axial and radial parenchyma cells, as well as resin ducts, which account for c. 10% of the xylem in conifers [*Hacke et al.,* 2015], are by definition ignored. Moreover, by using a proportion of wall area, the density of the solid cell wall is also omitted from the anatomical density measurement.

The use of wood anatomical density and its cellular constituents, lumen and wall dimensions has long been hampered in climate sensitivity studies by methodological limitations and time-consuming data production. This has resulted in a low number of samples (trees) processed, a low number of rings (years) considered, and a low number of anatomical features per ring measured, typically along only a few radial files of cells (Figure 2). In fact, anatomical density has never been used directly to reconstruct climate, but several studies have found good correspondence to X-ray densitometry [*Björklund et al.,* 2017; *Decoux et al.,* 2004; *Rathgeber et al.,* 2006; *Wang et al.,* 2002]. However, strong summer temperature signals in the anatomical parameter of cell wall thickness of the latewood have been reported [*Fonti et al.,* 2013; *Sidorova et al.,* 2012; *Wang et al.,* 2002; *Yasue et al.,* 2000], and *Panyushkina et al.* [2003] reconstructed 352 years of summer temperature in northeast Siberia with this parameter. More recent studies profited from methodological improvements (see below), which allows a >10-fold increase in the number of measured tracheids, while still reducing the time requirement. This allowed for more detailed studies into, for example, climate drivers of wood formation in *Picea abies* along an elevational gradient in the Italian Alps [*Castagneri et al.,* 2017] or hydroclimate reconstruction in Nevada based on earlywood tracheid lumen diameter of *Pinus longaeva* [*Ziaco et al.,* 2016].

The general procedure to produce wood anatomical density involves 1) the preparation of thin sections of 10-20 µm thickness using a microtome, 2) staining the section with a reagent such as safranin to increase contrast, 3) capturing high-resolution imagery of the section and 4) measuring the tracheid dimensions in the anatomical images with image analysis techniques [*Gärtner & Schweingruber,* 2013; *von Arx et al.,* 2016]. The tracheids should be cut orthogonally and the section thickness should be kept constant within a dataset as deviations in both aspects will change the measured tracheid wall and lumen dimensions [*Decoux et al.,* 2004; *Elliott & Brook,* 1967; *von Arx et al.,* 2016]. Cutting can produce cracks and broken tracheid walls that reduce data quality and efficiency of image analysis, but these issues can be largely avoided when stabilizing the wood before cutting [*Schneider & Gärtner,* 2013; *von Arx et al.,* 2016]. Images of anatomical samples are then manually captured with a camera mounted on a microscope with a resolution of c. 1-2 pixels/µm, and multiple overlapping images are stitched to form an overall composite image of the anatomical sample using image-stitching software [*von Arx et al.,* 2016]. This time-consuming digitization of entire anatomical sections can be improved in efficiency and quality by using automated microscope systems or thin-section slide-scanners that automatically batch-process multiple anatomical samples [*Castagneri et al., 2018*; *Pacheco et al.,* 2018]. There are also alternative approaches to avoid preparing anatomical sections and directly capture anatomical features from the leveled wood surfaces. One such approach is to activate the autofluorescence of wood with a helium neon laser light source and using a confocal microscope for image capture [*Liang et al.,* 2013]. Another approach is to meticulously polish the wood surface before image capturing with a microscope system, where lumina are either filled with non-reactive resin [*Arzac et al.,* 2018] or wood dust to enhance the contrast [*Evans,* 1994]. Independent from the sample processing and image capturing approach, image analysis software is subsequently used for measurement of tracheid dimensions. There are many different software programs used, from generic programs shipped with microscope systems and the freely available ImageJ (Rasband 1997-2019), to dedicated programs such as WinCELL (Regent Instruments Inc., Québec, Canada) and ROXAS [*Prendin et al.,* 2017; *von Arx & Carrer,* 2014]. Generic programs often allow the automation of tracheid lumen measurements, while wall thickness measurements have to be performed manually for each tracheid. Dedicated programs automatically measure lumen dimensions and the thickness of tracheid walls. WinCELL can provide tangential thicknesses and ROXAS can provide both tangential and radial thicknesses. Having tracheid lumen area or diameter and wall thickness, a geometric tracheid model can be used to derive the proportion of wall area to overall cell area as wood anatomical density [*Decoux et al., 2004*; *Vaganov et al.,* 2009]. ROXAS is currently the only program capable of automatically and directly measuring the wood anatomical density of each tracheid cell, which avoids making any geometric assumptions on tracheid shapes. Finally, radial profiles of density can be created based on individual radial files (Figure 2) [*Peters et al.,* 2018] or based on position of the tracheid in the ring.

4 Full-scale comparison experiment with commonly used techniques

As a literature-based review of technical measurements is necessarily limited by subtle but important unknowns in the comparability of the original measurements and techniques, we address this by performing an in-depth experiment whereby 17 separate laboratories performed an extensive array of measurements of density-related parameters using a range of techniques for this review.

4.1 Experimental design

In this experiment we analysed 30 datasets using five different microdensitometry techniques (namely Walesch, Itrax, Nanowood 3D XCT, BI and anatomical density, see Table 1 for dataset Laboratory, Country, System and Short ID). For specific hardware and software configuration, and sample preparation procedures and treatments used for each dataset in the experiment we refer to Table S1-S3.

4.1.1 Tree-ring material

The laboratories/techniques in the study measured wood density on 29 mature living *Pinus sylvestris* (Scots pine) trees from the cool and moist boreal forest zone close to the latitudinal tree line (North-eastern Finland, 200 m a.s.l., 68.9°N 28.2°E) (Figure 4). This site and species were selected to be analogous to samples collected for temperature reconstruction purposes [e.g., *Esper et al.,* 2012]. The sample material consisted of miniature logs cut from the felled trees (ca. 30 cm axial log length, harvested at ca. 2.7 m stem height), which were large enough to produce unique sub sample sets for at least the 17 laboratories included in this study. The trees were felled and sampled after the completed growing season of 2014 coordinated by the Finnish Forest Research Institute (METLA). Each laboratory was allotted a random subset consisting of 3 radii from each of the 29 trees, 87 samples in total (Figure 4c). The dataset produced by each laboratory is comparable to those produced in standard tree-ring investigations. The laboratories were responsible for their own sample preparation and measurements following their own established procedures.

***FIGURE 4** Sample material used for the comparison experiment. a) Site location where samples were harvested (red dot), and b) photograph of the sample site. c) A subset of the sampled material. White dashed lines illustrate how discs were cut from the miniature logs and black dashed lines illustrate how sample wedges were cut from each disc. d) Examples of i) an image* *of reflected light typically used for blue intensity, ii) X-ray image, and iii) photograph of stained micro-section [von Arx et al., 2016] used for wood anatomical determination of density. In contrast to the reflected light and X-ray based density derivations, anatomical density is based on the analysis of individual tracheids, where anatomical density is defined as the proportion of cell wall area in relation to the full tracheid area for all tracheids of interest.*

4.1.2 Chronology development and trend analysis

The tree-rings in the wood material were visually cross-dated [*sensu Yamaguchi,* 1991], and the dating of the measurements was statistically checked with the software COFECHA [*Holmes,* 1983]. Note that all laboratories measured unique samples from the same trees. Missing rings and immeasurable sections will vary slightly among labs, but are not considered to have any systematic effect on the results with such a robust replication. From the dated tree rings, inter-annual time-series of maximum density, minimum density, and average ring density were extracted from the measurement profiles for each technique, accompanied by the total ring width. For the un-calibrated techniques (those techniques that do not provide a density unit (e.g., g/cm^3)) the parameters are expressed as maximum, minimum and ring averages of absorbed light (BI scale 0-255) or proportion of wall area (anatomical density scale 0-100%). Whereas the un-calibrated BI and anatomical techniques do not provide wood density *per se*, their measurements are representations of density, and therefore we will use the notation **mxd** when we simply refer to the maximum corresponding parameters for all techniques.

Tree-ring chronologies used within the field of dendroclimatology are usually constructed as arithmetic mean value functions of all samples after removing biological age-trends in a detrending and standardization process [*Fritts,* 1976]. Here we average samples without detrending allowing the chronologies to be compared in terms of overall trends. In fact, detrending methods that aim to preserve long-term trends, such as regional curve standardization (RCS) and its variants [e.g., *Briffa et al.,* 1992], are not suitable for material consisting of only even-aged living trees [*Melvin & Briffa,* 2011]. The RCS concept builds on the alignment of all measurement series by their first growth year, representing the overall biological growth trend, whereupon this growth trend in the form of a mathematical function is subtracted from each individual measurement. If only even-aged living trees are included in this exercise, environmental growth trends may still persist in the overall average of age-aligned growth, and is then subsequently also removed from the individual measurements. An alternative type of detrending employs individual data adaptive fitting of mathematical functions [*Cook,* 1985]. This more invasive type of detrending removes the overall trend in each indexed series, and all indices will be adjusted to have similar mean values [*Cook et al.,* 1995], i.e. if overall trends are going to be explored, this type of detrending should be avoided. Persistent trends in the raw **mxd** chronologies were determined with the Mann-Kendall non-parametric monotonic trend test of computing slope, and significance of slope [*Burkey,* 2006]. The trend analysis was conducted on **mxd** chronologies converted to z-scores (i.e., the mean was subtracted from each value and divided by the standard deviation) over the period 1800-2013 CE.

4.1.3 Climate response analysis

When the **mxd** and ring width chronologies were correlated with local monthly temperature data, the tree-ring data were detrended and standardized with cubic smoothing splines (50% frequency response cut-off at 25-years) [*Cook & Peters,* 1981] to remove age / size related trends. Similar data-treatment was utilized for meteorological data retrieved from the CRUTEM4 (5° gridded monthly dataset) [*Osborn & Jones,* 2014]. The grid-point centered over the sampling-site comprised data spanning 1876 to the present. Moreover, the strength of the common signal among trees was quantified by the average pair-wise correlation of all tree-ring series; the *Rbar* statistic [*Wigley et al.,* 1984], similarly calculated on detrended data.

4.1.4 Re-calibrating mean levels of microdensitometric techniques

Mass/volume-based density (here denoted $\rho_{M/V}$ expressed as g/dm^3) was used to re-calibrate the microdensitometric measurements [*sensu Mothe et al.,* 1998]. Both mass and volume were determined on samples acclimatized at c. 50% relative humidity and a temperature of c. 20 °C. The $\rho_{M/V}$ was determined most often by using simple pycnometric methods i.e. water displacement (see Text S1). Samples (typically 1-3 cm^3 in size) intended for $\rho_{M/V}$ were prepared from wood material axially adjacent to the samples used for the microdensitometric analyses (here denoted ρ_{Micro}). The actual calendar years present in the $\rho_{M/V}$ samples were determined and subsequently ρ_{Micro} for the same years, i.e., ring density over the same years (often >100 years) was integrated. Tree averages were calculated when more than one sample per tree was measured. $\rho_{M/V}$ measurements were produced for all X-ray and anatomically based techniques, but not for the BI techniques. ρ_{Micro} was thereafter regressed against $\rho_{M/V}$, also for the BI techniques, using the tree average $\rho_{M/V}$ from the X-ray techniques. The obtained regression coefficients were then used in transfer functions to re-calibrate raw measurement values of all techniques to ring density but also to maximum and minimum density. Note that this procedure is different from the correction factor proposed by *Lenz et al.* [1976] because it is not only concerned with the X-ray attenuation difference between the wood sample material and the material standard used for the initial calibration of X-ray based techniques. It is also designed to re-calibrate X-ray based techniques, and un-calibrated techniques, regardless of what mechanism causes discrepancies.

4.1.5 Exploring the apparent measurement resolution of microdensitometric techniques

In Figure 1 we conceptually showed that measurement resolution can have a large impact on obtained **mxd** and to some degree also on minimum density measurements. It is therefore important to explore if measurement resolution has practical implications on real data, such as the sample material we use here. The measurement resolution of the anatomical technique is based on the tracheid cell unit and the radial cell diameter of latewood cells can be <10 µm, which is typically finer than the finest sensor aperture of 10 µm for the Itrax and Walesch techniques, and also the pixel or voxel pitch of the BI and 3D XCT techniques. With the anatomical technique we can moreover easily simulate reduced measurement resolution by increasing the aperture for which the anatomical density profile is integrated. Accordingly, ten anatomical density datasets derived from the same cell measurements were created with the measurement resolution based on the apertures 10, 20, 30, 40, 50, 60, 80, 100, 120 and 160 µm to cover the range of measurement resolutions of the other techniques. These 10 datasets allow us to understand how systematic changes in measurement resolution influence the measurement properties. Because the density of the xylem changes almost exclusively as a function of its tracheid dimensions, we use the differently resolved anatomical datasets to help estimate the apparent resolution of the other techniques that might depend upon e.g., both the clarity of X-ray images and the physical sensor configuration.

Studying Figure 1 we recognize that the amplitude of profiles within narrow rings are suppressed relative to the wider rings, i.e. as measurement resolution is lowered, the **mxd** for narrow rings is systematically lowered compared with **mxd** for wide rings. It follows that the correlation between **mxd** and ring width, r[**mxd**, ring width], should artificially increase when measurement resolution is lowered due to growing bias in measured **mxd**. We therefore use r[**mxd**, ring width] to explore consequences of measurement resolution. The **mxd** datasets were normalized and the ring-width datasets were kept untreated for the correlation analysis because the absolute value of ring width is central for the measurement resolution. Due to the potentially non-linear character of this bias (large bias for narrow rings and little bias, if any, for wide rings), the Spearman rank correlation coefficient was used. We make the assumption that the most accurate estimate of the relationship between **mxd** and ring width is obtained with the highest measurement resolution, provided by anatomical density. Note that we do not assume that r[**mxd**, ring width] should be as close to zero as possible. Instead, we assume that the anatomical **mxd** datasets can act as a reference for the r[**mxd**, ring width] analysis. Moreover, we conduct repeated correlations of all the **mxd** datasets to the set of anatomical maximum density datasets. Throughout the course of this experiment, we inform the other analyses with results from the range of measurement resolutions of the anatomical datasets.

When apparent measurement resolutions of the non-anatomical datasets were indirectly established with r[**mxd**, ring width] and the correlation between **mxd** and anatomical maximum density, we divided the datasets into two groups henceforth classified as high-resolution and low-resolution datasets. For both groups we further experimentally divided each dataset into narrow- and wide-ring sub-datasets. That is, in each dataset, **mxd** from rings narrower than the overall median ring width of 400 μm were used to form a first sub-dataset, and **mxd** from rings wider than 400 μm were used to form a second dataset. From these sub-datasets, two new **mxd** chronologies were constructed for each laboratory, both with roughly half the replication of the complete datasets. Temperature signal (correlation) and overall trend analyses were then repeated on the sub-datasets and compared with the results obtained with the original complete **mxd** datasets. The analyses were also stratified on the two groups of apparent measurement resolution.

Table 1 *Dataset short ID, where the suffix B denotes blue intensity, X denotes X-ray and T denotes computed tomography. Moreover, laboratory, country, technique, hardware, software and the associated nominal resolution is presented for each dataset. We define the nominal resolution as the size of each pixel in the sample image for BI techniques, the analysis step width or sensor aperture for X-ray techniques, or the bandwidth used to collect cells for anatomical density integrations.*

Short ID.	Laboratory	Country	Technique	Hardware	Software	Nominal resolution
GreiB	DendroGreif	Germany	Blue intensity	Flatbed scanner	Windendro™	~4 µm
SwanB	Swansea	UK	Blue intensity	Flatbed scanner	Windendro™	~25 µm
WSLB	WSL Birmensdorf	Switzerland	Blue intensity	Flatbed scanner	Windendro™	~16 µm
LTRRB	LTRR Tucson	USA	Blue intensity	Flatbed scanner	Windendro™	~11 µm
StAB	St. Andrews	UK	Blue intensity	Flatbed scanner	Coorecorder™	~8 µm
SileB	Silesia	Poland	Blue intensity	Flatbed scanner	Coorecorder™	~11 µm
WPUB	WPU New Jersey	USA	Blue intensity	Flatbed scanner	Coorecorder™	~11 µm
LDEOB	LDEO New York	USA	Blue intensity	Flatbed scanner	Coorecorder™	~8 µm
IANIB	IANIGLA Mendoza	Argentina	Blue intensity	Flatbed scanner	Coorecorder™	~11 µm
UIbkB	ATRG Innsbruck	Austria	Blue intensity	Photography	Lignovision™	~3 µm
SthmX	Stockholm	Sweden	Radiodensitometry	Itrax ™	Windendro™	20 µm
CETEX	CETEMAS	Spain	Radiodensitometry	Itrax™	Windendro™	20 µm
GreifX	DendroGreif	Germany	Radiodensitometry	Itrax™	Windendro™	10 µm
GentT	Woodlab UGent	Belgium	Computed Tomography	Nanowood	DHXCT2016	17.5 µm
GentT*	Woodlab UGent	Belgium	Computed Tomography	Nanowood	DHXCT2016	17.5 µm*
WSLX	WSL Birmensdorf	Switzerland	Radiodensitometry	Walesch Electronics™	Dendro2003™	≥10 µm
KrasX	SIF Krasnoyarsk	Russia	Radiodensitometry	Walesch Electronics™	Dendro2003™	≥10 µm
DresdX	Dresden	Germany	Radiodensitometry	Walesch Electronics™	Dendro2003™	≥10 µm
MainX	Mainz	Germany	Radiodensitometry	Walesch Electronics™	Dendro2003™	≥10 µm
XianX	SKL Xi'an	China	Radiodensitometry	Walesch Electronics™	Dendro2003™	≥10 µm
AD160[µ]	WSL Birmensdorf	Switzerland	Anatomical density	Photography	ROXAS	160 µm
AD120	WSL Birmensdorf	Switzerland	Anatomical density	Photography	ROXAS	120 µm
AD100	WSL Birmensdorf	Switzerland	Anatomical density	Photography	ROXAS	100 µm
AD80	WSL Birmensdorf	Switzerland	Anatomical density	Photography	ROXAS	80 µm
AD60	WSL Birmensdorf	Switzerland	Anatomical density	Photography	ROXAS	60 µm
AD50	WSL Birmensdorf	Switzerland	Anatomical density	Photography	ROXAS	50 µm
AD40	WSL Birmensdorf	Switzerland	Anatomical density	Photography	ROXAS	40 µm
AD30	WSL Birmensdorf	Switzerland	Anatomical density	Photography	ROXAS	30 µm
AD20	WSL Birmensdorf	Switzerland	Anatomical density	Photography	ROXAS	20 µm
AD10	WSL Birmensdorf	Switzerland	Anatomical density	Photography	ROXAS	10 µm

GentT*, second dataset from Gent: MXD is derived only with the 20% densest voxels within the sensor aperture and the measurement plane.

[µ] In the short ID. of anatomical datasets, the numbers indicate the bandwidth (µm) used to derive anatomical density.

4.2 Experimental outcome

4.2.1 Basic data comparison

In this experiment, a consortium of 17 laboratories developed and analyzed 30 datasets consisting of 200+ year-long chronologies. We derived four different tree-ring parameters constituted by up to three samples per 29 trees. Each overall parameter-average chronology in Figure 5 thus consists of c. 15,000 measurement points, and each annual average of parameter-chronologies consist of up to 87 measurement points. The **mxd** data have notable spreads in average values (Figure 5, Table S4). Each technique category exhibits coefficients of variation (CV) around 10%. The spread in ring density is also considerable for the BI technique and for the X-ray techniques CV = 20% and 10% respectively, but close to zero (0.4%) variation for the anatomical ring density parameters.

FIGURE 5 *Chronologies of different parameters and technique categories. a) Top panel shows raw-data chronologies from X-ray based minimum density, full ring density and maximum density. Corresponding raw data for the un-calibrated BI technique are presented just below, and results for the anatomical density technique in the bottom panel. b) Short segments of X-ray based, BI based or anatomically based annual maxima (MXD or corresponding parameters), with laboratory indicated with short ID's and color-coding. Note that the Lab names are listed on an ordinal scale based on the quantitative mean values. The red tones indicate Walesch, green tones Itrax, orange X-ray computed tomography and blue tones blue intensity techniques, respectively. The b) panels show the systematic nature of discrepancies among laboratories and techniques.*

4.2.2 Inter-annual variability is strongly coherent among all techniques

There is a high degree of inter-annual similarity among different **mxd**, as well as ring width datasets. The average pair-wise chronology correlation is r = 0.94 (r_{range} = 0.85-0.97) for **mxd** and r = 0.98 (r_{range} = 0.95-0.99) for ring width (Table S4-S5). Whereas the chronology inter-correlation is higher for ring width than **mxd**, the between-tree Rbar = 0.59 ($Rbar_{range}$ = 0.48-0.67) of **mxd** is higher than for ring width at Rbar = 0.45 ($Rbar_{range}$ = 0.35-0.49). Corresponding ring density statistics for all techniques are r = 0.95 (r_{range} = 0.92-0.97) and Rbar = 0.50 ($Rbar_{range}$ = 0.45-0.56).

4.2.3 Subtle differences of the inter-annual temperature correlation

The correlations to temperature of the different ring width datasets are very similar, with significant correlations only for July at r = 0.5 (0.47-0.53) (Figure S1). All **mxd** datasets express significant (α < 0.05) correlations with the April through September temperatures (Figure 6). However, there are some notable and perhaps important differences among techniques. 9 out of 10 maximum BI datasets exhibit the highest correlations in July and are slightly lower in May and August, and lower still in April, June and September. The Walesch MXD datasets all have pronounced MJJA correlations with the highest correlations in August, and with slightly lower correlations for April and September. The Greifswald Itrax and Gent CT MXD datasets display intermediate correlation structure to the BI and Walesch techniques and the two other Itrax MXD datasets have correlation structure similar to the BI based **mxd** datasets. The anatomical **mxd** datasets show systematic patterns in climate correlations depending upon the measurement resolution. 10-40 μm resolution anatomical **mxd** datasets exhibit pronounced May, June and August correlations, with slightly weaker correlations for April, July and September. 50-60 μm datasets possess correlation structures similar to Walesch datasets, and the 80-160 μm datasets have correlation structures similar to BI, Itrax and GentT datasets.

FIGURE 6 *Monthly temperature correlations for the **mxd** parameters with the CRUTEM4 5° gridded temperature data [Osborn & Jones, 2014]. Significant (α < 0.05) monthly correlations are marked with a white dot.*

4.2.4 Datasets exhibit notable differences in long-term trends

We observe substantial differences in the long-term trends in the averaged raw **mxd** chronologies. All Walesch, the two GentT, one Itrax and three BI based **mxd** datasets have significant positive trends (α < 0.05) (Figure 7a), whereas seven BI and two Itrax datasets lack significant positive trends. The slope coefficients for the anatomical **mxd** datasets gradually decrease with reduced measurement resolution, and the 120-160 μm datasets lack significant positive trends. In Figure 7b two arbitrarily chosen mean datasets with and without significant trends are presented to visualize how different temperature histories could potentially be inferred from using different measurement systems. The **mxd** data points of the last 30 years may be nearly at, or alternatively nearly 1 standard deviation above the long-term mean. Conversely, the first 30 years may deviate from the mean by either nearly -1 standard deviation, or again, be nearly equivalent to the long-term mean.

FIGURE 7 *a) Slope coefficients from the Mann-Kendall trend test presented as boxplots stratified on technique and category of technique. Individual slope coefficients are indicated with filled circles. Filled circles with red tones indicate Walesch, green tones Itrax, orange X-ray computed tomography and blue tones blue intensity techniques, respectively. Corresponding Lab names are inset on an ordinal scale adjacent to the colored circles. Prior to trend analysis all **mxd** chronologies were converted to z-scores. The slope coefficients were determined on data covering the time period 1800-2013 CE. The dashed horizontal line indicates significance (α < 0.05). b) Two different **mxd** datasets (WSLB and AD10) was chosen to illustrate the difference in datasets with and without significant trends. The third b) panel displays average CRUTEM4 5° gridded April-September temperature data [Osborn & Jones, 2014], converted to z-scores, enveloping the sampling site.*

4.2.5 Re-calibration of microdensitometric data

According to the regression of sample averages of ring density from all techniques, ρ_{Micro} (i.e., X-ray sample density, Anatomical sample density or sample BI) against $\rho_{M/V}$, (i.e., the sample mass/volume) it is clear that many datasets deviate substantially from the expected density values estimated with $\rho_{M/V}$ (Figure 8).

FIGURE 8 *Scatter plots between sample measurements of mass/volume $\rho_{M/V}$ and the sample averages derived from microdensitometric measurements ρ_{Micro}. $\rho_{M/V}$ thus refers to the gravimetric/volumetric density of the sample from tree X, and ρ_{Micro} refers to the integrated ring density observed over exactly the same amount of rings from tree X as the $\rho_{M/V}$ contains* *(usually >100 rings). Simple least square regressions are fitted including confidence bounds around the best fit, with explained variance (R^2) and Mean squared error (MSE) presented for all technique datasets. The mean offset of X-ray based techniques from mass/volume based estimates are presented as "bias" in the corresponding panels. For calibrated techniques, mass/volume measurements were made on the same wedges as the measurements of X-ray or anatomical density. Mass/volume based estimates on the exact same samples were only performed for GentT. For BI data, mass/volume measurements were borrowed from the X-ray labs' $\rho_{M/V}$ measurements from the same or closest wedge position in the tree. The red tones indicate Walesch, green tones Itrax, orange X-ray computed tomography and blue tones blue intensity techniques respectively.*

The deviations occur both in average values and in variance, illustrated by the mean and the slope offset from the 1:1 line, respectively. The offsets are systematic as evidenced by a high amount of explained variance in the regressions. This opens up reliable options to use the regression coefficients in transfer functions to re-calibrate the X-ray density parameters as well as BI-based and wood anatomically based density parameters. The regression coefficients in the re-calibration should not only harmonize the mean levels of the data but also the overall variance. The re-calibration produced data that express little spread in the ring density parameters across technique-categories (Figure 9b-d), where original X-ray based ring density data often had c. ±10% offsets (Figure 9a). Re-calibrated X-ray based **mxd** display reduced but still substantial spread (Figure 9b). The re-calibrated BI and anatomically based **mxd** parameters exhibit similar spreads as the X-ray based **mxd** (Figure 9c and d). The measurement resolution has a large impact on anatomical **mxd** mean levels with mean values ranging from 594-789 g/dm^3 (Figure 9d). A similar spread and presumed error/bias as observed by the spread of values from individual laboratories measuring with X-ray and BI based techniques of 571-825 g/dm^3.

FIGURE 9 *Boxplots of the mean levels of the original max, ring and min density datasets in a), as well as re-calibrated X-ray based **mxd**, ring- and minimum density data in b). c) contains re-calibrated BI-based data and d) re-calibrated anatomically based data. The red tones indicate Walesch, green tones ITRAX, orange X-ray computed tomography and blue tones blue intensity techniques, respectively. Lab names are placed on an ordinal scale adjacent to the boxplots based on their quantitative values.*

4.2.6 Apparent measurement resolution of microdensitometric data

As the anatomical density measurement resolution decreases from 10 to 160 µm, correlations between **mxd** and ring width systematically increase from 0.14 to 0.67 (Figure 10a). The non-anatomical datasets exhibit correlation coefficients with a range of r = 0.3-0.68, and display similar patterns in their scatter (Figure S2). As predicted, the dependence of **mxd** towards ring width is more tightly coupled for narrow rings at lower measurement resolutions (Figure 10b). While the nominal measurement resolutions of non-anatomical datasets (Table 1) range between 4-25 µm, the r[**mxd**, ring width] of eight BI, two Itrax, and the first GentT datasets correspond to the r[**mxd**, ring width] of 80-160 µm measurement resolution. The r[**mxd**, ring width] of the Walesch systems, two BI, one Itrax and the second GentT* datasets correspond to the r[**mxd**, ring width] of 40-60 µm measurement resolution. The nominal resolution thus seems to be an indicator of little importance, especially for BI techniques that utilize commercial flatbed scanners. Thus, in the following, we refer to a binary division of apparent measurement resolution (greater or less than ~70 µm) as low vs. high measurement resolution datasets respectively (Figure 10a). If however, the differences in r[**mxd**, ring width] were somehow substantially affected by different techniques measuring different physical properties of the wood, or if various techniques were associated with different levels of measured noise, this would question the ability of r[**mxd**, ring width] to act as a predictor of apparent measurement resolution. However, when each non-anatomical **mxd** dataset is correlated to the range of anatomical **mxd** datasets, correlations peak (r > 0.94) at 80-120 µm for BI datasets, 50-60 µm for Walesch datasets and 60 or 120 for Itrax datasets and 60 or 80 for GentT datasets (Figure 11). It is highly unlikely to achieve correlation peaks of 0.94 for all technique datasets with anatomical measurements (Figure 11) if some of the **mxd** datasets are correlated at 0.15 with ring width and others at 0.7 with ring width for any of the two reasons mentioned above. Moreover, it is highly unlikely that different X-ray techniques (e.g., Walesch and Itrax) measure different things in the wood, where we in fact also observe a large range in r[**mxd**, ring width] of 0.3-0.65. This further corroborates the concept of identifying the non-anatomical datasets' apparent measurement resolution through the r[**mxd**, ring width] exercise, as a useful estimator compared to the nominal resolution. Figure S3 illustrates the weak relationship between nominal resolution and apparent resolution estimated with either of the approaches introduced in Figures 10 and 11.

FIGURE 10 *Spearman rank correlations between **mxd** and ring width, r[**mxd**, ring width], presented as boxplots a) stratified by technique category. A low and high measurement resolution classification of datasets is defined by the dashed grey line. Dataset ID's are placed on the quantitative y-scale to represent each measurement point in the boxplot with a slight displacement on the x-axis to increase readability. b) Scatterplots between **mxd** and ring width illustrating the increased dependence of **mxd** to ring width with reduced measurement resolution. The red tones indicate Walesch, green tones Itrax, orange X-ray computed tomography and blue tones blue intensity techniques, respectively. The full set of scatter plots can be found in Figure S2.*

FIGURE 11 *Correlation of each **mxd** chronology against the range of anatomical **mxd** datasets r[**mxd**$_x$, **mxd**$_y$]. a) Includes BI based datasets, b) includes X-ray datasets and c) includes the average of Itrax in green, the average of all BI datasets in blue and the average of all Walesch datasets in red, but also each anatomical **mxd** dataset correlated with the range of anatomical datasets in different shades of grey. Peak correlations indicate which resolution of the anatomical **mxd** is most similar to each non-anatomical **mxd** dataset. The peak correlation of each dataset is indicated with the dataset ID where colors facilitate the identification of the corresponding line. Along the x-axis, the dataset IDs are placed at the peak of each specific r[**mxd**$_x$, **mxd**$_y$], and on the y-axis, the dataset ID's are placed in the order of appearance based on Table 1.*

All high measurement resolution datasets in the study have significant positive trends and most of them explain 50% of the high frequency variance of April-September temperatures (Figure 12). In contrast, most low measurement resolution datasets lack positive trends and explain less than 50% of the high-frequency variance in the temperature data. Moreover, high measurement resolution chronologies built only from **mxd** from narrow rings retain their positive trends, while low measurement resolution **mxd** chronologies built from narrow rings retain the absence of a positive trend. However, the low measurement resolution **mxd** chronologies built from wide rings all attain significant positive trends and the slope coefficients are more similar to the complete high measurement resolution **mxd** chronologies and also to the high measurement resolution **mxd** chronologies built from wide rings. All high measurement resolution **mxd** chronologies composed solely of narrow rings lose their ability to explain 50% of the variance in temperature data, except for the 10-30 µm measurement resolution anatomical datasets. Many of the low measurement resolution **mxd** chronologies built from narrow rings lose much of the temperature sensitivity altogether. However, the low measurement resolution **mxd** chronologies built from wide rings advance towards explaining 50% of the variance in temperature data, and the range of explained variances for both high measurement resolution and low measurement resolution is reduced.

***FIGURE 12** The figure shows overall **mxd** chronology trends (Mann-Kendall slope coefficients) a), and temperature correlations b). Trends and temperature correlations are presented as boxplots stratified on high measurement resolution and low measurement resolution datasets in each panel, where each laboratory is indicated as a filled circle within the corresponding boxes. The dataset ID's are listed on an ordinal scale adjacent to the boxes. The red tones indicate Walesch, green tones ITRAX, orange X-ray computed tomography and blue tones blue intensity techniques, respectively. The left panels show the complete **mxd** datasets and the center and right panels present the results when all datasets are split into **mxd** chronologies based only on narrow or wide rings, respectively.*

5 Synthesis of empirical findings and existing knowledge

"The main present problem concerns the comparison of results between laboratories, as the data obtained from the densitometric records change with the data acquisition system and with the radiation technique itself. The most important parameter is the slit width, which governs the resolution. This is not even the same by the stationary X-ray method…" (the precursor to the Walesch technique) "…*which is yet the simplest and the most widely used. Thus a characteristic as important as the maximum annual density never means the same thing, since it increases when the slit width decreases."*

Polge [1978]

Although, many studies have expressed similar opinions [*Evans,* 1994; *Jacquin et al.,* 2017; *Lenz et al.,* 1976; *Parker et al.,* 1985; *Vaganov et al.,* 2006], more recent studies empirically comparing measurement approaches usually only briefly touch upon this central topic [*De Ridder et al.,* 2010; *Mannes et al.,* 2007; *Park & Telewski* 1993] or do not consider measurement resolution at all [*Björklund et al., 2014*; *Kazcka et al.,* 2018], but see *Helama et al.* [2012]. Therefore we reiterate 40 years on, the relevance of Hubert Polge's problem statement, and elaborate further on this issue, finding that it could be even more profound in the study of climatic change than any works to date have recognized.

5.1 Consolidating the notion of inherent differences in mean levels of wood density measurements

Our comparison experiment confirmed that state-of-the-art X-ray based microdensitometric measurements exhibit a large variation of mean levels for measured density parameters, but also demonstrate errors when compared with densities derived with mass/volume based approaches. Similar errors were obtained for the un-calibrated techniques. Even if we were able to re-calibrate the data with mass/volume-based density approaches, the variation in the **mxd** parameter was not harmonized to an acceptable degree.

5.1.1 Incomparable mean levels of **mxd** *data require special attention*

While previous research has indicated potential challenges in smaller comparisons [*Clauson & Wilson,* 1991; *De Ridder et al.,* 2010; *Gunnarson et al.,* 2012; *Helama et al.,* 2012; *Ivkovich & Koshy,* 1997; *Mannes et al.,* 2007; *Melvin et al.,* 2013; *Park & Telewski,* 1993], our results firmly consolidate that the **mxd** measurement in practice continues to be inherently dependent on measurement idiosyncrasies despite that the fact that the anatomical principle of **mxd** having been defined [*Vaganov et al.,* 2006]. This awareness requires that when building **mxd** chronologies for climate reconstructions aiming to preserve multi-centennial variability [e.g., *Cook et al.,* 1995], data combined from different laboratories or techniques must at a minimum be scaled to a common mean and standard deviation prior to amalgamation [*Esper et al.,* 2014; *McCarroll et al.,* 2013; *Melvin et al.,* 2013; *Zhang et al.,* 2015]. *Helama et al.,* [2012] cautions that routinely applied procedures to remove the age/size related trends in tree-ring data (e.g., using a single detrending curve in “regional curve standardization” (RCS) [*Briffa & Melvin,* 2011]) should not be applied on a single dataset where differently sourced data are merged. The problem mainly arises if sample materials of mixed sources possess different means due to differing measurement protocols and partly cover different time periods. An example of this can be observed in Figure S4. This example demonstrates the findings of *Melvin et al.* [2013] and *Zhang et al.* [2015] of how a combination of data derived by two laboratories with only partial temporal overlap can obscure underlying environmental trends even if these trends are present in both datasets separately. Alternatively, combined data must be standardized separately, i.e. trends, means, and variances of all constituent tree-ring series should be appropriately harmonized, and then compared and combined [e.g., *Helama et al.,* 2012]. However, with this approach the multi-centennial time-scale variability could be severely suppressed [*Cook et al.,* 1995]. Note that these requirements are essential even when the data are derived from the same technique, or at the same lab at different time periods [*Esper et al.,* 2014; *Klesse et al.,* 2015].

5.1.2 Incomparable mean levels of ring density data can be easily alleviated

While it is conceptually determined that **mxd** and minimum density parameters are dependent on measurement resolution, this is not the case for the ring density parameter. Nevertheless, we showed that the X-ray based ring density parameter exhibits notable differences among laboratories and techniques. The discrepancies in mean levels of ring density among different datasets prior to re-calibration result from the accumulated effects of using different devices, different setup of each device, different radiation techniques, different image-analysis software and parameterization, different calibration standard material, different analysis microenvironment, differences in sample preparation and chemical treatment, etc. Thus our experiment shows that the correction factors derived by *Lenz et al.* [1976], at best, are applicable only for the specific device they were developed on, because even the ring density of the different Walesch devices vary substantially. Thus the correction factors do not properly reflect the cell wall chemistry differences of different species compared to the chemistry of the material standard. They rather reflect currently indefinable measurement/calibration artefacts that likely are different on all measurement devices in operation (see the many differences among techniques and laboratories in Table S1-S3).

With high confidence, we can rule out that the observed differences are related to actual differences in ring density of the wood samples. This is because the samples were randomly distributed to the laboratories in the experiment, and also because the sample material produces nearly identical ring width chronologies (Figure S5). Hence, ring density seemingly used without mass/volume-based re-calibration in biomass estimations [*Babst et al.,* 2014b; *Bouriaud et al.,* 2015; *Vanoppen et al.,* 2018] introduces a false sense of uncertainty-reduction when estimates can differ by up to 20% from one laboratory to the next. By re-calibrating data, we achieved marked improvements of estimates. These improvements were also found to be true when applied to BI and anatomical techniques. Therefore, in future work we recommend that microdensitometric measurements should be re-calibrated [*Mothe et al.,* 1998; *Evans,* 1994] on a chronology-by-chronology basis, and results be disclosed [*sensu De Ridder et al.,* 2010]. This implies that the correction factors *Lenz et al.* [1976] derived with gravimetric/volumetric methods more than 40 years ago are obsolete.

Fortunately, the additional re-calibrating measurement scheme constitutes only a minor fraction of the time needed to make the microdensitometric measurements (see Text S1 for an example of instructions). By demonstrating that this simple re-calibration can be successful using fast and inexpensive BI-based density derivations, we further open up new frontiers for the application of microdensitometric ring density. In ecology, wood density is often regarded as an important covariate with functional and competitive traits of species [*Chave et al.,* 2009]. Denser wood is known to convey greater mechanical stability [*Jacobsen et al.,* 2007; *Niklas,* 1995; *Poorter,* 2008; *Pratt et al.,* 2007], and be associated with reduced leaf size [*Wright et al.,* 2007] and lower mortality rates in diverse tropical forests [*Chave et al.,* 2009]. A more available and still accurate pathway to wood density could potentially be used to effectively complement spatial and species based analyses to focus also on variation over time; over the lifespan of trees [e.g., *DeBell et al.,* 2004], and in particular across environmental changes and gradients. This development would not only promote a more detailed understanding of ecosystem processes, but could also benefit forest inventories and inform parameterization to reduce uncertainties associated with current dynamic global vegetation models (DGVMs) [e.g., *Sitch et al.,* 2008].

5.2 Apparent measurement resolution has a profound impact on mxd data

5.2.1 A major influence of mean level offsets in re-calibrated data

At its core, the empirical experiment of this review was not designed to identify which of the specific measurement artefacts mentioned above are the primary determinants for the observed differences. However, by re-calibrating data with mass/volume-based methods, we do not require addressing and correcting the variable sources for these errors at the laboratory specific level. Rather we can focus on practical and general solutions and procedures which can be implemented by all laboratories. In fact, the re-calibration allows us to reduce the sources of discrepancy to two aspects: uncertainty in the re-calibration regression, and the apparent measurement resolution. The aggregation of datasets on low- vs. high-regression uncertainty does not result in a reduced spread of mean levels for datasets with low regression uncertainty, as would be expected if this aspect was influential (we refer to Figure S6 for these results). However, we can empirically establish that apparent measurement resolution is a major influence on mean levels of **mxd** data by knowing that the only difference among anatomical **mxd** datasets is measurement resolution. The simple indicator of apparent measurement resolution, r[**mxd**, ring width], allows us, by comparison, to show that apparent measurement resolution also had a fundamental impact on the mean levels of the non-anatomical **mxd** data, because aggregating datasets based on measurement resolution results in significantly different distributions of mean levels. These findings are very much in tune with existing knowledge of how measurement resolution theoretically would affect **mxd** mean levels [*Evans,* 1994; *Jacquin et al.,* 2017; *Lenz et al.,* 1976; *Parker et al.,* 1985; *Polge,* 1978; *Vaganov et al.,* 2006]

5.2.2 A subtle but distinct influence on the inter-annual variation

Continuing the above line of reasoning, the differences in inter-annual variation among anatomical **mxd** datasets is, by definition, also a product of measurement resolution. By pair-wise successively correlating non-anatomical **mxd** datasets to the measurement resolution range of anatomical **mxd** datasets, peak correlations are consistently obtained at the (indirectly determined) apparent measurement resolution, r[**mxd**, ring width], suggesting that apparent measurement resolution is central also here. It has, however, been cautioned that BI and X-ray based techniques may not measure exactly the same properties in the wood [e.g., *Buckley et al.,* 2018; *Kaczka et al.,* 2018]. *McCarroll et al.* [2002] suggested that BI is more closely related to lignin content because of the reflective/absorptive properties of this compound, while X-ray techniques inherently measure all the aggregated compounds of the wood [*Schweingruber et al.,* 1978]. It can further be cautioned that anatomical density is not the same as the X-ray techniques as anatomical measurements do not account for variability in density of the solid cell wall [*Decoux et al.,* 2004; *Zobel & Van Buijtenen,* 1989]. These concerns may be valid, but are likely of secondary significance for the following two reasons: 1) There are, in some instances, marked differences in correlation coefficients between anatomical **mxd** chronology-pairs, that are by definition driven by measurement resolution. 2) Peak correlations between pairs of non-anatomical techniques and corresponding anatomical datasets are almost identical to the correlation between corresponding pairs of ring width: average r[$\mathbf{mxd}_x$, $\mathbf{mxd}_y$] = 0.96, and average r[ring width_x, ring width_y] = 0.97. Consequently, apparent measurement resolution can represent the limited but tangible differences among datasets. Whereas the technique-specific treatment of the cell wall, be it an integrated measure as with the X-ray technique, ignored by the anatomical technique, or integrated more or less incorrectly by the BI technique, is less likely to represent or explain any important discrepancies among datasets. These findings further develop the arguments presented in Section 2, where evidence from the literature is used to infer that the intra- and inter-annual variability of wood density are mainly determined by changes in anatomical dimensions. If the cell wall density is rather invariable [*Decoux et al.,* 2004] and the cell wall color controlled by fungi/bacteria/resin staining mainly affects >decadal scales, it therefore stands to reason that measurement resolution is of utmost importance to explain differences among microdensitometric techniques at *inter-annual* time-scales.

5.2.3 Intriguing influence on the temperature signal

By comparing the correlation with summer temperature among anatomical datasets of known measurement resolution to corresponding datasets of indirectly determined apparent measurement resolution, a very close association is observed. At lower measurement resolutions, the r[**mxd**, ring width] is relatively high, which translates to an **mxd** temperature signal more similar to the temperature signal of ring width. The **mxd** temperature signals of the low measurement resolution datasets indeed reveal more pronounced July correlations. These correlations become systematically lower with increasing measurement resolution. Interestingly, the July correlation is further weakened in the highest measurement resolution anatomical **mxd** datasets, a feature not present in any non-anatomical datasets in our experiment, but a typical characteristic of, in particular *Picea sp.* and to some degree also *Pinus sp.* MXD data from the Northern Hemisphere (NH) [*Björklund et al.,* 2017; *Büntgen et al.,* 2017; *Schweingruber et al.,* 1978]. An explanation for this could be that data from these studies in general do not include the very narrow rings present in this experimental sample material, and the dependence of **mxd** to ring width is therefore reduced. An alternative, but not mutually exclusive explanation could be that the *Picea sp.* ring width of the NH network has very weak mid-summer temperature correlations [*Björklund et al.,* 2017; *Briffa et al.,* 2002], and a measurement-induced likeness to ring width does not enhance the mid-summer correlation of **mxd** data. Though the underlying mechanisms behind this mid-summer decline remain unresolved, they can most likely be attributed to the asynchronous and sometimes conflicting interplay among cell-formation, cell-expansion and stored resources for cell-wall thickening [*Björklund et al.,* 2017; *Cuny et al.,* 2015].

5.2.4 The cause of overall trend differences in chronologies

We further detected slightly differing overall trends in **mxd** chronologies – a difference also found in *Helama et al.* [2012] comparing age-aligned MXD data from Itrax and Walesch. We discuss two potential sources for this discrepancy. Firstly, trends could vary because of differences in apparent measurement resolution. In our experiment, narrow rings were shown to be artificially associated with low **mxd** values, and biological growth trends of conifers typically describe a life-long exponential decline in ring width [*Melvin,* 2004], also evident from the ring width chronologies of the experiment (Figure S5). Hence, low apparent measurement resolution techniques would be associated with more negative overall trends compared to high apparent measurement resolution techniques. Secondly, trend differences may be detected if some techniques are more sensitive to heartwood-sapwood transitions. This is the case for BI technique [*Björklund et al.,* 2014, 2015; *Buckley et al.,* 2018; *Rydval et al.,* 2014], but may also affect X-ray techniques if resin extraction is omitted [*Helama et al.,* 2010; *Schweingruber et al.,* 1978]. Aligning **mxd** chronologies from both BI and X-ray techniques on heartwood/sapwood dates instead of calendar dates, reveals that there is a small negative step around the time of heartwood/sapwood transition (Figure S7). The high apparent measurement resolution anatomical **mxd** do not have this feature. However, low apparent measurement resolution anatomical **mxd** develop a similar step in trend as the other techniques. Because the anatomical method is not based on light intensity, but proportion of cell wall, a step in trend around the time of heartwood/sapwood transition must be related to some other feature of the measurements than simply the color or density difference caused by heartwood/sapwood transition. When we separated data based on apparent measurement resolution we obtained a significant difference between high apparent measurement resolution and low apparent measurement resolution datasets with regard to their trends. Note also that some X-ray techniques, with presumably reduced sensitivity to heartwood/sapwood transitions are classified as low apparent measurement resolution datasets and some BI datasets are classified as high apparent measurement resolution datasets. Thus, in this study, apparent measurement resolution rather than heartwood/sapwood transitions most likely cause the observed trend differences in the **mxd** parameter. Nonetheless, ambient color differences within and between samples have conclusively been shown to distort decadal to multi-centennial variability for BI techniques [*Björklund et al.,* 2014; *Wilson et al.,* 2017], and this bias may additionally contribute to trend distortion caused by apparent measurement resolution for other more diverse sample materials. In particular, the utilisation of preserved historical, snag and/or sub-fossil material [*Wilson et al.,* 2004; *Björklund et al.,* 2014, *Rydval et al.,* 2017] to extend living datasets further back in time – the norm for most millennial-long chronologies – pose serious challenges. This is because preserved wood will in all scenarios be darker than their living tree counterparts. Preserved wood can become incredibly dark in tannin and iron rich lake and peaty environments. If this darkening of the wood is not considered, it will impose a “warm” bias, as darker colours are here associated with higher densities. Moreover, in *Larix sp.* the high content of extractives in their heartwood [*Grabner et al*., 2005] may challenge the success of chemical extraction and result in noticeable heartwood/sapwood differences even for X-ray microdensitometry.

5.2.5 Statistical treatment of trend differences

Trend differences among datasets are diminished if typical standardization/detrending procedures, such as individual data-adaptive approaches (one curve function per tree) [*Cook & Peters,* 1981; *Melvin & Briffa,* 2008] or collective data-adaptive approaches (one curve function for all trees) [*Briffa et al.,* 1992] are applied (results not shown). Similar findings were previously also shown by *Helama et al.* [2012]. Dataset trends all become neutral and may be associated with loss of important climate information. To retain a positive trend after standardization in these data, more deterministic methods have to be employed. One such approach could be to employ functions that are not allowed to track persistent positive trends. This approach could be justified because of the preconceived notion that after the juvenile growth phase [*Melvin,* 2004] tree-ring series should not systematically have wider rings or denser latewood with increasing age. Thus, such a feature would most likely be related to climate. This approach would, however, not be able to retain a positive trend in **mxd** data that does not have any positive trend to begin with. Another approach would be to sample more trees, covering earlier time periods, preferably several generations, and employ RCS standardization [*Melvin & Briffa,* 2011]. An artificial measurement-resolution induced trend in the data should be similar for all generations within a dataset, and removing the common age/growth variance from all series should result in the retention of net positive or negative trends of specific generations for all techniques. To achieve this result, extensive and diverse sets of sample materials are needed [*Esper et al.,* 2003; *Melvin & Briffa,* 2011]. While differences in mean levels appear straightforward to compensate with statistical scaling, trend differences among data sources require much more scrutiny and care. The only way to quantify the environmental trends is by accurately identifying the biological growth-trend, and this is not an easy task [*Peters et al.,* 2014] especially if different data sources can have different age/size related growth trends due to apparent measurement resolution.

5.2.6 Potential component in the "divergence problem" of Northern forests?

In dendroclimatology there is a longstanding debate as to whether ring width and **mxd** chronologies display a trend mismatch or loss of response in recent decades to growing season temperature. This is often referred to as the divergence problem [*D'Arrigo et al.,* 2008; *Esper & Frank,* 2009; *Stine & Huybers,* 2014]. If this phenomenon has scientific merit as an unmatched decline or loss of response in ring width during recent decades, corresponding **mxd** data derived from low apparent measurement resolution techniques may also inherit these features even if they are not present in the **mxd** data as an environmentally induced trend. Any decline in ring width, be it on annual, decadal or centennial scale will prompt a proportionally exaggerated decline in **mxd** values if apparent measurement resolution is low. That is, under this hypothesis, measurement resolution is not the cause of the "true" divergence, there must first be an environmental driver hampering ring width growth for divergence to be detected in **mxd**. Alternatively, the divergence problem is not induced by environmental drivers but a problem of disentangling biological growth trends from environmental growth trends, expressed during the difficult decomposition of the two [*Esper & Frank,* 2009]. Consider that most dendroclimatological chronologies have an increasing mean age of trees closer to the sampling date [*Nehrbass-Ahles et al.,* 2014], and this is almost always associated with a decline in ring-width due to the age/size trends of most conifers [*Fritts,* 1976]. Thus **mxd** data at more modern dates will be similarly suppressed if measurement resolution is low. In this sense, it would be worth revisiting original chronologies and reconstructions exhibiting divergence, and jointly examine ring width and **mxd** for conspicuously tight associations when ring widths are narrow.

5.2.7 Mitigating differences caused by measurement resolution

In the experiment detailed herein, we showed that wide–ring **mxd** chronologies (**mxd** from only >400 μm wide rings) obtain trends and temperature signals more similar to high measurement resolution techniques. This is quite remarkable considering that only half of the sample material is compared to the full dataset. Even the least replicated GentT datasets exhibit these features. All narrow-ring **mxd** chronologies exhibit the opposite features. Such a marked deterioration of performance from wide-ring **mxd** chronologies to narrow-ring **mxd** chronologies again corroborates the hypothesis that apparent measurement resolution is very important. Moreover, this also shows that it may be possible to mitigate this bias in chronologies. We show that this mitigation can be achieved with a simple omission of **mxd** data measured from narrow rings, but we recommend finding other solutions that do not discard valuable data, such as adopting percentile chronologies instead of mean chronology approaches [*Stine & Huybers,* 2017] or statistically modeling-out similarities of **mxd** to ring width prior to use [*sensu Kirdyanov et al.,* 2007]. It is interesting to note that if a smaller amount of information within the aperture and measurement track is utilized, it has a positive effect on the performance of the data. This is exemplified by the GentT* dataset that only uses the 20% densest voxels to derive the **mxd** parameter, compared to the original GentT dataset that utilizes 100%. This feature, in the DHXCT image analysis software, but also relatedly implemented in CooRecorder™, may be an interesting approach to increase apparent measurement resolution after X-ray or visible light scanning has been performed. Taking more care in matching the measurement sensor obliquity across ring boundaries should also be addressed. Software development, where sensor shapes can adapt to curving ring boundaries could potentially be a very valuable feature and means of addressing this issue. Of course it is of fundamental importance to increase or maintain a high quality in the image capturing process. For X-ray techniques, except 3D X-ray computed tomography, the fiber-angle control during sample preparation is of utmost importance. If fibers deviate even slightly from the parallel direction of the X-ray beam, a blurred, unfocused image will result. This will reduce the apparent measurement resolution even if image analysis hardware and software specify 10 or 20 µm apertures (nominal resolution). If images are of high quality, the use of narrow analysis sensor apertures is preferable (at least down to 10 µm). For the BI technique, it appears that a move towards increased scanning resolution or high-resolution photography may be beneficial, as indicated through comparison of the UIbkB dataset with the other BI datasets produced with flatbed scanners. However, as a technique where economy and accessibility are selling points; further advances in image-analysis rather than hardware may be the more likely future priority.

5.3. Synopsis

With this review, in tandem with an empirical comparison experiment, we demonstrate the need, and provide a simple methodological outline, for mass/volume based re-calibration to accurately estimate ring density values (see Text S1 for an example of instructions). The mean levels of ring density should not be considered absolute values unless a gravimetric/volumetric re-calibration has been conducted. It should further be considered best practice to keep track of system stability and reproducibility through time. We note also that if a re-calibration is implemented, the set of "correction factors" introduced by *Lenz et al.,* [1976] also becomes redundant for **mxd** and minimum density.

The mean levels of **mxd** and minimum density are never comparable even if a re-calibration has been implemented because of inherently different apparent measurement resolutions between different techniques and laboratories. This conclusion is based on existing theoretical knowledge corroborated with empirical evidence presented in this review. In fact, this review has demonstrated that the apparent measurement resolution of a sample is even more fundamental than existing work appears to have conveyed. In our experiments specifically, we observe substantial biases using data measured from narrow rings, which can influence the long-term trend in measurements and the resulting temperature signals obtained where such data are used in palaeoclimatology. We recommend efforts to increase apparent measurement resolution in the laboratory, and to consider analytical techniques to enhance the precision of the **mxd** signal.

Because the mean values of minimum density and **mxd** are without direct comparison (their comparability is obscured by measurement resolution) the main aim of both system operators and developers should be geared towards sharp radiographs [*Vaganov et al., 2006*], as opposed to accurate density transformations [*Moschler & Winistorfer,* 1990]. The assumption made in calibrating a heterogeneous material such as wood into density using a homogenous calibration material appears to be sufficiently representative in terms of assigning each measurement conducted in the same lab to a relative scale. However, the calibration reference cannot be reliably used to derive comparable **mxd** measurements at different labs due to apparent resolution biases.

We therefore recommend that special care is needed when working with past measurements, data produced using various technologies, or from different laboratories. When combining differently sourced density datasets, each needs to be treated individually prior to their combination.

We emphasize that wood density, as perceived by all techniques, is effectively a representation of the proportion of cell wall in the tracheids of the xylem. Except for the important caveat that cell-wall discoloration can be overwhelming on >multi-decadal scales for reflected light techniques such as BI, the most fundamental difference among microdensitometric techniques at inter-annual time-scales is their apparent measurement resolution.

Finally, despite all the analytical challenges of producing microdensitometric measurements for global change research, we underscore that the merits – the tight association with growing season temperatures, the ability to represent volcanic cooling, and its reduced biological memory compared to ring width – position **mxd** as the current gold standard of high-resolution paleoclimatology for temperature reconstructions.

Acknowledgments, Samples, and Data

We sincerely thank three anonymous referees for valuable critique to an earlier version of the manuscript. We further acknowledge the shared expertise of Etienne Szymanski and Peter Herter of WALESCH Electronic and Anders Rindby of Cox Analytical Systems during a workshop arranged as part of the coordination of the inter-comparison experiment (Section 4 of this review). We thank two diligent technicians; Patrick Züst and Basil Frefel for assistance in producing the wood anatomically based dataset.

This work was mainly funded by the Swiss National Science Foundation (grants iTREE CRSII3_136295 and P300P2_ 154543). J.B. further gratefully acknowledge financial support by the Transnational Access to Research Infrastructures activity in the 7th Framework Programme of the EC under the Trees4Future project (no. 284181). G.v.A. was supported by a grant from the Swiss State Secretariat for Education, Research and Innovation SERI (SBFI C14.0104). J.B. & G.v.A. were also supported by the Swiss National Science Foundation SNSF (Project XELLCLIM no. 200021_182398). MR acknowledges funding through the EVA4.0 project (CZ.02.1.01/0.0/0.0/16_019/0000803). P.F. was supported by the Swiss National Science Foundation (grant no. 150205, LOTFOR). T. D. M was supported by Ghent University Special Research Fund PhD grant (BOF.DOC.2014.0037.01). R.K. and K.J. was Supported by the National Science Centre project DEC-2013/11/B/ST10/04764 (Poland). A.H. and R.S-S are grateful to Juan Majada for providing support for this study and Laura González Sánchez, Mara Arrojo and Fernando Quintana who assisted in the CETEMAS´laboratory. R.S-S. was supported by a Postdoctoral grant (IJCI-2015-25845, FEDER funds). A.V.K. was supported by the Russian Science Foundation (project 18-14-00072). J.E, C.H. and M.K. were supported by the German Science Foundation (grants Inst 247/665-1 FUGG, ES 161/9-1 and HA 8048/1-1). M.W. and T.S. were supported by the Leibnitz Association (project BaltRap) and M.W. supported by the German Science Foundation (grants Inst 247/665-1 FUGG, ES 161/9-1 and Wi 2680 /8-1). K.N. was supported by the Austrian Science Fund FWF (grant no. I 1183-N19). L.A-H., R.O. and R.D. were supported by the US National Science Foundation (NSF) grants AGS-15-02150, PLR-15-04134 and PLR-16-03473. U.B. received funding from the project “SustES - Adaptation strategies for sustainable ecosystem services and food security under adverse environmental conditions” (CZ.02.1.01/0.0/0.0/16_019/0000797). R.W. was supported by NERC grant NE/K003097/1. N.J.L. received support from the UK NERC (NE/P011527/1) and EU project “Millennium” 017008. M.M. and V.T. were supported by US NSF CAREER grant AGS-1349942.

Data produced for this study are made available through the Supporting Information (Data S1), where also Meta data (technique and parameterization) for each dataset are described (Tables S1-S3).

References

Allen, K. J., Cook, E. R., Evans, R., Francey, R., Buckley, B. M., Palmer, J. G., ... & Baker, P. J. (2018). Lack of cool, not warm, extremes distinguishes late 20th Century climate in 979-year Tasmanian summer temperature reconstruction. *Environmental Research Letters*, *13*(3), 034041.

Allen, K. J., Drew, D. M., Downes, G. M., Evans, R., Cook, E. R., Battaglia, M., & Baker, P. J. (2013). A strong regional temperature signal in low- elevation Huon pine. *Journal of Quaternary Science*, *28*(5), 433-438.

Allen, K. J., Nichols, S. C., Evans, R., Cook, E. R., Allie, S., Carson, G., ... & Baker, P. J. (2015). Preliminary December–January inflow and streamflow reconstructions from tree rings for western Tasmania, southeastern Australia. *Water Resources Research*, *51*(7), 5487-5503.

Anchukaitis, K. J., Breitenmoser, P., Briffa, K. R., Buchwal, A., Büntgen, U., Cook, E. R., ... & Grudd, H. (2012). Tree rings and volcanic cooling. *Nature Geoscience*, *5*(12), 836.

Anchukaitis, K. J., D’Arrigo, R. D., Andreu-Hayles, L., Frank, D., Verstege, A., Curtis, A., ... & Cook, E. R. (2013). Tree-ring-reconstructed summer temperatures from northwestern North America during the last nine centuries. *Journal of Climate*, *26*(10), 3001-3012.

Anchukaitis, K. J., Wilson, R., Briffa, K. R., Büntgen, U., Cook, E. R., D'Arrigo, R., ... & Hegerl, G. (2017). Last millennium Northern Hemisphere summer temperatures from tree rings: Part II, spatially resolved reconstructions. *Quaternary Science Reviews*, *163*, 1-22.

Antonova, G. F., & Stasova, V. V. (1997). Effects of environmental factors on wood formation in larch (Larix sibirica Ldb.) stems. *Trees*, *11*(8), 462-468.

Arzac, A., López-Cepero, J. M., Babushkina, E. A., & Gomez, S. (2018). Applying methods of hard tissues preparation for wood anatomy: Imaging polished samples embedded in polymethylmethacrylate. *Dendrochronologia*, *51*, 76-81.

Austin, A. T., & Ballaré, C. L. (2010). Dual role of lignin in plant litter decomposition in terrestrial ecosystems. *Proceedings of the National Academy of Sciences*, 20090936.

Auty, D., Achim, A., Macdonald, E., Cameron, A. D., & Gardiner, B. A. (2014). Models for predicting wood density variation in Scots pine. *Forestry: An International Journal of Forest Research*, *87*(3), 449-458.

Babst, F., Alexander, M. R., Szejner, P., Bouriaud, O., Klesse, S., Roden, J., ... & Trouet, V. (2014a). A tree-ring perspective on the terrestrial carbon cycle. *Oecologia*, *176*(2), 307-322.

Babst, F., Bouriaud, O., Papale, D., Gielen, B., Janssens, I. A., Nikinmaa, E., ... & Grünwald, T. (2014b). Above- ground woody carbon sequestration measured from tree rings is coherent with net ecosystem productivity at five eddy- covariance sites. *New Phytologist*, *201*(4), 1289-1303.

Babst, F., Frank, D., Büntgen, U., Nievergelt, D., & Esper, J. (2009). Effect of sample preparation and scanning resolution on the Blue Reflectance of Picea abies. *TRACE Proc*, *7*, 188-195.

Baker, T. R., Phillips, O. L., Malhi, Y., Almeida, S., Arroyo, L., Di Fiore, A., ... & Lewis, S. L. (2004). Variation in wood density determines spatial patterns inAmazonian forest biomass. *Global Change Biology*, *10*(5), 545-562.

Bergsten, U., Lindeberg, J., Rindby, A., & Evans, R. (2001). Batch measurements of wood density on intact or prepared drill cores using x-ray microdensitometry. *Wood Science and Technology*, *35*(5), 435-452.

Björklund, J. (2014). *Tree-rings and climate-Standardization, proxy-development, and Fennoscandian summer temperature history*. PhD thesis. Department of Earth Sciences, University of Gothen- burg. http://www.gvc.gu.se/forskning/klimat/paleoklimat/GULD/ Publications/thesises-and-reports/

Björklund, J. A., Gunnarson, B. E., Krusic, P. J., Grudd, H., Josefsson, T., Östlund, L., & Linderholm, H. W. (2013). Advances towards improved low-frequency tree-ring reconstructions, using an updated Pinus sylvestris L. MXD network from the Scandinavian Mountains. *Theoretical and applied climatology*, *113*(3-4), 697-710.

Björklund, J. A., Gunnarson, B. E., Seftigen, K., Esper, J., & Linderholm, H. W. (2014). Blue intensity and density from northern Fennoscandian tree rings, exploring the potential to improve summer temperature reconstructions with earlywood information. *Climate of the Past*, *10*(2), 877-885.

Björklund, J., Gunnarson, B. E., Seftigen, K., Zhang, P., & Linderholm, H. W. (2015). Using adjusted blue intensity data to attain high-quality summer temperature information: a case study from Central Scandinavia. *The Holocene*, *25*(3), 547-556.

Björklund, J., Seftigen, K., Schweingruber, F., Fonti, P., Arx, G., Bryukhanova, M. V., ... & Frank, D. C. (2017). Cell size and wall dimensions drive distinct variability of earlywood and latewood density in Northern Hemisphere conifers. *New Phytologist*, *216*(3), 728-740.

Black, B. A., Boehlert, G. W., & Yoklavich, M. M. (2005). Using tree-ring crossdating techniques to validate annual growth increments in long-lived fishes. *Canadian Journal of Fisheries and Aquatic Sciences*, *62*(10), 2277-2284.

Bouriaud, O., Teodosiu, M., Kirdyanov, A. V., & Wirth, C. (2015). Influence of wood density in tree-ring-based annual productivity assessments and its errors in Norway spruce. *Biogeosciences*, *12*(20), 6205-6217.

Bowyer, J. L., & Shmulski, R. H. JG 2003. Forest Products and Wood Science: An Introduction.

Briffa, K. R., Bartholin, T. S., Eckstein, D., Jones, P. D., Karlén, W., Schweingruber, F. H., & Zetterberg, P. (1990). A 1,400-year tree-ring record of summer temperatures in Fennoscandia. *Nature*, *346*(6283), 434.

Briffa, K. R., Jones, P. D., Bartholin, T. S., Eckstein, D., Schweingruber, F. H., Karlen, W., ... & Eronen, M. (1992). Fennoscandian summers from AD 500: temperature changes on short and long timescales. *Climate dynamics*, *7*(3), 111-119.

Briffa, K. R., & Melvin, T. M. (2011). A closer look at regional curve standardization of tree-ring records: justification of the need, a warning of some pitfalls, and suggested improvements in its application. In *Dendroclimatology* (pp. 113-145). Springer, Dordrecht.

Briffa, K. R., Jones, P. D., Schweingruber, F. H., & Osborn, T. J. (1998). Influence of volcanic eruptions on Northern Hemisphere summer temperature over the past 600 years. *Nature*, *393*(6684), 450.

Briffa, K. R., Osborn, T. J., & Schweingruber, F. H. (2004). Large-scale temperature inferences from tree rings: a review. *Global and planetary change*, *40*(1-2), 11-26.

Briffa, K. R., Osborn, T. J., Schweingruber, F. H., Jones, P. D., Shiyatov, S. G., & Vaganov, E. A. (2002). Tree-ring width and density data around the Northern Hemisphere: Part 1, local and regional climate signals. *The Holocene*, *12*(6), 737-757.

Britez, M. R. D., Sergent, A. S., Meier, A. M., Bréda, N., & Rozenberg, P. (2014). Wood density proxies of adaptive traits linked with resistance to drought in Douglas fir (Pseudotsuga menziesii (Mirb.) Franco). *Trees*, *28*(5), 1289-1304.

Brown, H. P., Panshin, A. J., & Forsaith, C. C. (1949). Textbook of wood technology. Vol. 1. Structure, identification, defects and uses of the commercial woods of the United States. *Textbook of wood technology. Vol. 1. Structure, identification, defects and uses of the commercial woods of the United States.*

Bryukhanova, M., & Fonti, P. (2013). Xylem plasticity allows rapid hydraulic adjustment to annual climatic variability. *Trees*, *27*(3), 485-496.

Buckley, B. M., Hansen, K. G., Griffin, K. L., Schmiege, S., Oelkers, R., D'Arrigo, R. D., ... & Wilson, R. J. (2018). Blue intensity from a tropical conifer's annual rings for climate reconstruction: An ecophysiological perspective. *Dendrochronologia*, *50*, 10-22.

Büntgen, U., Frank, D., Grudd, H., & Esper, J. (2008). Long-term summer temperature variations in the Pyrenees. *Climate Dynamics*, *31*(6), 615-631.

Büntgen, U., Frank, D. C., Kaczka, R. J., Verstege, A., Zwijacz-Kozica, T., & Esper, J. (2007). Growth responses to climate in a multi-species tree-ring network in the Western Carpathian Tatra Mountains, Poland and Slovakia. *Tree physiology*, *27*(5), 689-702.

Büntgen, U., Frank, D. C., Nievergelt, D., & Esper, J. (2006). Summer temperature variations in the European Alps, AD 755–2004. *Journal of Climate*, *19*(21), 5606-5623.

Büntgen, U., Frank, D., Trouet, V., & Esper, J. (2010). Diverse climate sensitivity of Mediterranean tree-ring width and density. *Trees*, *24*(2), 261-273.

Büntgen, U., Krusic, P. J., Verstege, A., Sangüesa-Barreda, G., Wagner, S., Camarero, J. J., ... & Tegel, W. (2017). New tree-ring evidence from the Pyrenees reveals Western Mediterranean climate variability since medieval times. *Journal of Climate*, *30*(14), 5295-5318.

Büntgen, U., Raible, C. C., Frank, D., Helama, S., Cunningham, L., Hofer, D., ... & Esper, J. (2011). Causes and consequences of past and projected Scandinavian summer temperatures, 500–2100 AD. *Plos One*, *6*(9), e25133.

Burkey, J. (2006). A non-parametric monotonic trend test computing Mann-Kendall Tau, Tau-b, and Sen's slope written in Mathworks-MATLAB implemented using matrix rotations. *King County, Department of Natural Resources and Parks, Science and Technical Services Section: Seattle, WA*.

Camarero, J. J., Fernández-Pérez, L., Kirdyanov, A. V., Shestakova, T. A., Knorre, A. A., Kukarskih, V. V., & Voltas, J. (2017). Minimum wood density of conifers portrays changes in early season precipitation at dry and cold Eurasian regions. *Trees*, *31*(5), 1423-1437.

Camarero, J. J., Rozas, V., & Olano, J. M. (2014). Minimum wood density of Juniperus thurifera is a robust proxy of spring water availability in a continental Mediterranean climate. *Journal of biogeography*, *41*(6), 1105-1114.

Cameron, A. D., Gardiner, B. A., Ramsay, J., & Drewett, T. A. (2015). Effect of early release from intense competition within high density natural regeneration on the properties of juvenile and mature wood of 40-year-old Sitka spruce (Picea sitchensis (Bong.) Carr.). *Annals of forest science*, *72*(1), 99-107.

Cameron, J. F., Berry, P. F., & Phillips, E. W. J. (1959). The determination of wood density using beta rays. *Holzforschung-International Journal of the Biology, Chemistry, Physics and Technology of Wood*, *13*(3), 78-84.

Campbell, R., McCarroll, D., Loader, N. J., Grudd, H., Robertson, I., & Jalkanen, R. (2007). Blue intensity in Pinus sylvestris tree-rings: developing a new palaeoclimate proxy. *The Holocene*, *17*(6), 821-828.

Campbell, R., McCarroll, D., Robertson, I., Loader, N. J., Grudd, H., & Gunnarson, B. (2011). Blue intensity in Pinus sylvestris tree rings: a manual for a new palaeoclimate proxy. *Tree-Ring Research*, *67*(2), 127-134.

Castagneri, D., Battipaglia, G., von Arx, G., Pacheco, A., & Carrer, M. (2018). Tree-ring anatomy and carbon isotope ratio show both direct and legacy effects of climate on bimodal xylem formation in Pinus pinea. *Tree physiology*.

Castagneri, D., Fonti, P., von Arx, G., & Carrer, M. (2017). How does climate influence xylem morphogenesis over the growing season? Insights from long-term intra-ring anatomy in Picea abies. *Annals of botany*, *119*(6), 1011-1020.

Chave, J., Coomes, D., Jansen, S., Lewis, S. L., Swenson, N. G., & Zanne, A. E. (2009). Towards a worldwide wood economics spectrum. *Ecology letters*, *12*(4), 351-366.

Che, M. L., Chen, B. Z., Wang, Y., & Guo, X. Y. (2014). Review of dynamic global vegetation models (DGVMs). *The journal of applied ecology*, *25*(1), 263-271.

Chen, F., Yuan, Y. J., Wei, W. S., Yu, S. L., Fan, Z. A., Zhang, R. B., ... & Shang, H. M. (2012). Temperature reconstruction from tree-ring maximum latewood density of Qinghai spruce in middle Hexi Corridor, China. *Theoretical and Applied Climatology*, *107*(3-4), 633-643.

Clauson, M. L., & Wilson, J. B. (1991). Comparison of video and x-ray for scanning wood density. *Forest products journal (USA)*.

Cleaveland, M. K. (1986). Climatic response of densitometric properties in semiarid site tree rings. *Tree-Ring Bulletin*.

Cook, E. R. (1985). *A Time Series Analysis Approach to Tree-Ring Standardization*, Ph.D. Thesis, The University of Arizona, Tucson.

Cook, E. R., Briffa, K. R., Meko, D. M., Graybill, D. A., & Funkhouser, G. (1995). The'segment length curse'in long tree-ring chronology development for palaeoclimatic studies. *The Holocene*, *5*(2), 229-237.

Cook, E. R., & Kairiukstis, L. A. (Eds.). (2013). *Methods of dendrochronology: applications in the environmental sciences*. Springer Science & Business Media.

Cook, E. R., & Peters, K. (1981). The smoothing spline: a new approach to standardizing forest interior tree-ring width series for dendroclimatic studies.

Cown, D. J., & Clement, B. C. (1983). A wood densitometer using direct scanning with X-rays. *Wood Science and Technology*, *17*(2), 91-99.

Cuny, H. E., Rathgeber, C. B., Frank, D., Fonti, P., & Fournier, M. (2014). Kinetics of tracheid development explain conifer tree- ring structure. *New Phytologist*, *203*(4), 1231-1241.

D'Arrigo, R., Wilson, R., & Anchukaitis, K. J. (2013). Volcanic cooling signal in tree ring temperature records for the past millennium. *Journal of Geophysical Research: Atmospheres*, *118*(16), 9000-9010.

D'Arrigo, R., Wilson, R., Liepert, B., & Cherubini, P. (2008). On the 'divergence problem' in northern forests: a review of the tree-ring evidence and possible causes. *Global and planetary change*, *60*(3-4), 289-305.

Dannenberg, M. P., & Wise, E. K. (2016). Seasonal climate signals from multiple tree ring metrics: A case study of Pinus ponderosa in the upper Columbia River Basin. *Journal of Geophysical Research: Biogeosciences*, *121*(4), 1178-1189.

Davi, N. K., Jacoby, G. C., & Wiles, G. C. (2003). Boreal temperature variability inferred from maximum latewood density and tree-ring width data, Wrangell Mountain region, Alaska. *Quaternary Research*, *60*(3), 252-262.

De Groote, S. R., Vanhellemont, M., Baeten, L., Van den Bulcke, J., Martel, A., Bonte, D., ... & Verheyen, K. (2018). Competition, tree age and size drive the productivity of mixed forests of pedunculate oak, beech and red oak. *Forest Ecology and Management*, *430*, 609-617.

De Mil, T., Vannoppen, A., Beeckman, H., Van Acker, J., & Van den Bulcke, J. (2016). A field-to-desktop toolchain for X-ray CT densitometry enables tree ring analysis. *Annals of botany*, *117*(7), 1187-1196.

De Ridder, M., Van den Bulcke, J., Vansteenkiste, D., Van Loo, D., Dierick, M., Masschaele, B., ... & Van Hoorebeke, L. (2010). High-resolution proxies for wood density variations in Terminalia superba. *Annals of botany*, *107*(2), 293-302.

DeBell, D. S., Singleton, R., Gartner, B. L., & Marshall, D. D. (2004). Wood density of young-growth western hemlock: relation to ring age, radial growth, stand density, and site quality. *Canadian Journal of Forest Research*, *34*(12), 2433-2442.

Decoux, V., Varcin, É., & Leban, J. M. (2004). Relationships between the intra-ring wood density assessed by X-ray densitometry and optical anatomical measurements in conifers. Consequences for the cell wall apparent density determination. *Annals of Forest Science*, *61*(3), 251-262.

Dierick, M., Van Loo, D., Masschaele, B., Boone, M., & Van Hoorebeke, L. (2010). A LabVIEW® based generic CT scanner control software platform. *Journal of X-ray Science and Technology*, *18*(4), 451-461.

Dierick, M., Van Loo, D., Masschaele, B., Van den Bulcke, J., Van Acker, J., Cnudde, V., & Van Hoorebeke, L. (2014). Recent micro-CT scanner developments at UGCT. *Nuclear Instruments and Methods in Physics Research Section B: Beam Interactions with Materials and Atoms*, *324*, 35-40.

Dolgova, E. (2016). June–September temperature reconstruction in the Northern Caucasus based on blue intensity data. *Dendrochronologia*, *39*, 17-23.

Downes, G. M., Evans, R., Benson, M., & Myers, B. (1994, May). Application of a new wood micro-structure analyser to the assessment of environmental effects on radiata pine tracheid dimensions. In *48th Appita Conference, Melbourne*.

Downes, G. M., Wimmer, R., & Evans, R. (2002). Understanding wood formation: gains to commercial forestry through tree-ring research. *Dendrochronologia*, *20*(1-2), 37-51.

Drew, D. M., Allen, K., Downes, G. M., Evans, R., Battaglia, M., & Baker, P. (2012). Wood properties in a long-lived conifer reveal strong climate signals where ring-width series do not. *Tree physiology*, *33*(1), 37-47.

Duan, J., & Zhang, Q. B. (2014). A 449 year warm season temperature reconstruction in the southeastern Tibetan Plateau and its relation to solar activity. *Journal of Geophysical Research: Atmospheres*, *119*(20), 11-578.

Düthorn, E., Schneider, L., Günther, B., Gläser, S., & Esper, J. (2016). Ecological and climatological signals in tree-ring width and density chronologies along a latitudinal boreal transect. *Scandinavian Journal of Forest Research*, *31*(8), 750-757.

Elliott, G. K. (1970). Wood density in conifers. Tech. Comm. No. 8, Commonwealth Forestry Bureau, Oxford, England.

Elliott, G. K., & Brook, S. E. G. (1967). Microphotometric technique for growth-ring analysis. *Journal of the Institute of wood Science*, (18), 24.

Emile-Geay, J., McKay, N. P., Kaufman, D. S., Von Gunten, L., Wang, J., Anchukaitis, K. J., ... & Henley, B. J. (2017). A global multiproxy database for temperature reconstructions of the Common Era. *Scientific data*, *4*, 170088.

Eschbach, W., Nogler, P., Schär, E., & Schweingruber, F. H. (1995). Technical advances in the radiodensitometrical determination of wood density. *Dendrochronologia*, *13*, 155-168.

Esper, J., Cook, E. R., Krusic, P. J., Peters, K., & Schweingruber, F. H. (2003). Tests of the RCS method for preserving low-frequency variability in long tree-ring chronologies. Tree Ring Res. 59, 81–98

Esper, J., Düthorn, E., Krusic, P. J., Timonen, M., & Büntgen, U. (2014). Northern European summer temperature variations over the Common Era from integrated tree- ring density records. *Journal of Quaternary Science*, *29*(5), 487-494.

Esper, J., George, S. S., Anchukaitis, K., D'Arrigo, R., Ljungqvist, F. C., Luterbacher, J., ... & Büntgen, U. (2018). Large-scale, millennial-length temperature reconstructions from tree-rings. *Dendrochronologia*, *50*, 81-90.

Esper, J., & Frank, D. (2009). Divergence pitfalls in tree-ring research. *Climatic Change*, *94*(3), 261-266.

Esper, J., Frank, D. C., Timonen, M., Zorita, E., Wilson, R. J., Luterbacher, J., ... & Verstege, A. (2012). Orbital forcing of tree-ring data. *Nature Climate Change*, *2*(12), 862.

Esper, J., Schneider, L., Smerdon, J. E., Schöne, B. R., & Büntgen, U. (2015). Signals and memory in tree-ring width and density data. *Dendrochronologia*, *35*, 62-70.

Esper, J., Wilson, R. J., Frank, D. C., Moberg, A., Wanner, H., & Luterbacher, J. (2005). Climate: past ranges and future changes. *Quaternary Science Reviews*, *24*(20-21), 2164-2166.

Evans, R. (1994). Rapid measurement of the transverse dimensions of tracheids in radial wood sections from Pinus radiata. *Holzforschung, 48(2),* 168-172

Evans, R., Downes, G. M., & Murphy, J. O. (1996). Application of new wood characterization technology to dendrochronology. In 'Tree Rings, Environment and Humanity'.(Eds JS Dean, DM Meko and TW Swetnam.) pp. 743–749. *Radiocarbon*.

Fletcher, J. M., & Hughes, J. F. (1970). Uses of X-rays for density determinations and dendrochronology. *Bull. Fac. For. Univ. BC*, (7), 41-54.

Fonti, P., Bryukhanova, M. V., Myglan, V. S., Kirdyanov, A. V., Naumova, O. V., & Vaganov, E. A. (2013). Temperature- induced responses of xylem structure of Larix sibirica (Pinaceae) from the Russian Altay. *American journal of botany*, *100*(7), 1332-1343.

Fonti, P., & Jansen, S. (2012). Xylem plasticity in response to climate. *New Phytologist*, *195*(4), 734-736.

Fonti, P., von Arx, G., García- González, I., Eilmann, B., Sass- Klaassen, U., Gärtner, H., & Eckstein, D. (2010). Studying global change through investigation of the plastic responses of xylem anatomy in tree rings. *New Phytologist*, *185*(1), 42-53.

Frank, D., Büntgen, U., Böhm, R., Maugeri, M., & Esper, J. (2007). Warmer early instrumental measurements versus colder reconstructed temperatures: shooting at a moving target. *Quaternary Science Reviews*, *26*(25-28), 3298-3310.

Frank, D., & Esper, J. (2005). Characterization and climate response patterns of a high-elevation, multi-species tree-ring network in the European Alps. *Dendrochronologia*, *22*(2), 107-121.

Franke, J., Frank, D., Raible, C. C., Esper, J., & Brönnimann, S. (2013). Spectral biases in tree-ring climate proxies. *Nature Climate Change*, *3*(4), 360.

Fritts, H. C. (1976). *Tree rings and climate*. New York, NY, USA: Academic Press INC.

Fuentes, M., Salo, R., Björklund, J., Seftigen, K., Zhang, P., Gunnarson, B., ... & Linderholm, H. W. (2018). A 970-year-long summer temperature reconstruction from Rogen, west-central Sweden, based on blue intensity from tree rings. *The Holocene*, *28*(2), 254-266.

Fukazawa, K. (1992). Ultraviolet microscopy. In *Methods in lignin chemistry* (pp. 110-121). Springer, Berlin, Heidelberg.

Gartner, B. L. (1995). Patterns of xylem variation within a tree and their hydraulic and mechanical consequences. In *Plant stems* (pp. 125-149).

Gärtner, H., & Nievergelt, D. (2010). The core-microtome: a new tool for surface preparation on cores and time series analysis of varying cell parameters. *Dendrochronologia*, *28*(2), 85-92.

Gärtner, H., & Schweingruber, F. H. (2013). *Microscopic preparation techniques for plant stem analysis*. Verlag Dr. Kessel.

Gindl, W., Grabner, M., & Wimmer, R. (2000). The influence of temperature on latewood lignin content in treeline Norway spruce compared with maximum density and ring width. *Trees*, *14*(7), 409-414.

Grabner, M., Müller, U., Gierlinger, N., & Wimmer, R. (2005). Effects of heartwood extractives on mechanical properties of larch. *Iawa Journal*, *26*(2), 211-220.

Green, H. V. (1963). *Wood Quality Studies: A Scanning Microphotometer for Automatically Measuring and Recording Certain Wood Characteristics*. Pulp and Paper Research Institute of Canada.

Green, H. V. (1965). Wood characteristics IV: The study of wood characteristics by means of a photometric technique. Woodl. Res. Index Pulp Pap. *Res. Inst. Can*, (167).

Grissino-Mayer, H. D. (1997). Computer assisted, independent observer verification of tree-ring measurements. *Tree-Ring Bulletin*.

Guay, R., Gagnon, R., & Morin, H. (1992). A new automatic and interactive tree ring measurement system based on a line scan camera. *The Forestry Chronicle*, *68*(1), 138-141.

Guillet, S., Corona, C., Stoffel, M., Khodri, M., Lavigne, F., Ortega, P., ... & Davi, N. (2017). Climate response to the Samalas volcanic eruption in 1257 revealed by proxy records. *Nature geoscience*, *10*(2), 123.

Gunnarson, B. E., Josefsson, T., Linderholm, H. W., & Östlund, L. (2012). Legacies of pre-industrial land use can bias modern tree-ring climate calibrations. *Climate Research*, *53*(1), 63-76.

Gunnarson, B. E., Linderholm, H. W., & Moberg, A. (2011). Improving a tree-ring reconstruction from west-central Scandinavia: 900 years of warm-season temperatures. *Climate Dynamics*, *36*(1-2), 97-108.

Hacke, U. G., Lachenbruch, B., Pittermann, J., Mayr, S., Domec, J. C., & Schulte, P. J. (2015). The hydraulic architecture of conifers. In *Functional and ecological xylem anatomy* (pp. 39-75). Springer, Cham.

Haines, H. A., Gadd, P. S., Palmer, J., Olley, J. M., Hua, Q., & Heijnis, H. (2018). A new method for dating tree-rings in trees with faint, indeterminate ring boundaries using the Itrax core scanner. *Palaeogeography, Palaeoclimatology, Palaeoecology*, *497*, 234-243.

Hannrup, B., Danell, Ö., Ekberg, I., & Moëll, M. (2007). Relationships between wood density and tracheid dimensions in Pinus sylvestris L. *Wood and Fiber Science*, *33*(2), 173-181.

Hansen, J., Turk, R., Vogg, G., Heim, R., & Beck, E. (1997). Conifer carbohydrate physiology: updating classical views. *Trees: contributions to modern tree physiology*.

Harris, M. J. (1969). The use of beta rays in determining wood properties. N.Z.J. Sci. 12, 395-451.

Helama, S., Bégin, Y., Vartiainen, M., Peltola, H., Kolström, T., & Meriläinen, J. (2012). Quantifications of dendrochronological information from contrasting microdensitometric measuring circumstances of experimental wood samples. *Applied Radiation and Isotopes*, *70*(6), 1014-1023.

Helama, S., Vartiainen, M., Holopainen, J., Mäkelä, H. M., Kolström, T., & Meriläinen, J. (2014). A palaeotemperature record for the Finnish Lakeland based on microdensitometric variations in tree rings. *Geochronometria*, *41*(3), 265-277.

Helama, S., Vartiainen, M., Kolström, T., & Meriläinen, J. (2010). Dendrochronological investigation of wood extractives. *Wood science and technology*, *44*(2), 335-351.

Hevia, A., Sánchez-Salguero, R., Camarero, J. J., Buras, A., Sangüesa-Barreda, G., Galván, J. D., & Gutiérrez, E. (2018). Towards a better understanding of long-term wood-chemistry variations in old-growth forests: A case study on ancient Pinus uncinata trees from the Pyrenees. *Science of the Total Environment*, *625*, 220-232.

Holmes, R. L. (1983). Program COFECHA user's manual. *Laboratory of Tree-Ring Research, The University of Arizona, Tucson*.

Ifju, G., Wellwood, R. W., & Wilson, J. W. (1965). Relationship between certain intra-increment measurements in Douglas-fir. *Pulp Pap. Mag. Can*, *66*, T475-T483.

Ivkovich, M., & Koshy, M. P. (1997). Wood density measurement: comparison of X-ray, photometric, and morphometric methods. In *Proceedings of the 26th Biannual Meeting of the Canadian Tree Improvement Association (CTIA/IUFRO), International Workshop on Wood Quality, Québec, Que. Edited by SY Zhang, R. Gosselin, and G. Chauret. Forintek Canada Corp., Sainte-Foy, Que. pp. II* (pp. 55-58).

Jackson, J. B., Mourou, M., Labaune, J., Whitaker, J. F., Duling III, I. N., Williamson, S. L., ... & Mourou, G. A. (2009). Terahertz pulse imaging for tree-ring analysis: a preliminary study for dendrochronology applications. *Measurement Science and Technology*, *20*(7), 075502.

Jacobsen, A. L., Pratt, R. B., Ewers, F. W., & Davis, S. D. (2007). Cavitation resistance among 26 chaparral species of southern California. *Ecological Monographs*, *77*(1), 99-115.

Jacquin, P., Longuetaud, F., Leban, J. M., & Mothe, F. (2017). X-ray microdensitometry of wood: A review of existing principles and devices. *Dendrochronologia*, *42*, 42-50.

Jagels, R., & Telewski, F. W. (1990). Computer-aided image analysis of tree rings. *Methods of dendrochronology: Applications in the environmental sciences*, 76-93.

Jones, P. D., Briffa, K. R., Osborn, T. J., Lough, J. M., Van Ommen, T. D., Vinther, B. M., ... & Schmidt, G. A. (2009). High-resolution palaeoclimatology of the last millennium: a review of current status and future prospects. *The Holocene*, *19*(1), 3-49.

Jones, P. D., Briffa, K. R., & Schweingruber, F. H. (1995). Tree- ring evidence of the widespread effects of explosive volcanic eruptions. *Geophysical Research Letters*, *22*(11), 1333-1336.

Kaczka, R. J., Spyt, B., Janecka, K., & Musioł, R. (2017). The Blue Intensity proxy for> 400 years growing season temperature reconstruction from the Tatra Mountains. *TRACE*, *15*, 23-30.

Kaczka, R. J., Spyt, B., Janecka, K., Beil, I., Büntgen, U., Scharnweber, T., ... & Wilmking, M. (2018). Different maximum latewood density and blue intensity measurements techniques reveal similar results. *Dendrochronologia*, *49*, 94-101.

Kanowski, P., & Wright, J. (1985). Effects of resin extraction on optically determined density of Pinus caribaea Morelet and P. oocarpa Schiede. *The Commonwealth Forestry Review*, 29-31.

Katsevich, A. (2002). Theoretically exact filtered backprojection-type inversion algorithm for spiral CT. *SIAM Journal on Applied Mathematics*, *62*(6), 2012-2026.

Kellogg, R. M., Sastry, C. B. R., & Wellwood, R. W. (1975). Relationships between cell-wall composition and cell-wall density. *Wood and Fiber Science*, *7*(3), 170-177.

Kellogg, R. M., & Wangaard, F. F. (1969). Variation in the cell-wall density of wood. *Wood and Fiber Science*, *1*(3), 180-204.

Kennedy, R. W. (1966). Intra-increment variation and heritability of specific gravity, parallel-to-grain tensile strength, stiffness and tracheid length in clonal Norway spruce. *Tappi*, *49*(7), 292-296.

Kirdyanov, A. V., Vaganov, E. A., & Hughes, M. K. (2007). Separating the climatic signal from tree-ring width and maximum latewood density records. *Trees*, *21*(1), 37-44.

Klesse, S., Ziehmer, M., Rousakis, G., Trouet, V., & Frank, D. (2015). Synoptic drivers of 400 years of summer temperature and precipitation variability on Mt. Olympus, Greece. *Climate dynamics*, *45*(3-4), 807-824.

Klippel, L., Krusic, P. J., Konter, O., St. George, S., Trouet, V., & Esper, J. (2018). A 1200+ year reconstruction of temperature extremes for the northeastern Mediterranean region. *International Journal of Climatology*.

Kusec, D. J. (1972). Twin-blade saw for precision machining of increment cores. *Wood Fiber*, 4(1), 44-49.

Lachenbruch, B., & McCulloh, K. A. (2014). Traits, properties, and performance: how woody plants combine hydraulic and mechanical functions in a cell, tissue, or whole plant. *New Phytologist*, *204*(4), 747-764.

Larsson, L. (2014). CooRecorder and Cdendro programs of the CooRecorder/Cdendro package version 7.7.

Lee, T. C., Zwiers, F. W., & Tsao, M. (2008). Evaluation of proxy-based millennial reconstruction methods. *Climate Dynamics*, *31*(2-3), 263-281.

Lenz, O., Schär, E., & Schweingruber, F. H. (1976). Methodische Probleme bei der radiographisch-densitometrischen Bestimmung der Dichte und der Jahrringbreiten von Holz. *Holzforschung-International Journal of the Biology, Chemistry, Physics and Technology of Wood*, *30*(4), 114-123.

Lesnino, G. (1994). The laser-sandblasting method: a new method for the qualitative annual ring analysis of conifers. *Wood science and technology*, *28*(2), 159-171.

Levanič, T., Gričar, J., Gagen, M., Jalkanen, R., Loader, N. J., McCarroll, D., ... & Robertson, I. (2009). The climate sensitivity of Norway spruce [Picea abies (L.) Karst.] in the southeastern European Alps. *Trees*, *23*(1), 169.

Liang, H., Lyu, L., & Wahab, M. (2016). A 382-year reconstruction of August mean minimum temperature from tree-ring maximum latewood density on the southeastern Tibetan Plateau, China. *Dendrochronologia*, *37*, 1-8.

Liang, W., Heinrich, I., Simard, S., Helle, G., Liñán, I. D., & Heinken, T. (2013). Climate signals derived from cell anatomy of Scots pine in NE Germany. *Tree physiology*, *33*(8), 833-844.

Linderholm, H. W., Björklund, J., Seftigen, K., Gunnarson, B. E., & Fuentes, M. (2015). Fennoscandia revisited: a spatially improved tree-ring reconstruction of summer temperatures for the last 900 years. *Climate Dynamics*, *45*(3-4), 933-947.

Lloyd, J. A. (1978). Distribution of extractives in Pinus radiata earlywood and latewood. *New Zealand Journal of Forestry Science*, *8*(2), 288-294.

Luckman, B. H., Briffa, K. R., Jones, P. D., & Schweingruber, F. H. (1997). Tree-ring based reconstruction of summer temperatures at the Columbia Icefield, Alberta, Canada, AD 1073-1983. *The Holocene*, *7*(4), 375-389.

Luckman, B. H., & Wilson, R. J. S. (2005). Summer temperatures in the Canadian Rockies during the last millennium: a revised record. *Climate Dynamics*, *24*(2-3), 131-144.

Maes, S. L., Vannoppen, A., Altman, J., Van den Bulcke, J., Decocq, G., De Mil, T., ... & Vanhellemont, M. (2017). Evaluating the robustness of three ring-width measurement methods for growth release reconstruction. *Dendrochronologia*, *46*, 67-76.

Mannes, D., Lehmann, E., Cherubini, P., & Niemz, P. (2007). Neutron imaging versus standard X-ray densitometry as method to measure tree-ring wood density. *Trees*, *21*(6), 605-612.

Marian, J. E., & Stumbo, D. A. (1960). A new method of growth ring analysis and the determination of density by surface texture measurements. *Forest Science*, *6*(3), 276-91.

McCarroll, D., Loader, N. J., Jalkanen, R., Gagen, M. H., Grudd, H., Gunnarson, B. E., ... & Boettger, T. (2013). A 1200-year multiproxy record of tree growth and summer temperature at the northern pine forest limit of Europe. *The Holocene*, *23*(4), 471-484.

McCarroll, D., Pettigrew, E., Luckman, A., Guibal, F., & Edouard, J. L. (2002). Blue reflectance provides a surrogate for latewood density of high-latitude pine tree rings. *Arctic, Antarctic, and Alpine Research*, *34*(4), 450-453.

Melvin, T. (2004). *Historical growth rates and changing climatic sensitivity of boreal conifers* (Doctoral dissertation, University of East Anglia).

Melvin, T. M., & Briffa, K. R. (2008). A “signal-free” approach to dendroclimatic standardisation. *Dendrochronologia*, *26*(2), 71-86.

Melvin, T. M., Grudd, H., & Briffa, K. R. (2013). Potential bias in ‘updating’tree-ring chronologies using regional curve standardisation: Re-processing 1500 years of Torneträsk density and ring-width data. *The Holocene*, *23*(3), 364-373.

Mills, C. M., Crone, A., Wood, C., & Wilson, R. (2017). Dendrochronologically Dated Pine Buildings from Scotland: The SCOT2K Native Pine Dendrochronology Project. *Vernacular Architecture*, *48*(1), 23-43.

Moehring, D. M., Grano, C. X., & Bassett, J. R. (1975). Xylem development of loblolly pine during irrigation and simulated drought. *Res. Pap. SO-110. New Orleans, LA: US Department of Agriculture, Forest Service, Southern Forest Experiment Station. 8 p.*, *110*.

Moschler Jr, W. W., & Winistorfer, P. M. (1990). Direct scanning densitometry: an effect of sample heterogeneity and aperture area. *Wood and fiber science*, *22*(1), 31-38.

Mothe, F., Duchanois, G., Zannier, B., & Leban, J. M. (1998). Analyse microdensitométrique appliquée au bois: méthode de traitement des données utilisée à l'Inra-ERQB (programme Cerd). In *Annales des sciences forestières* (Vol. 55, No. 3, pp. 301-313). EDP Sciences.

Nehrbass- Ahles, C., Babst, F., Klesse, S., Nötzli, M., Bouriaud, O., Neukom, R., ... & Frank, D. (2014). The influence of sampling design on tree- ring- based quantification of forest growth. *Global change biology*, *20*(9), 2867-2885.

Niklas, K. J. (1995). Plant height and the properties of some herbaceous stems. *Annals of Botany*, *75*(2), 133-142.

Nock, C. A., Geihofer, D., Grabner, M., Baker, P. J., Bunyavejchewin, S., & Hietz, P. (2009). Wood density and its radial variation in six canopy tree species differing in shade-tolerance in western Thailand. *Annals of botany*, *104*(2), 297-306.

O'Donnell, A. J., Allen, K. J., Evans, R. M., Cook, E. R., Trouet, V., & Baker, P. J. (2016). Wood density provides new opportunities for reconstructing past temperature variability from southeastern Australian trees. *Global and Planetary Change*, *141*, 1-11.

Olano, J. M., Linares, J. C., García-Cervigón, A. I., Arzac, A., Delgado, A., & Rozas, V. (2014). Drought-induced increase in water-use efficiency reduces secondary tree growth and tracheid wall thickness in a Mediterranean conifer. *Oecologia*, *176*(1), 273-283.

Osborn, T. J., & Jones, P. (2014). The CRUTEM4 land-surface air temperature data set: construction, previous versions and dissemination via Google Earth. *Earth System Science Data*, *6*(1), 61-68.

Österreicher, A., Weber, G., Leuenberger, M., & Nicolussi, K. (2015). Exploring blue intensity-comparison of blue intensity and MXD data from Alpine spruce trees. In *TRACE–Tree Rings in Archaeology, Climatology and Ecology* (Vol. 13, pp. 56-61).

Pacheco, A., Camarero, J. J., Ribas, M., Gazol, A., Gutierrez, E., & Carrer, M. (2018). Disentangling the climate-driven bimodal growth pattern in coastal and continental Mediterranean pine stands. *Science of The Total Environment*, *615*, 1518-1526.

Panyushkina, I. P., Hughes, M. K., Vaganov, E. A., & Munro, M. A. (2003). Summer temperature in northeastern Siberia since 1642 reconstructed from tracheid dimensions and cell numbers of Larix cajanderi. *Canadian Journal of Forest Research*, *33*(10), 1905-1914.

Park, W. K., & Telewski, F. W. (1993). Measuring maximum latewood density by image analysis at the cellular level. *Wood and Fiber Science*, *25*(4), 326-332.

Parker, M. L., & Henoch, W. E. S. (1971). The use of Engelmann spruce latewood density for dendrochronological purposes. *Canadian Journal of Forest Research*, *1*(2), 90-98.

Parker, M. L., & Jozsa, L. A. (1973). Dendrochronological investigations along the Mackenzie, Liard and South Nahanni rivers, NWT Part I: Using tree damage to date landslides, ice jamming and flooding. *Hydrological aspects of northern pipeline development. Information Canada. Ottawa, Cat*, (R27-172), 313-464.

Parker, M. L., Taylor, F. G., Doyle, T. W., Foster, B. E., Cooper, C., & West, D. C. (1985). *Radiation densitometry in tree-ring analysis: a review and procedure manual* (No. ORNL/FPO-85/73). Oak Ridge National Lab., TN (USA).

Pereira, H., Graça, J., & Rodrigues, J. C. (2003). Wood chemistry in relation to quality. *Wood quality and its biological basis*, 53-86.

Peters, R. L., Balanzategui, D., Hurley, A. G., von Arx, G., Prendin, A. L., Cuny, H. E., ... & Fonti, P. (2018). RAPTOR: Row and position tracheid organizer in R. *Dendrochronologia*, *47*, 10-16.

Peters, R. L., Groenendijk, P., Vlam, M., & Zuidema, P. A. (2015). Detecting long- term growth trends using tree rings: a critical evaluation of methods. *Global change biology*, *21*(5), 2040-2054.

Petit, G., & Crivellaro, A. (2014). Comparative axial widening of phloem and xylem conduits in small woody plants. *Trees*, *28*(3), 915-921.

Plomion, C., Leprovost, G., & Stokes, A. (2001). Wood formation in trees. *Plant physiology*, *127*(4), 1513-1523.

Polge, H. (1963). Une nouvelle méthode de détermination de la texture du bois-L'analyse densitométrique de clichés radiographiques. Ann. Ec. Natl. Eaux Forets St. Rech. Exper. 20(4), 530-581.

Polge, H. (1965a). *New investigations on wood by densitometric analysis of radiographs*. Inst. Natl. Rech. Agron., Cant. Natl. Rech. For., Nancy, France.

Polge, H. (1965b). The use of curves of density variation for the study of environmental factors and in particular of climatic factors. *International Union of Forestry Research Organizations Proceedings*, *2*, 1-8.

Polge, H. (1966). Établissement des courbes de variation de la densité du bois par exploration densitométrique de radiographies d'échantillons prélevés à la tarière sur des arbres vivants: applications dans les domaines Technologique et Physiologique. In *Annales des sciences forestières* (Vol. 23, No. 1, pp. I-206). EDP Sciences.

Polge, H. (1970). The use of X-ray densitometric methods in dendrochronology. *Tree-ring bulletin*.

Polge, H. (1978). Fifteen years of wood radiation densitometry. *Wood Science and Technology*, *12*(3), 187-196.

Poorter, L. (2008). The relationships of wood-, gas-and water fractions of tree stems to performance and life history variation in tropical trees. *Annals of botany*, *102*(3), 367-375.

Pratt, R. B., Jacobsen, A. L., Ewers, F. W., & Davis, S. D. (2007). Relationships among xylem transport, biomechanics and storage in stems and roots of nine Rhamnaceae species of the California chaparral. *New Phytologist*, *174*(4), 787-798.

Prendin, A. L., Petit, G., Carrer, M., Fonti, P., Björklund, J., & von Arx, G. (2017). New research perspectives from a novel approach to quantify tracheid wall thickness. *Tree physiology*, *37*(7), 976-983.

Pritzkow, C., Heinrich, I., Grudd, H., & Helle, G. (2014). Relationship between wood anatomy, tree-ring widths and wood density of Pinus sylvestris L. and climate at high latitudes in northern Sweden. *Dendrochronologia*, *32*(4), 295-302.

Rathgeber, C. B., Decoux, V., & Leban, J. M. (2006). Linking intra-tree-ring wood density variations and tracheid anatomical characteristics in Douglas fir (Pseudotsuga menziesii (Mirb.) Franco). *Annals of Forest Science*, *63*(7), 699-706.

Raven, P. H., Evert, R. F., & Eichhorn, S. E. (2005). *Biology of plants*. Macmillan.

Rinn, F. R. A. N. K. (1996). Resistographic visualization of tree-ring density variations. *Tree Rings, Environment, and Humanity. Radiocarbon*, *1996*, 871-878.

Rosner, S., Světlík, J., Andreassen, K., Børja, I., Dalsgaard, L., Evans, R., ... & Solberg, S. (2013). Wood density as a screening trait for drought sensitivity in Norway spruce. *Canadian Journal of Forest Research*, *44*(2), 154-161.

Rossi, S., Deslauriers, A., & Anfodillo, T. (2006). Assessment of cambial activity and xylogenesis by microsampling tree species: an example at the Alpine timberline. *Iawa Journal*, *27*(4), 383-394.

Rydval, M., Druckenbrod, D. L., Svoboda, M., Trotsiuk, V., Janda, P., Mikoláš, M., ... & Wilson, R. (2018). Influence of sampling and disturbance history on climatic sensitivity of temperature-limited conifers. *The Holocene*, *28*(10), 1574-1587.

Rydval, M., Gunnarson, B. E., Loader, N. J., Cook, E. R., Druckenbrod, D. L., & Wilson, R. (2017b). Spatial reconstruction of Scottish summer temperatures from tree rings. *International Journal of Climatology*, *37*(3), 1540-1556.

Rydval, M., Larsson, L. Å., McGlynn, L., Gunnarson, B. E., Loader, N. J., Young, G. H., & Wilson, R. (2014). Blue intensity for dendroclimatology: should we have the blues? Experiments from Scotland. *Dendrochronologia*, *32*(3), 191-204.

Rydval, M., Loader, N. J., Gunnarson, B. E., Druckenbrod, D. L., Linderholm, H. W., Moreton, S. G., ... & Wilson, R. (2017a). Reconstructing 800 years of summer temperatures in Scotland from tree rings. *Climate Dynamics*, *49*(9-10), 2951-2974.

Savidge, R. A. (2003). Tree growth and wood quality. *Wood quality and its biological basis*, 1-29.

Scharnweber, T., Hevia, A., Buras, A., van der Maaten, E., & Wilmking, M. (2016). Common trends in elements? Within-and between-tree variations of wood-chemistry measured by X-ray fluorescence—A dendrochemical study. *Science of the Total Environment*, *566*, 1245-1253.

Schinker, M. G., Hansen, N., & Spiecker, H. (2003). High-frequency densitometry-a new method for the rapid evaluation of wood density variations. *IAWA Journal*, *24*(3), 231-239.

Schneider, L., & Gärtner, H. (2013). The advantage of using a starch based non-Newtonian fluid to prepare micro sections. *Dendrochronologia*, *31*(3), 175-178.

Schneider, L., Smerdon, J. E., Büntgen, U., Wilson, R. J., Myglan, V. S., Kirdyanov, A. V., & Esper, J. (2015). Revising midlatitude summer temperatures back to AD 600 based on a wood density network. *Geophysical Research Letters*, *42*(11), 4556-4562.

Schnell, G. R., & Sell, J. (1989). Image-analytical measurement of cell wall portion and wood density-method of preparation and measurement technique. *Holz als Roh-und Werkstoff (Germany, FR)*.

Schweingruber, F. H. (1988). *Tree rings: Basics and Applications of Dendrochronology*. Kluwer Academic Publishers, Dordrecht, Netherlands; Boston, Massachusetts, USA. 276 S.

Schweingruber, F. H., Bartholin, T., Schaur, E., & Briffa, K. R. (1988). Radiodensitometric-dendroclimatological conifer chronologies from Lapland (Scandinavia) and the Alps (Switzerland). *Boreas*, *17*(4), 559-566.

Schweingruber, F. H., Börner, A., & Schulze, E. D. (2011). *Atlas of stem anatomy in herbs, shrubs and trees* (Vol. 1). Springer Science & Business Media.

Schweingruber, F. H., & Briffa, K. R. (1996). Tree-ring density networks for climate reconstruction. In *Climatic variations and forcing mechanisms of the last 2000 years* (pp. 43-66). Springer, Berlin, Heidelberg.

Schweingruber, F. H., Briffa, K. R., & Nogler, P. (1993). A tree-ring densitometric transect from Alaska to Labrador. *International Journal of Biometeorology*, *37*(3), 151-169.

Schweingruber, F. H., Fritts, H. C., Bräker, O. U., Drew, L. G., & Schär, E. (1978). The X-ray technique as applied to dendroclimatology. *Tree-Ring Bulletin*.

Seidl, R., Thom, D., Kautz, M., Martin-Benito, D., Peltoniemi, M., Vacchiano, G., ... & Lexer, M. J. (2017). Forest disturbances under climate change. *Nature Climate Change*, *7*(6), 395.

Sheppard, P. R. (2007). Overcoming extraneous wood color variation during low-magnification reflected-light image analysis of conifer tree rings. *Wood and fiber science*, *31*(2), 106-115.

Sheppard, P. R., Graumlich, L. J., & Conkey, L. E. (1996). Reflected-light image analysis of conifer tree rings for reconstructing climate. *The Holocene*, *6*(1), 62-68.

Sheppard, P., & Singavarapu, S. (2006). Solving the ‘magnification irony’ in reflected-light image analysis of conifer tree-rings using a microscope. *Journal of Imaging Science and Technology*, *50*(3), 304-308.

Sheppard, P. R., & Wiedenhoeft, A. (2007). An advancement in removing extraneous color from wood for low-magnification reflected-light image analysis of conifer tree rings. *Wood and fiber science. Vol. 39, no. 1 (2007): pages 173-183.*

Siau, J. F. (1984). *Transport processes in wood* (Vol. 2). Springer Science & Business Media.

Sidorova, O. V., Saurer, M., Myglan, V. S., Eichler, A., Schwikowski, M., Kirdyanov, A. V., ... & Siegwolf, R. T. (2012). A multi-proxy approach for revealing recent climatic changes in the Russian Altai. *Climate Dynamics*, *38*(1-2), 175-188.

Simard, S., Giovannelli, A., Treydte, K., Traversi, M. L., King, G. M., Frank, D., & Fonti, P. (2013). Intra-annual dynamics of non-structural carbohydrates in the cambium of mature conifer trees reflects radial growth demands. *Tree Physiology*, *33*(9), 913-923.

Sitch, S., Huntingford, C., Gedney, N., Levy, P. E., Lomas, M., Piao, S. L., ... & Jones, C. D. (2008). Evaluation of the terrestrial carbon cycle, future plant geography and climate‐ carbon cycle feedbacks using five Dynamic Global Vegetation Models (DGVMs). *Global Change Biology*, *14*(9), 2015-2039.

Sperry, J. S., Hacke, U. G., & Pittermann, J. (2006). Size and function in conifer tracheids and angiosperm vessels. *American journal of botany*, *93*(10), 1490-1500.

Spyt, R., Kaczka, R. J., Ksciuczyk, K., & Zawadzka, M. (2016). Zastosowanie intensywności odbicia światła niebieskiego w datowaniu drewna historycznego. *Studia i Materiały Centrum Edukacji Przyrodniczo-Leśnej*, *18*(3 [48]).

Stamm, A. J., & Sanders, H. T. (1966). Specific gravity of wood substance of loblolly pine as affected by chemical composition. *Tappi*, *49*(9), 397.

Starheim, C. C., Smith, D. J., & Prowse, T. D. (2013). Multi‐ century reconstructions of Pacific salmon abundance from climate‐ sensitive tree rings in west central British Columbia, Canada. *Ecohydrology*, *6*(2), 228-240.

Stine, A. R., & Huybers, P. (2014). Arctic tree rings as recorders of variations in light availability. *Nature communications*, *5*, 3836.

Stine, A. R., & Huybers, P. (2017). Implications of Liebig's law of the minimum for tree-ring reconstructions of climate. *Environmental Research Letters*, *12*(11), 114018.

Stoffel, M., Khodri, M., Corona, C., Guillet, S., Poulain, V., Bekki, S., ... & Beniston, M. (2015). Estimates of volcanic-induced cooling in the Northern Hemisphere over the past 1,500 years. *Nature Geoscience*, *8*(10), 784.

Stokes, M. A., & Smiley, T. L. (1968). Tree-ring dating. *Tree-ring dating*.

Sun, Y., Wang, L., Chen, J., & Duan, J. (2012). Reconstructing mean maximum temperatures of May–August from tree-ring maximum density in North Da Hinggan Mountains, China. *Chinese science bulletin*, *57*(16), 2007-2014.

Taylor, K. E., Stouffer, R. J., & Meehl, G. A. (2012). An overview of CMIP5 and the experiment design. *Bulletin of the American Meteorological Society*, *93*(4), 485-498.

Telewski, F. W., Burns, J. M., & Ulan, L. (1986). A thin-section technique for x-ray densitometric analysis of narrow tree-ring series. Pages 651-657 *in* G. C. Jacoby and J. Hornbeck, eds. Proceedings of the international symposium on ecological aspects of tree-ring analysis. August 17-21, 1986, Marymount College, Tarrytown, NY.

Tene, A., Tobin, B., Dyckmans, J., Ray, D., Black, K., & Nieuwenhuis, M. (2011). Assessment of tree response to drought: validation of a methodology to identify and test proxies for monitoring past environmental changes in trees. *Tree physiology*, *31*(3), 309-322.

Thetford, R. D., D'Arrigo, R. D., & Jacoby, G. C. (1991). An image analysis system for determining densitometric and ring-width time series. *Canadian Journal of Forest Research*, *21*(10), 1544-1549.

Trachsel, M., Kamenik, C., Grosjean, M., McCarroll, D., Moberg, A., Brázdil, R., ... & Friedrich, M. (2012). Multi-archive summer temperature reconstruction for the European Alps, AD 1053–1996. *Quaternary Science Reviews*, *46*, 66-79.

Trouet, V., Panayotov, M. P., Ivanova, A., & Frank, D. (2012). A pan-European summer teleconnection mode recorded by a new temperature reconstruction from the northeastern Mediterranean (ad 1768–2008). *The Holocene*, *22*(8), 887-898.

Tsoumis, G. (1964). Microscopic measurement of the amount of cell wall substance in wood and its relationship to specific gravity. *Tappi*, *47*(11), 675-677.

Tyree, M. T., & Zimmermann, M. H. (2002). Hydraulic architecture of whole plants and plant performance. In *Xylem structure and the ascent of sap* (pp. 175-214). Springer, Berlin, Heidelberg.

Uggla, C., Magel, E., Moritz, T., & Sundberg, B. (2001). Function and dynamics of auxin and carbohydrates during earlywood/latewood transition in Scots pine. *Plant physiology*, *125*(4), 2029-2039.

Vaganov, E. A., Anchukaitis, K. J., & Evans, M. N. (2011). How well understood are the processes that create dendroclimatic records? A mechanistic model of the climatic control on conifer tree-ring growth dynamics. In *Dendroclimatology* (pp. 37-75). Springer, Dordrecht.

Vaganov, E. A., Hughes, M. K., & Shashkin, A.V. (2006). *Growth Dynamics of Conifer Tree Rings: Images of Past and Future Environments*. Springer.

Vaganov, E. A., Schulze, E. D., Skomarkova, M. V., Knohl, A., Brand, W. A., & Roscher, C. (2009). Intra-annual variability of anatomical structure and δ 13 C values within tree rings of spruce and pine in alpine, temperate and boreal Europe. *Oecologia*, *161*(4), 729-745.

Van den Bulcke, J., Wernersson, E. L., Dierick, M., Van Loo, D., Masschaele, B., Brabant, L., ... & Hendriks, C. L. L. (2014). 3D tree-ring analysis using helical X-ray tomography. *Dendrochronologia*, *32*(1), 39-46.

Vanhellemont, M., Sousa-Silva, R., Maes, S. L., Van den Bulcke, J., Hertzog, L., De Groote, S. R., ... & Verheyen, K. (2019). Distinct growth responses to drought for oak and beech in temperate mixed forests. *Science of The Total Environment*, *650*, 3017-3026.

Vannoppen, A., Boeckx, P., De Mil, T., Kint, V., Ponette, Q., Van den Bulcke, J., ... & Muys, B. (2018). Climate driven trends in tree biomass increment show asynchronous dependence on tree-ring width and wood density variation. *Dendrochronologia*, *48*, 40-51.

Vannoppen, A., Maes, S., Kint, V., De Mil, T., Ponette, Q., Van Acker, J., ... & Muys, B. (2017). Using X-ray CT based tree-ring width data for tree growth trend analysis. *Dendrochronologia*, *44*, 66-75.

von Arx, G., & Carrer, M. (2014). ROXAS–A new tool to build centuries-long tracheid-lumen chronologies in conifers. *Dendrochronologia*, *32*(3), 290-293.

von Arx, G., Crivellaro, A., Prendin, A. L., Čufar, K., & Carrer, M. (2016). Quantitative wood anatomy—practical guidelines. *Frontiers in plant science*, *7*, 781.

Von Storch, H., Zorita, E., Jones, J. M., Dimitriev, Y., González-Rouco, F., & Tett, S. F. (2004). Reconstructing past climate from noisy data. *Science*, *306*(5696), 679-682.

Wang, L., Payette, S., & Bégin, Y. (2002). Relationships between anatomical and densitometric characteristics of black spruce and summer temperature at tree line in northern Quebec. *Canadian Journal of Forest Research*, *32*(3), 477-486.

Wigley, T. M., Briffa, K. R., & Jones, P. D. (1984). On the average value of correlated time series, with applications in dendroclimatology and hydrometeorology. *Journal of climate and Applied Meteorology*, *23*(2), 201-213.

Williamson, G. B., & Wiemann, M. C. (2010). Measuring wood specific gravity… correctly. *American Journal of Botany*, *97*(3), 519-524.

Wilson, R., Anchukaitis, K., Briffa, K. R., Büntgen, U., Cook, E., D'arrigo, R., ... & Hegerl, G. (2016). Last millennium northern hemisphere summer temperatures from tree rings: Part I: The long term context. *Quaternary Science Reviews*, *134*, 1-18.

Wilson, R., D'Arrigo, R., Andreu-Hayles, L., Oelkers, R., Wiles, G., Anchukaitis, K., & Davi, N. (2017a). Experiments based on blue intensity for reconstructing North Pacific temperatures along the Gulf of Alaska. *Climate of the Past*, *13*(8), 1007-1022.

Wilson, R. J., Esper, J., & Luckman, B. H. (2004). Utilising historical tree-ring data for dendroclimatology: a case study from the Bavarian Forest, Germany. *Dendrochronologia*, *21*(2), 53-68.

Wilson, R., Rao, R., Rydval, M., Wood, C., Larsson, L. Å., & Luckman, B. H. (2014). Blue Intensity for dendroclimatology: The BC blues: A case study from British Columbia, Canada. *The Holocene*, *24*(11), 1428-1438.

Wilson, R., Wilson, D., Rydval, M., Crone, A., Büntgen, U., Clark, S., ... & Linderholm, H. W. (2017). Facilitating tree-ring dating of historic conifer timbers using Blue Intensity. *Journal of Archaeological Science*, *78*, 99-111.

Wimmer, R. (1995). Intra-annual cellular characteristics and their implications for modeling softwood density. *Wood and fiber science*, *27*(4), 413-420.

Wodzicki, T. J. (1971). Mechanism of xylem differentiation in Pinus silvestris L. *Journal of Experimental Botany*, 670-687.

Wood, L. J., Smith, D. J., & Demuth, M. N. (2011). Extending the Place Glacier mass-balance record to AD 1585, using tree rings and wood density. *Quaternary Research*, *76*(3), 305-313.

Wood, L. J., & Smith, D. J. (2013). Climate and glacier mass balance trends from AD 1780 to present in the Columbia Mountains, British Columbia, Canada. *The Holocene*, *23*(5), 739-748.

Wood, L. J., & Smith, D. J. (2015). Intra-annual dendroclimatic reconstruction for northern British Columbia, Canada, using wood properties. *Trees*, *29*(2), 461-474.

Woodcock, D., & Shier, A. (2002). Wood specific gravity and its radial variations: the many ways to make a tree. *Trees*, *16*(6), 437-443.

Woods, F. W., & Lawhon, W. T. (1974). Gamma densitometry of increment cores. *Forest Science*, *20*(3), 269-271.

Wright, I. J., Ackerly, D. D., Bongers, F., Harms, K. E., Ibarra-Manriquez, G., Martinez-Ramos, M., ... & Poorter, L. (2006). Relationships among ecologically important dimensions of plant trait variation in seven Neotropical forests. *Annals of Botany*, *99*(5), 1003-1015.

Xing, P., Zhang, Q. B., & Lv, L. X. (2014). Absence of late-summer warming trend over the past two and half centuries on the eastern Tibetan Plateau. *Global and Planetary Change*, *123*, 27-35.

Yamaguchi, D. K. (1991). A simple method for cross-dating increment cores from living trees. *Canadian Journal of Forest Research*, *21*(3), 414-416.

Yanosky, T. M., & Robinove, C. J. (1986). Digital image measurement of the area and anatomical structure of tree rings. *Canadian journal of botany*, *64*(12), 2896-2902.

Yanosky, T. M., Robinove, C. J., & Clark, R. G. (1986). Progress in the image analysis of tree rings. In Jacoby, G.C. and Hornbeck, J.W., compilers, Proceedings, International Symposium on Ecological Aspects of Tree-Ring Analysis, Springfield, Virginia: National Technical Information Service, 658-65.

Yasue, K., Funada, R., Kobayashi, O., & Ohtani, J. (2000). The effects of tracheid dimensions on variations in maximum density of Picea glehnii and relationships to climatic factors. *Trees*, *14*(4), 223-229.

Yuan, Y. J., Zhang, T. W., Wei, W. S., Nievergelt, D., Verstege, A., Yu, S. L., ... & Esper, J. (2013). Development of tree-ring maximum latewood density chronologies for the western Tien Shan Mountains, China: Influence of detrending method and climate response. *Dendrochronologia*, *31*(3), 192-197.

Zhang, P., Björklund, J., & Linderholm, H. W. (2015). The influence of elevational differences in absolute maximum density values on regional climate reconstructions. *Trees*, *29*(4), 1259-1271.

Zhang, P., Linderholm, H. W., Gunnarson, B. E., Björklund, J., & Chen, D. (2016). 1200 years of warm-season temperature variability in central Scandinavia inferred from tree-ring density. *Climate of the Past*, *12*(6), 1297-1312.

Ziaco, E., Biondi, F., Rossi, S., & Deslauriers, A. (2016). Environmental drivers of cambial phenology in Great Basin bristlecone pine. *Tree physiology*, *36*(7), 818-831.

Zobel, B. J., & Van Buijtenen, J. P. (1989). Wood variation and wood properties. In *Wood Variation* (pp. 1-32). Springer, Berlin, Heidelberg.

Abbreviations

BI – Blue intensity (name for a technique that quantifies reflected or absorbed light from wood samples)
CRU – Climate Research Unit (University of East Anglia)
CT – Computed Tomography
DHXCT – Software (dendrochronological helical X-ray computed tomography)
mxd – Maximum latewood density derived with any technique, even those that do not initially calibrate values to density
MXD – Maximum latewood density derived with X-ray based techniques
Rbar – Average pair-wise correlation between tree-ring series
RCS – Regional Curve Standardization (A method to neutralize age related information but conserve average growth rates in tree-ring indices)
ρ – Density
$\rho_{M/V}$ – Density from mass divided by volume
ρ_{Micro} – Density from indirect techniques based on light transmission or reflection, or anatomical dimensions

Figure 1.

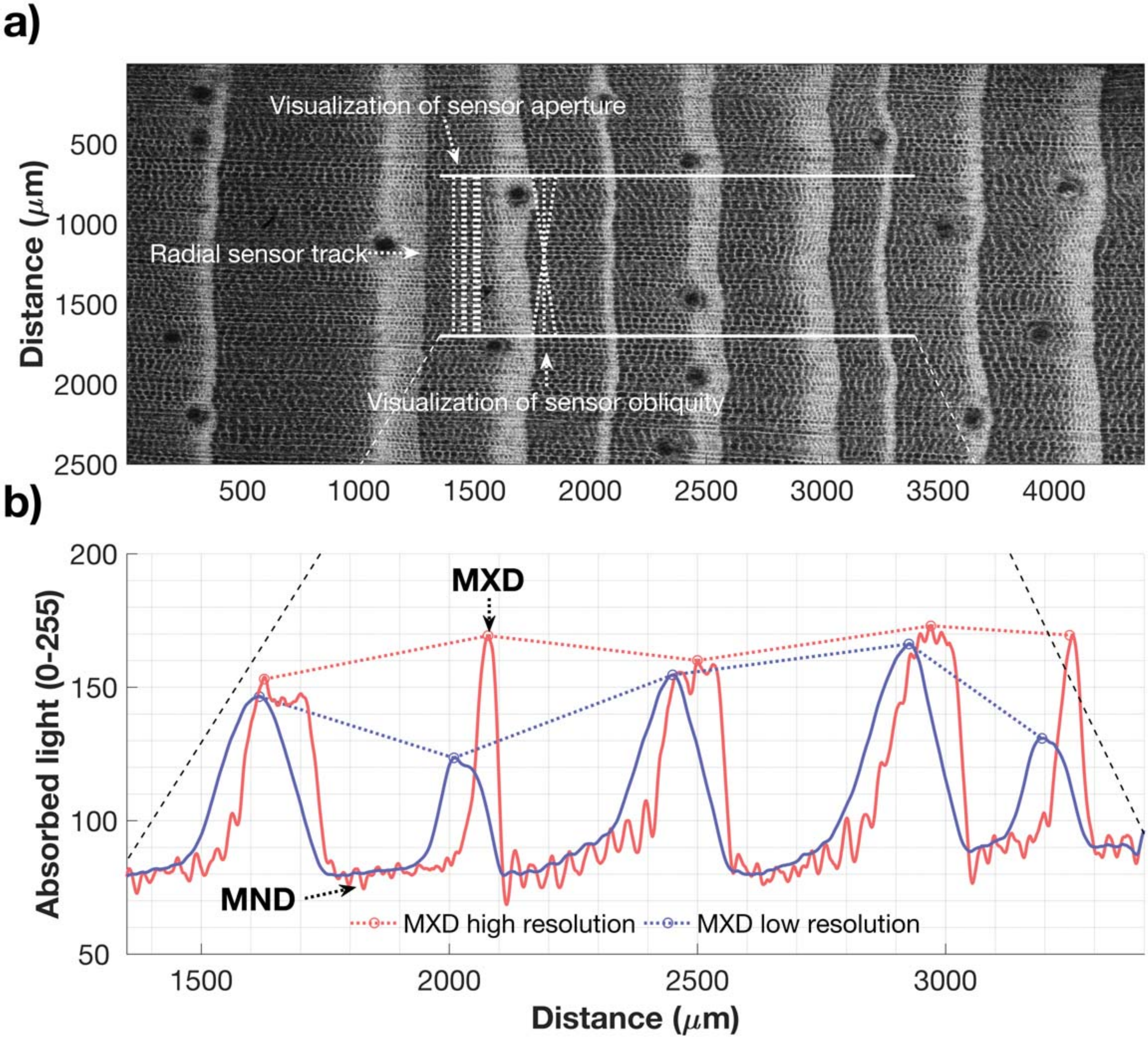

a)
Visualization of sensor aperture
Radial sensor track
Visualization of sensor obliquity
Distance (μm)
500
1000
1500
2000
2500
500
1000
1500
2000
2500
3000
3500
4000
b)
MXD
MND
MXD high resolution
MXD low resolution
Absorbed light (0-255)
200
150
100
50
1500
2000
2500
3000
Distance (μm)

Figure 2.

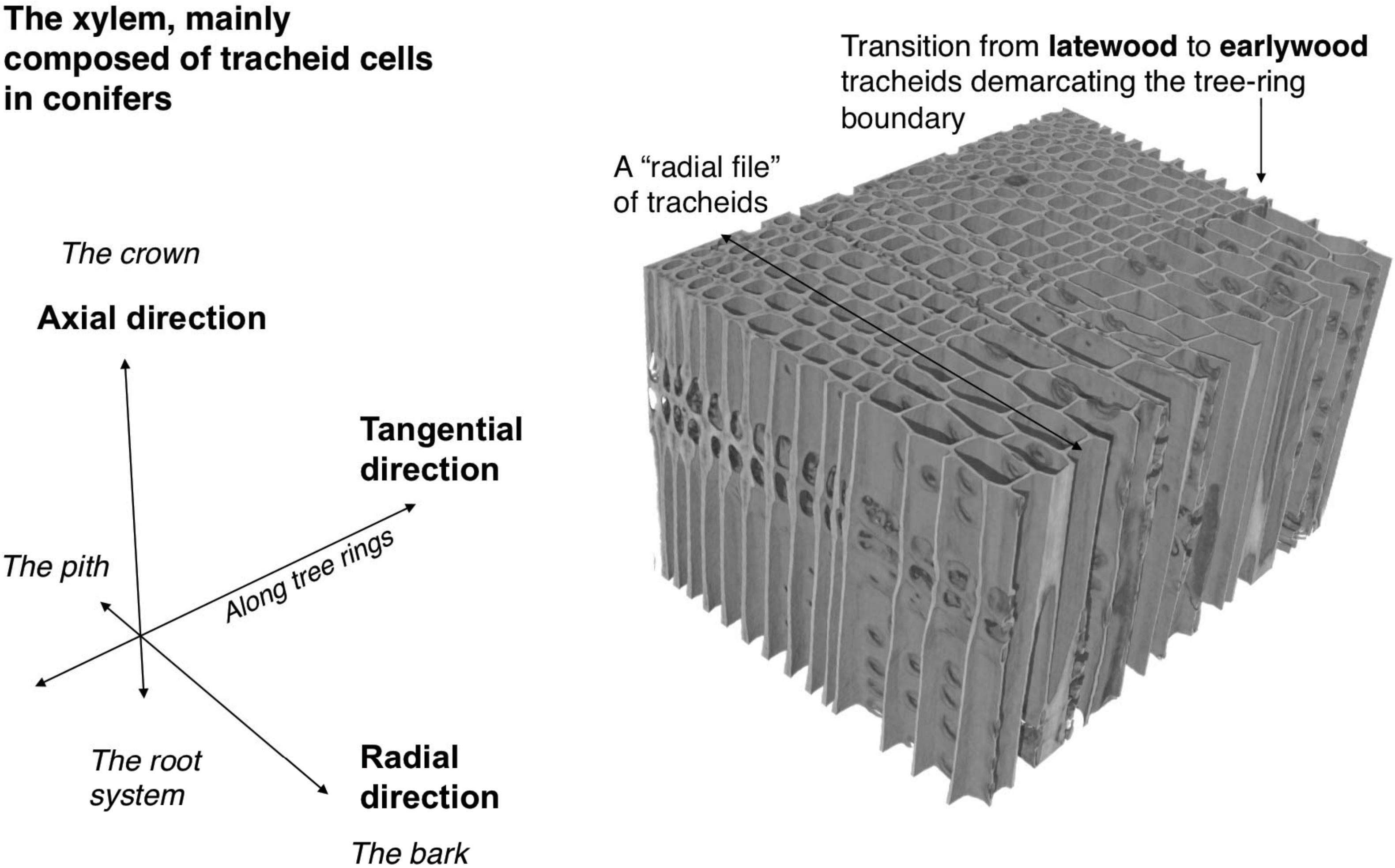
The xylem, mainly composed of tracheid cells in conifers
Transition from **latewood** to **earlywood** tracheids demarcating the tree-ring boundary
A “radial file” of tracheids
The crown
Axial direction
Tangential direction
Along tree rings
The pith
The root system
Radial direction
The bark

Figure3.

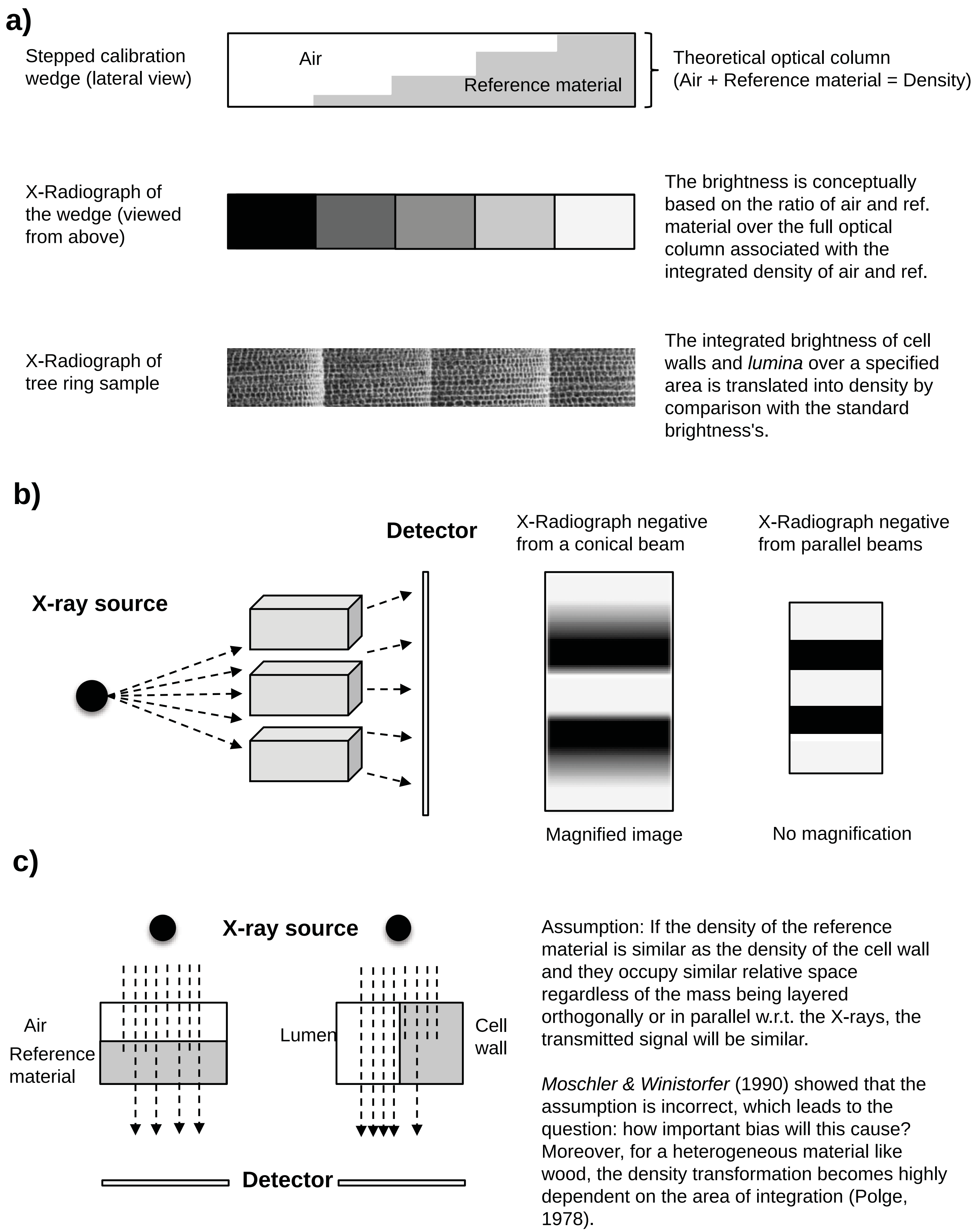
a)
Stepped calibration wedge (lateral view)
Air
Reference material
Theoretical optical column (Air + Reference material = Density)
X-Radiograph of the wedge (viewed from above)
The brightness is conceptually based on the ratio of air and ref. material over the full optical column associated with the integrated density of air and ref.
X-Radiograph of tree ring sample
The integrated brightness of cell walls and lumina over a specified area is translated into density by comparison with the standard brightness's.
b)
X-ray source
Detector
X-Radiograph negative from a conical beam
X-Radiograph negative from parallel beams
Magnified image
No magnification
c)
X-ray source
Air
Reference material
Lumen
Cell wall
Detector
Assumption: If the density of the reference material is similar as the density of the cell wall and they occupy similar relative space regardless of the mass being layered orthogonally or in parallel w.r.t. the X-rays, the transmitted signal will be similar.
Moschler & Winistorfer (1990) showed that the assumption is incorrect, which leads to the question: how important bias will this cause? Moreover, for a heterogeneous material like wood, the density transformation becomes highly dependent on the area of integration (Polge, 1978).

Figure 4.

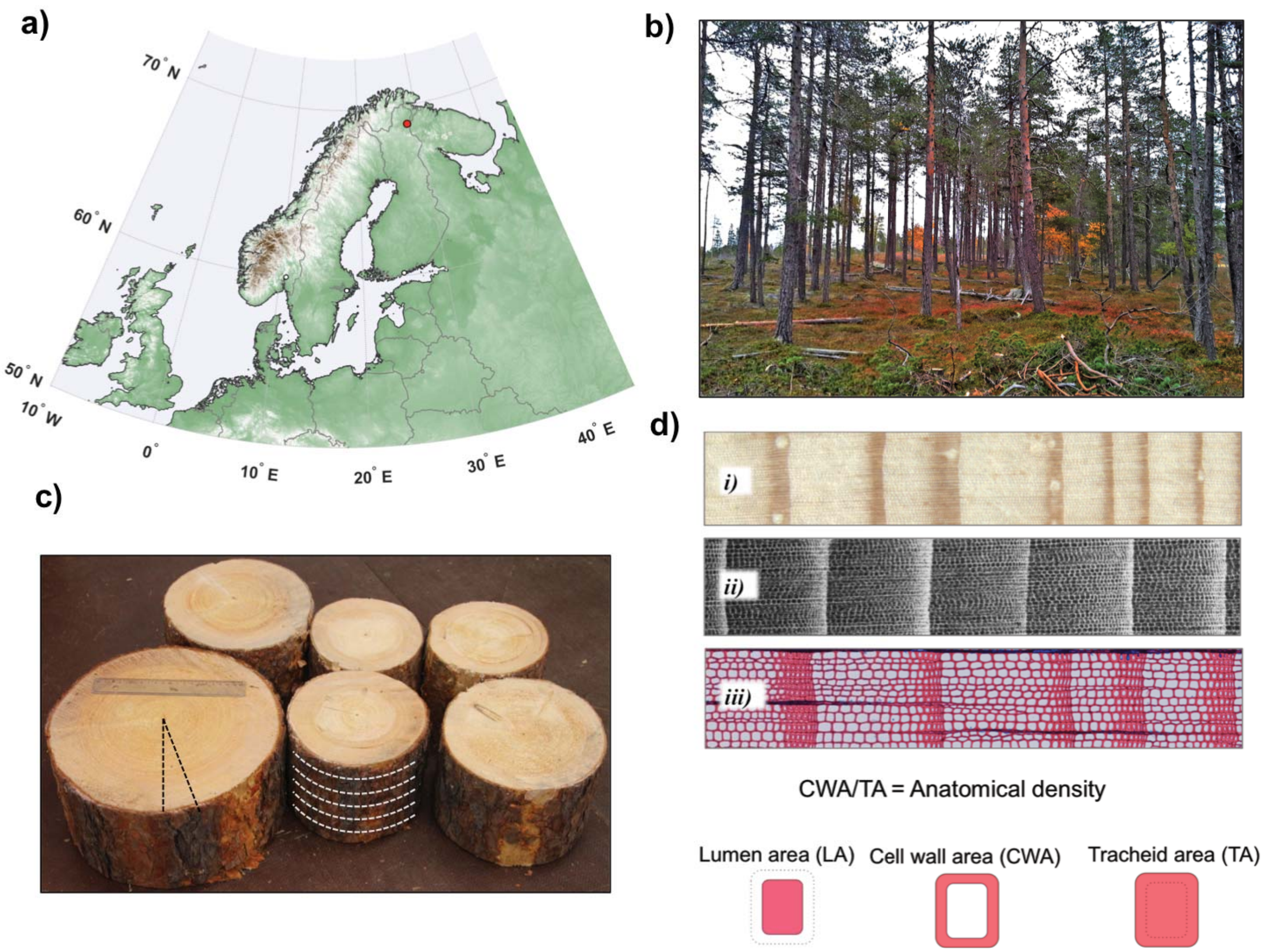

a)
70° N
60° N
50° N
10° W
0°
10° E
20° E
30° E
40° E
b)
c)
d)
i)
ii)
iii)
CWA/TA = Anatomical density
Lumen area (LA)
Cell wall area (CWA)
Tracheid area (TA)

Figure 5.

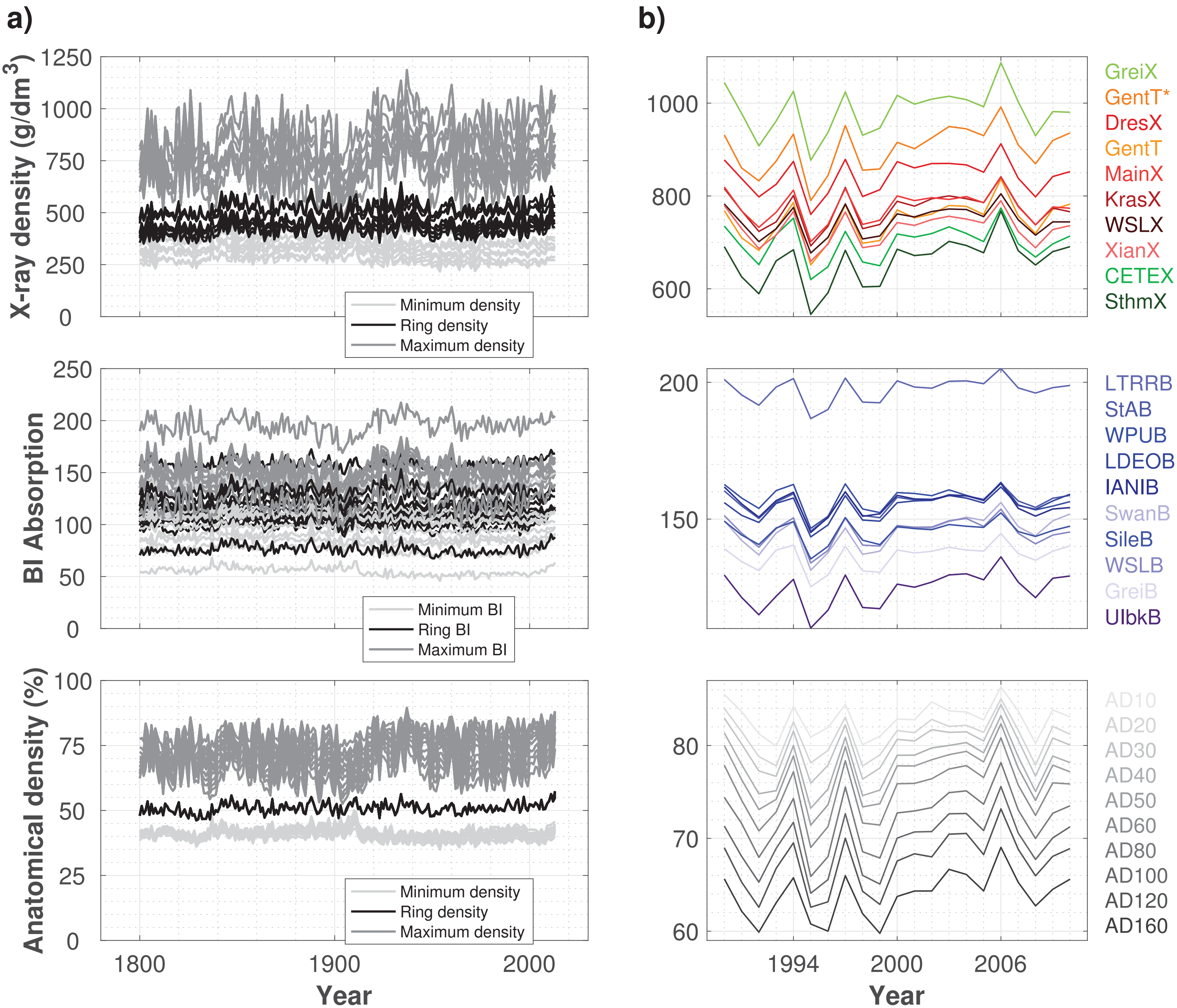

a)
b)
X-ray density (g/dm^3)
Minimum density
Ring density
Maximum density
BI Absorption
Minimum BI
Ring BI
Maximum BI
Anatomical density (%)
Minimum density
Ring density
Maximum density
Year
GreiX
GentT*
DresX
GentT
MainX
KrasX
WSLX
XianX
CETEX
SthmX
LTRRB
StAB
WPUB
LDEOB
IANIB
SwanB
SileB
WSLB
GreiB
UlbkB
AD10
AD20
AD30
AD40
AD50
AD60
AD80
AD100
AD120
AD160
Year

Figure 6.

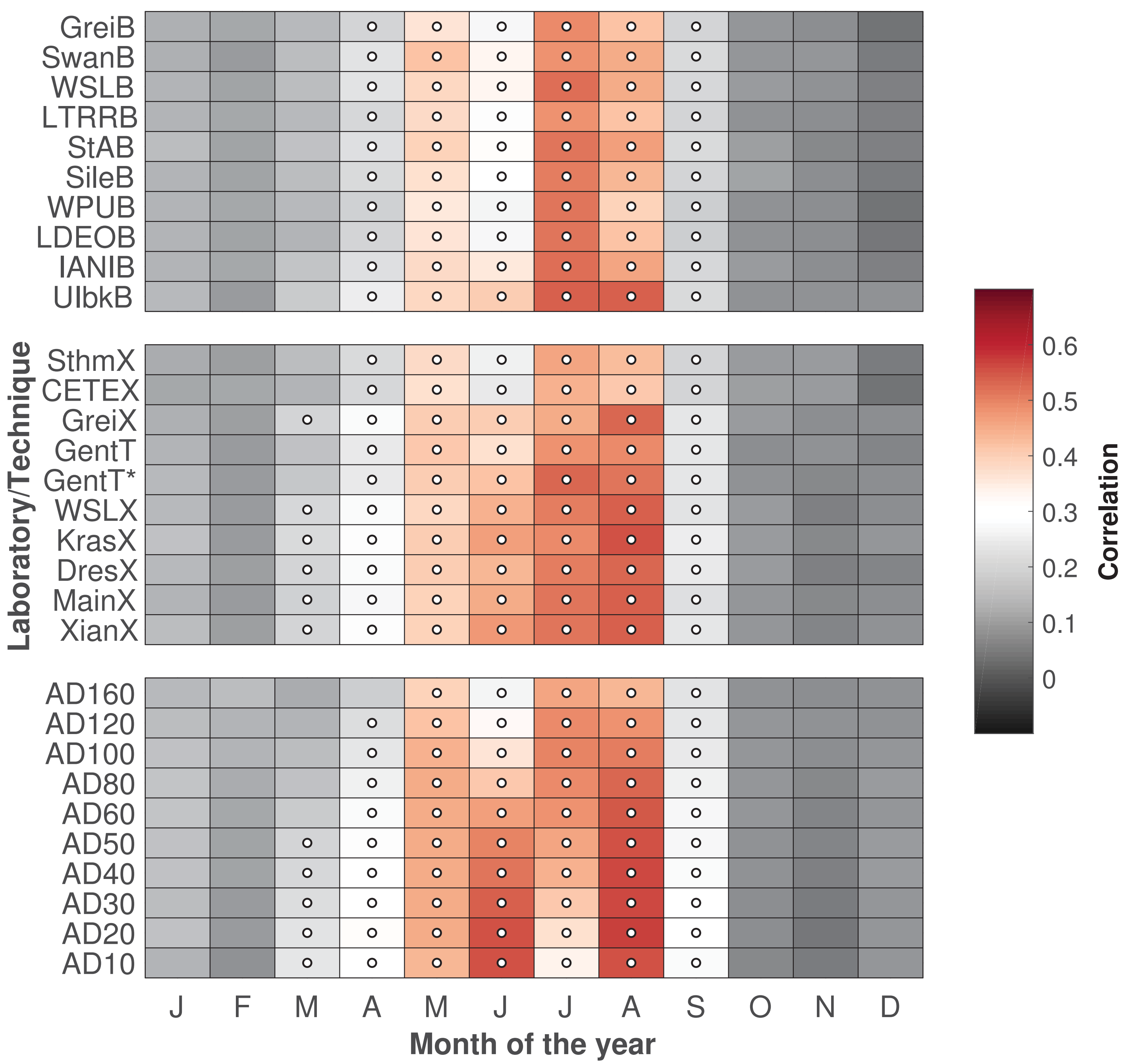

GreiB
SwanB
WSLB
LTRRB
StAB
SileB
WPUB
LDEOB
IANIB
UIbkB
SthmX
CETEX
GreiX
GentT
GentT*
WSLX
KrasX
DresX
MainX
XianX
AD160
AD120
AD100
AD80
AD60
AD50
AD40
AD30
AD20
AD10
Laboratory/Technique
J F M A M J J A S O N D
Month of the year
Correlation
0.6
0.5
0.4
0.3
0.2
0.1
0

Figure 7.

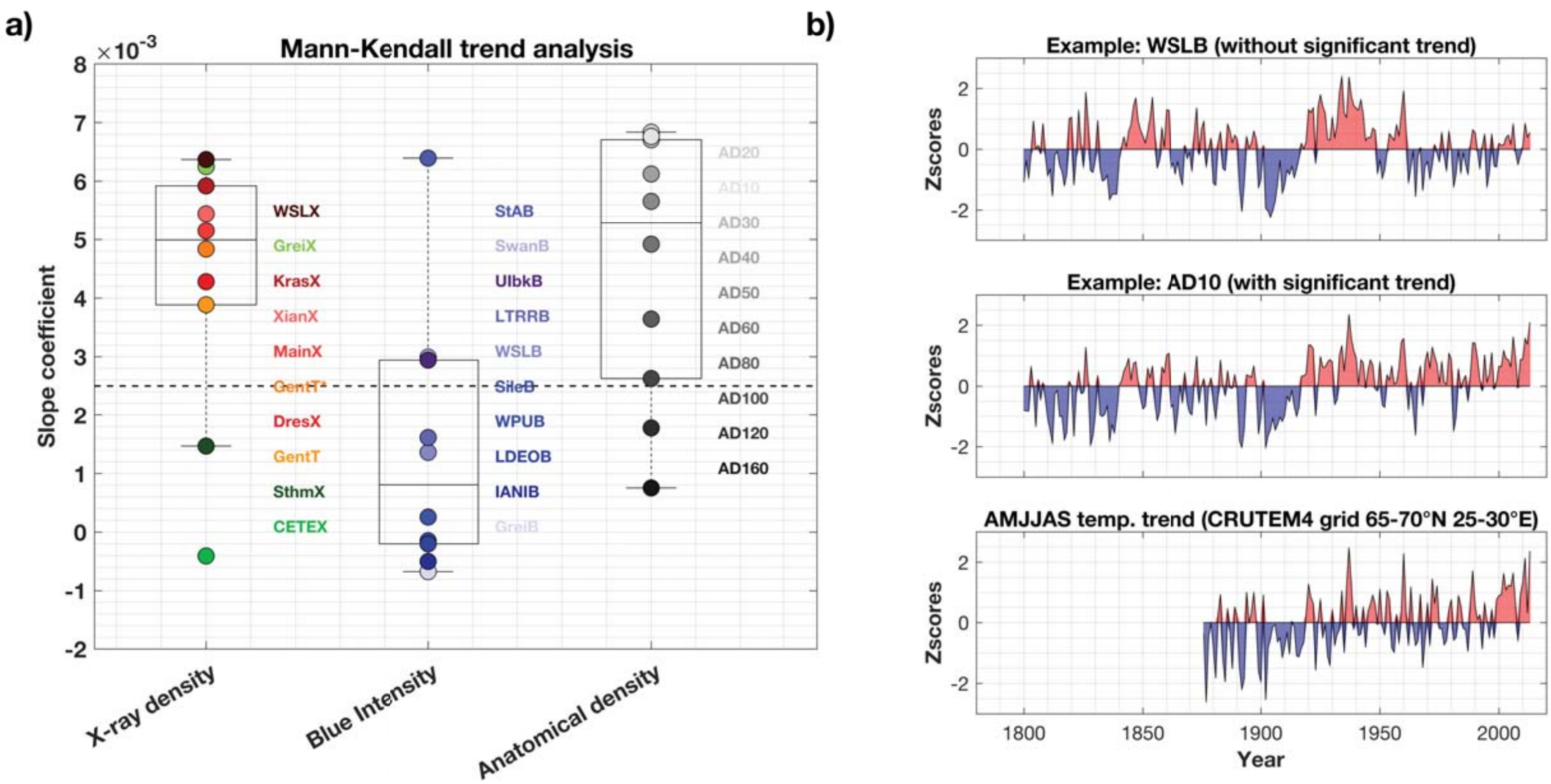

a)
Mann-Kendall trend analysis
×10^-3
Slope coefficient
X-ray density
Blue Intensity
Anatomical density
WSLX
GreiX
KrasX
XianX
MainX
GentT*
DresX
GentT
SthmX
CETEX
StAB
SwanB
UlbkB
LTRRB
WSLB
SileB
WPUB
LDEOB
IANIB
GreiB
AD20
AD10
AD30
AD40
AD50
AD60
AD80
AD100
AD120
AD160
b)
Example: WSLB (without significant trend)
Example: AD10 (with significant trend)
AMJJAS temp. trend (CRUTEM4 grid 65-70°N 25-30°E)
Zscores
Year

Figure 8.

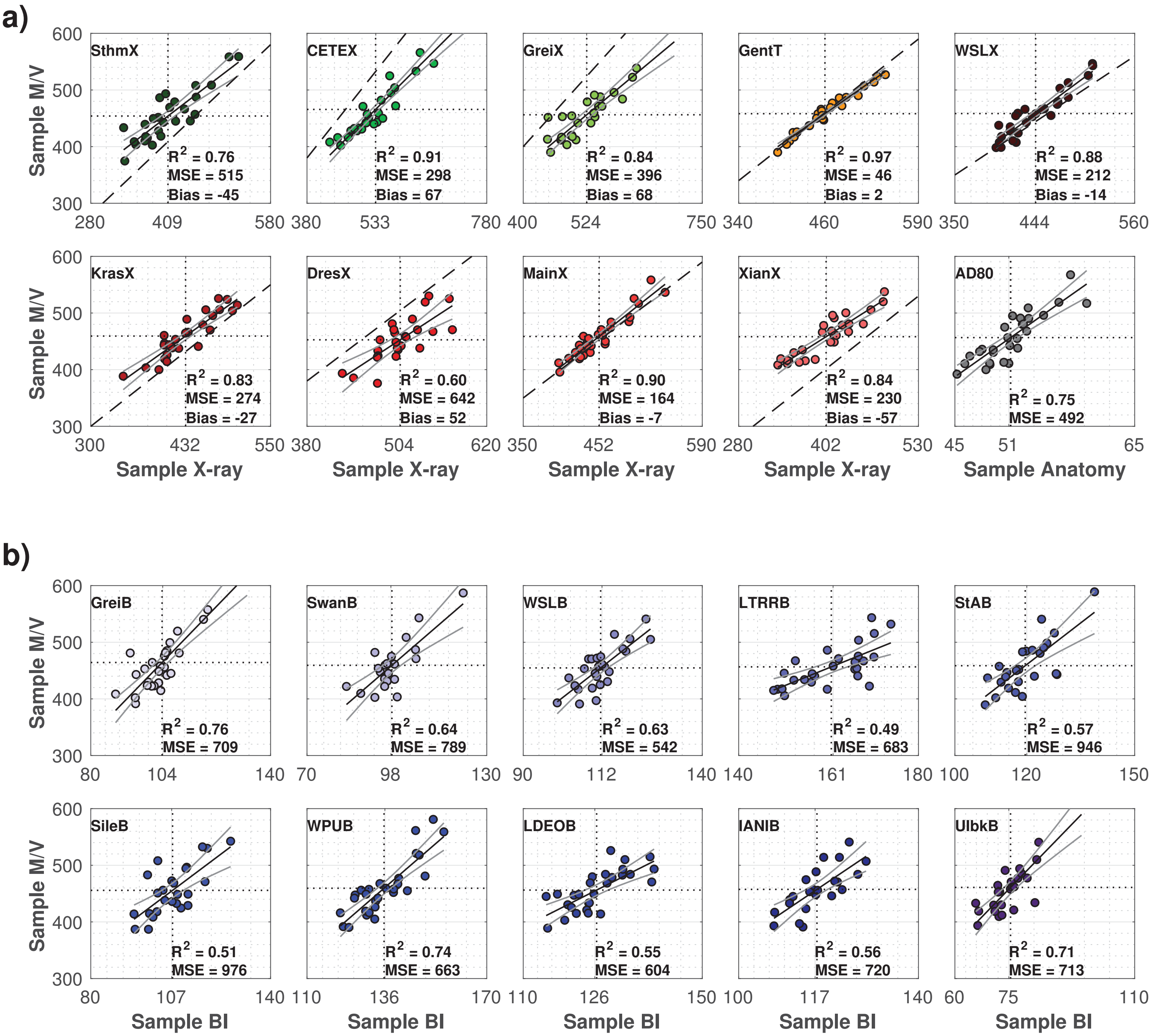

a)
b)
Sample M/V
Sample X-ray
Sample Anatomy
Sample BI
SthmX
R^2 = 0.76
MSE = 515
Bias = -45
CETEX
R^2 = 0.91
MSE = 298
Bias = 67
GreiX
R^2 = 0.84
MSE = 396
Bias = 68
GentT
R^2 = 0.97
MSE = 46
Bias = 2
WSLX
R^2 = 0.88
MSE = 212
Bias = -14
KrasX
R^2 = 0.83
MSE = 274
Bias = -27
DresX
R^2 = 0.60
MSE = 642
Bias = 52
MainX
R^2 = 0.90
MSE = 164
Bias = -7
XianX
R^2 = 0.84
MSE = 230
Bias = -57
AD80
R^2 = 0.75
MSE = 492
GreiB
R^2 = 0.76
MSE = 709
SwanB
R^2 = 0.64
MSE = 789
WSLB
R^2 = 0.63
MSE = 542
LTRRB
R^2 = 0.49
MSE = 683
StAB
R^2 = 0.57
MSE = 946
SileB
R^2 = 0.51
MSE = 976
WPUB
R^2 = 0.74
MSE = 663
LDEOB
R^2 = 0.55
MSE = 604
IANIB
R^2 = 0.56
MSE = 720
UlbkB
R^2 = 0.71
MSE = 713

Figure 9.

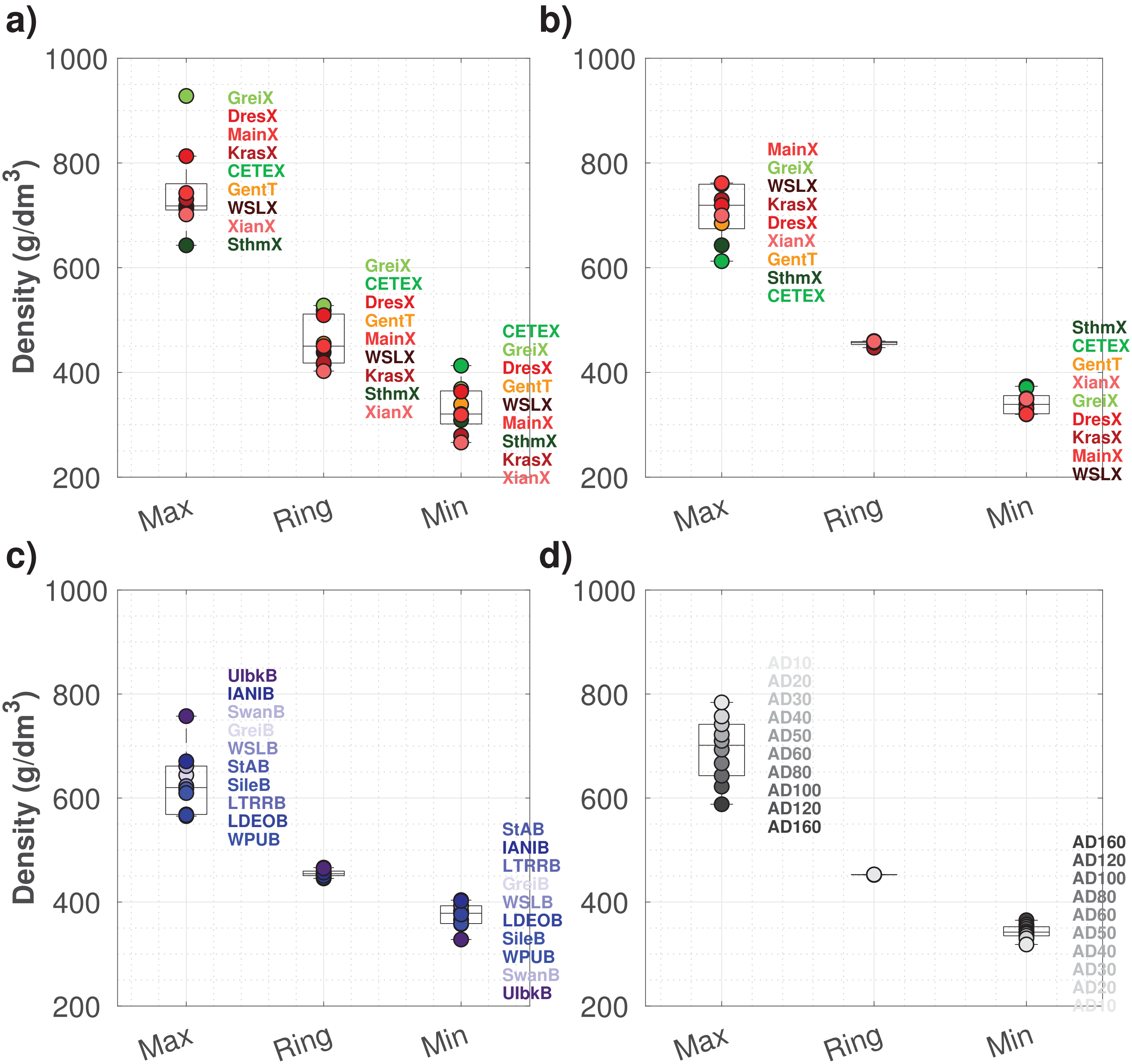

a)
b)
c)
d)
Density (g/dm^3)
1000
800
600
400
200
Max
Ring
Min
GreiX
DresX
MainX
KrasX
CETEX
GentT
WSLX
XianX
SthmX
UlbkB
IANIB
SwanB
GreiB
WSLB
StAB
SileB
LTRRB
LDEOB
WPUB
AD10
AD20
AD30
AD40
AD50
AD60
AD80
AD100
AD120
AD160

Figure 10.

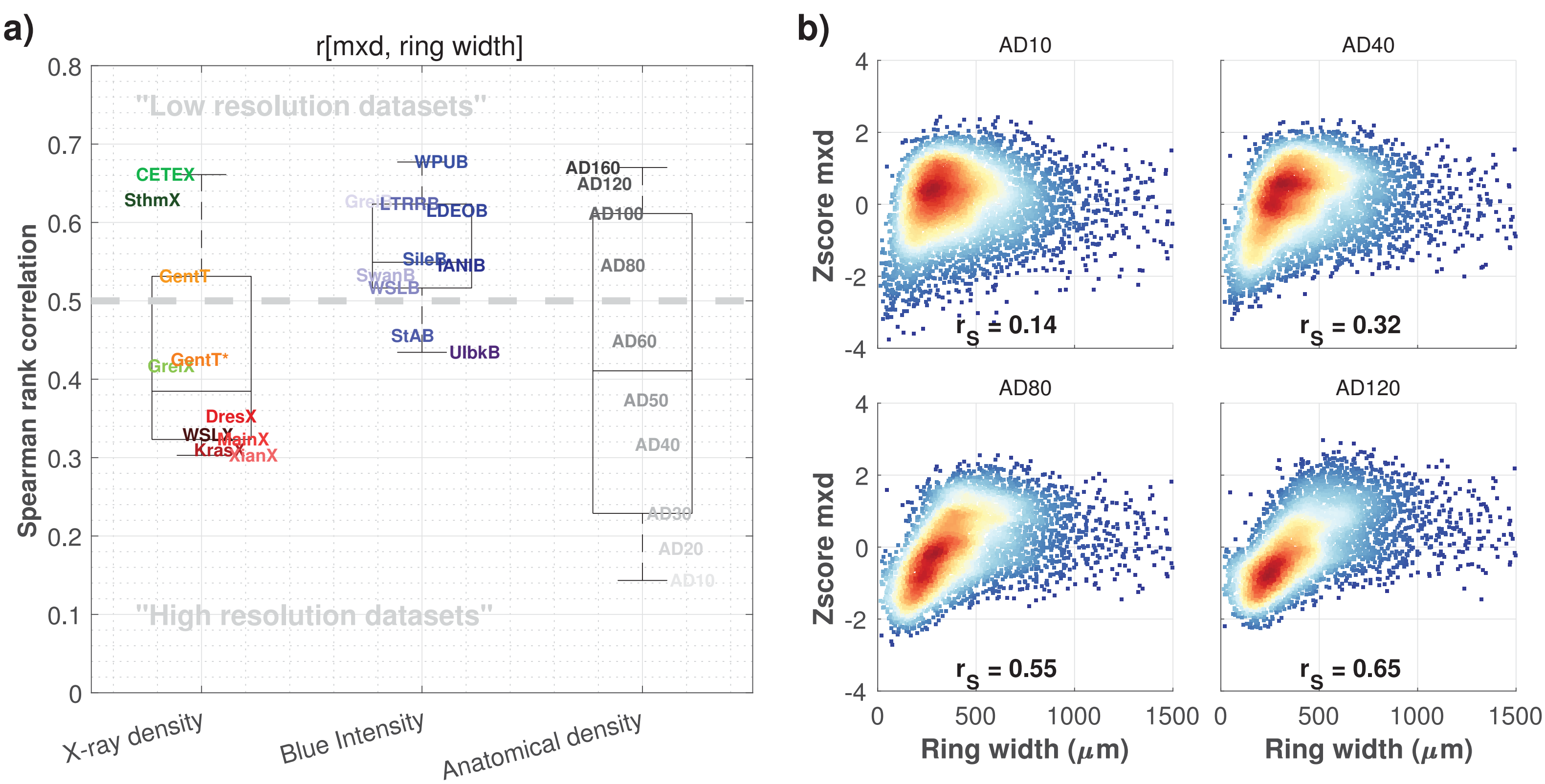
a)
r[mxd, ring width]
"Low resolution datasets"
"High resolution datasets"
Spearman rank correlation
CETEX
SthmX
GentT
GentT*
GreiX
DresX
WSLX
MainX
KrasX
XianX
WPUB
LTRRB
EDEOB
SileB
TANIB
SwanB
WSLB
StAB
UlbkB
AD160
AD120
AD100
AD80
AD60
AD50
AD40
AD30
AD20
AD10
X-ray density
Blue Intensity
Anatomical density
b)
AD10
AD40
AD80
AD120
Zscore mxd
r_S = 0.14
r_S = 0.32
r_S = 0.55
r_S = 0.65
Ring width (μm)

Figure 11.

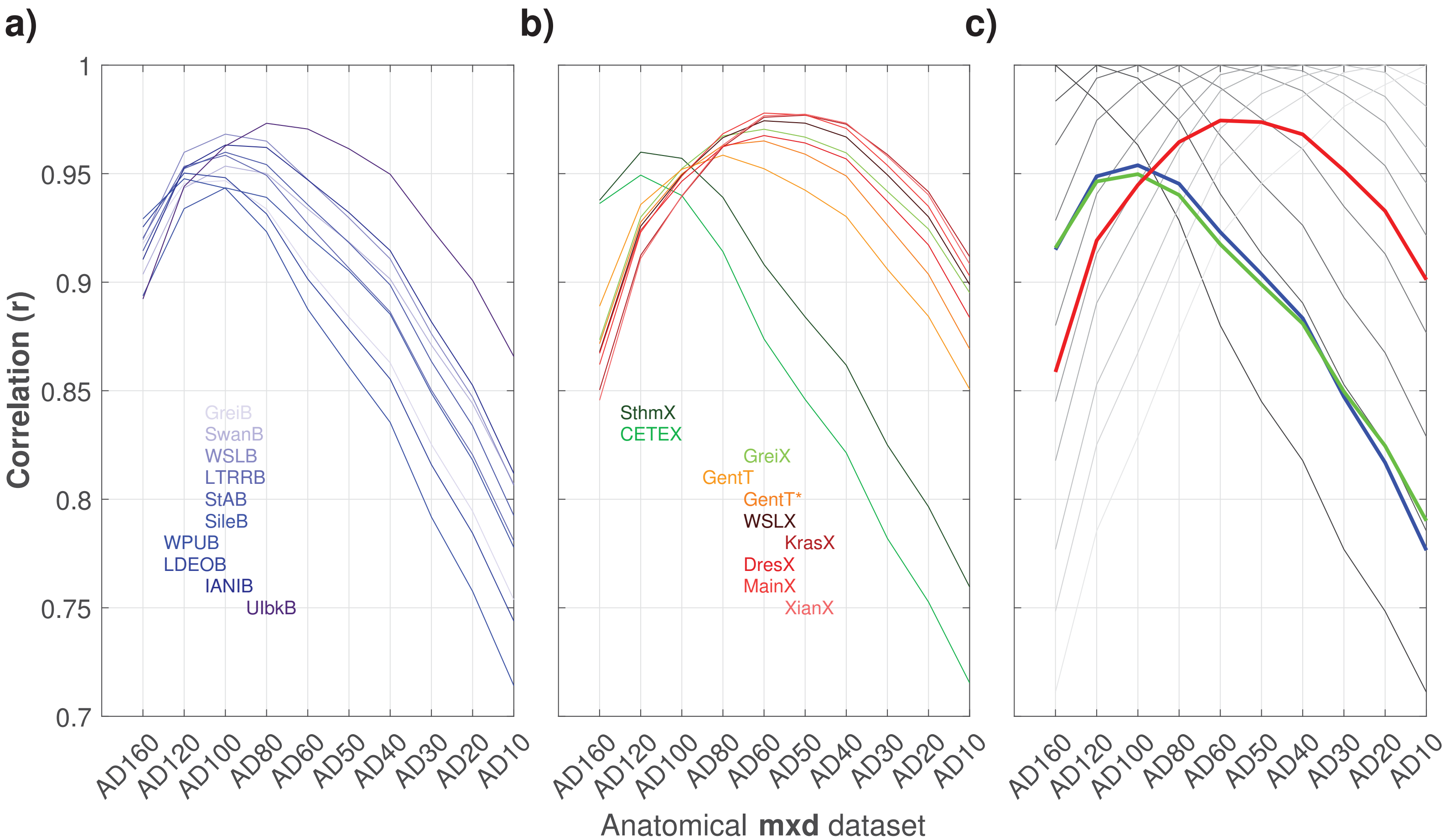

a)
b)
c)
Correlation (r)
1
0.95
0.9
0.85
0.8
0.75
0.7
AD160
AD120
AD100
AD80
AD60
AD50
AD40
AD30
AD20
AD10
GreiB
SwanB
WSLB
LTRRB
StAB
SileB
WPUB
LDEOB
IANIB
UIbkB
SthmX
CETEX
GreiX
GentT
GentT*
WSLX
KrasX
DresX
MainX
XianX
Anatomical mxd dataset

Figure 12.

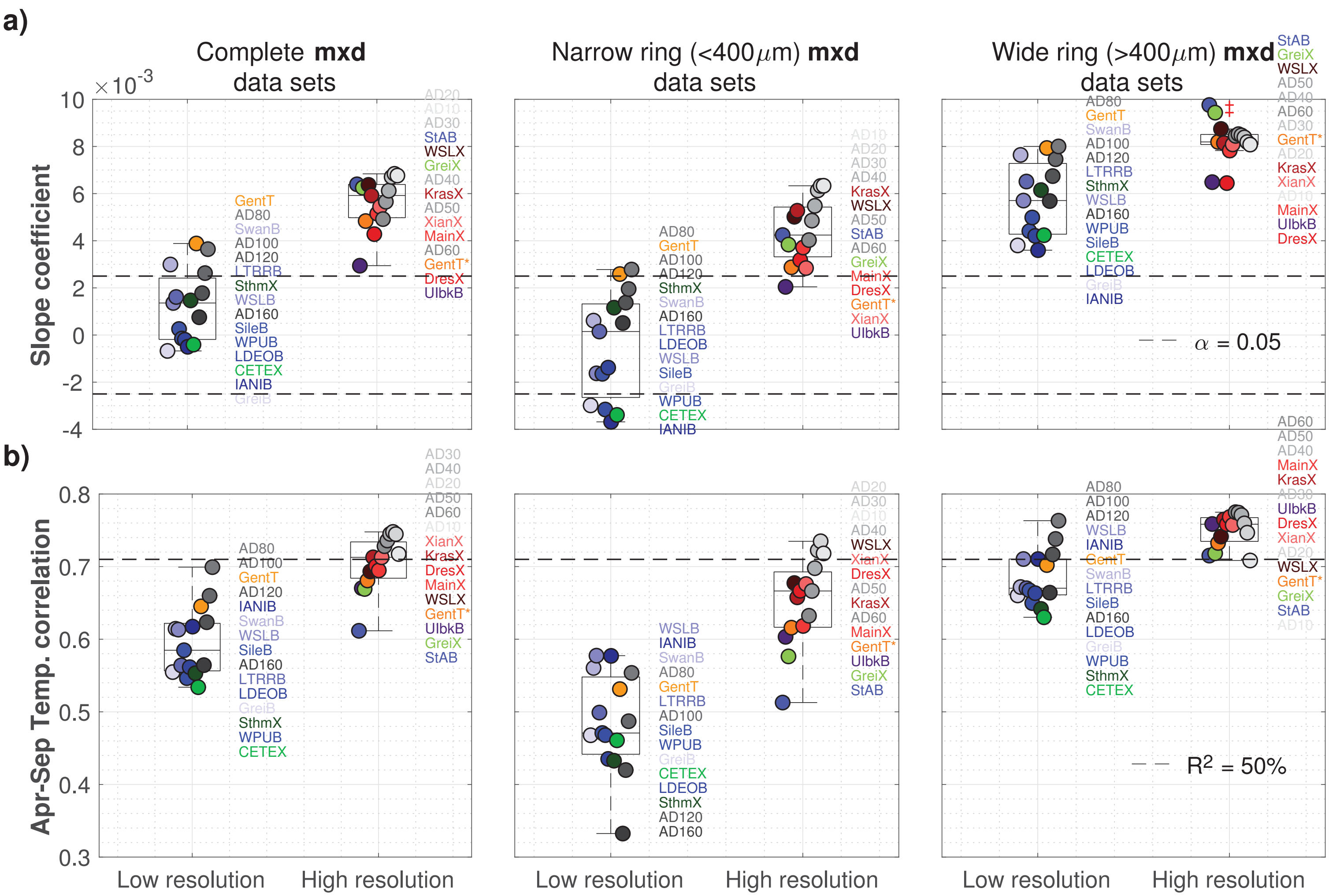

a)
Complete **mxd** data sets
Narrow ring (<400μm) **mxd** data sets
Wide ring (>400μm) **mxd** data sets
$\times 10^{-3}$
Slope coefficient
10
8
6
4
2
0
-2
-4
AD20 AD10 AD30 StAB WSLX GreiX AD40 KrasX AD50 XianX MainX AD60 GentT* DresX UlbkB
GentT AD80 SwanB AD100 AD120 LTRRB SthmX WSLB AD160 SileB WPUB LDEOB CETEX IANIB GreiB
AD10 AD20 AD30 AD40 KrasX WSLX AD50 StAB AD60 GreiX MainX DresX GentT* XianX UlbkB
AD80 GentT AD100 AD120 SthmX SwanB AD160 LTRRB LDEOB WSLB SileB GreiB WPUB CETEX IANIB
StAB GreiX WSLX AD50 AD40 AD60 AD30 GentT* AD20 KrasX XianX AD10 MainX UlbkB DresX
AD80 GentT SwanB AD100 AD120 LTRRB SthmX WSLB AD160 WPUB SileB CETEX LDEOB GreiB IANIB
‡
α = 0.05
b)
Apr-Sep Temp. correlation
0.8
0.7
0.6
0.5
0.4
0.3
AD30 AD40 AD20 AD50 AD60 AD10 XianX KrasX DresX MainX WSLX GentT* UlbkB GreiX StAB
AD80 AD100 GentT AD120 IANIB SwanB WSLB SileB AD160 LTRRB LDEOB GreiB SthmX WPUB CETEX
AD20 AD30 AD10 AD40 WSLX XianX DresX AD50 KrasX AD60 MainX GentT* UlbkB GreiX StAB
WSLB IANIB SwanB AD80 GentT LTRRB AD100 SileB WPUB GreiB CETEX LDEOB SthmX AD120 AD160
AD60 AD50 AD40 MainX KrasX AD30 UlbkB DresX XianX AD20 WSLX GentT* GreiX StAB AD10
AD80 AD100 AD120 WSLB IANIB GentT SwanB LTRRB SileB AD160 LDEOB GreiB WPUB SthmX CETEX
R^2 = 50%
Low resolution
High resolution